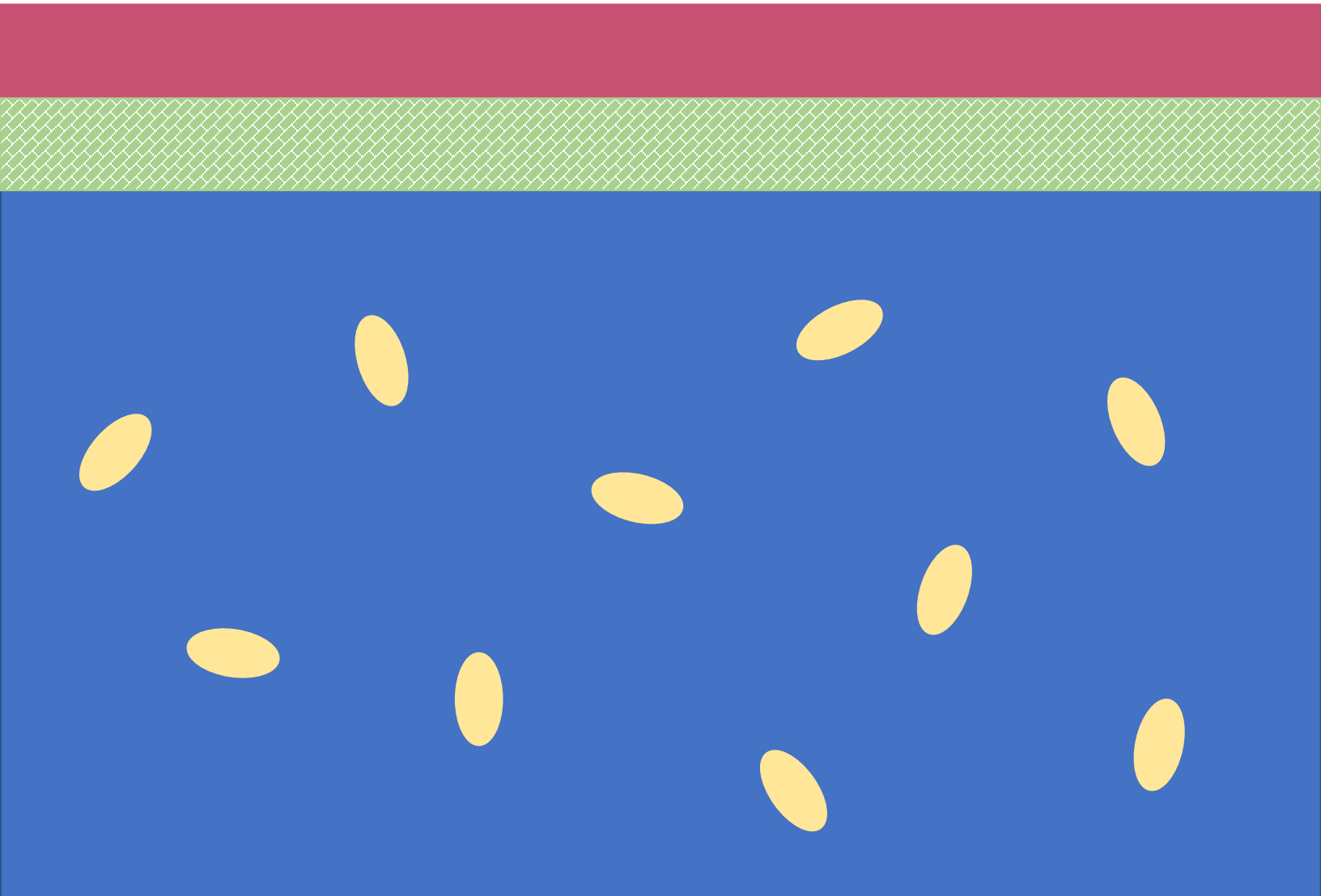






The Journal of
Cell Culture Models



Cover art credit: Olivia Atkins

Edited by Louis A. Roberts

-  Treatment/Medium
-  Keratinocytes
-  3D Collagen Gel
-  Fibroblasts

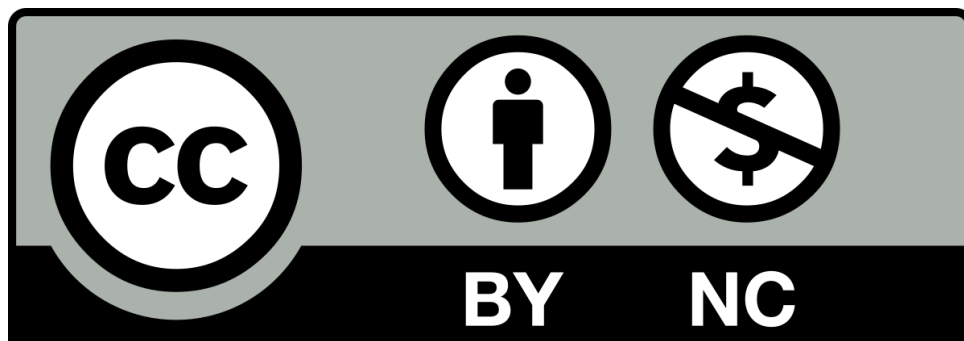
The Journal of Cell Culture Models

Louis A. Roberts

Worcester Polytechnic Institute

Worcester, MA

This work utilizes the Creative Commons under the Attribution-NonCommercial 4.0 International License (CC BY-NC 4.0.). You may share and adapt this work for noncommercial purposes provided you give appropriate credit.



Collection Description

While often cells are represented and pictured as discrete biological units, we aim to expand our vision where cells are more realistically considered as building blocks of tissues. By focusing on their interactions with other cell types and biocompatible materials, we can better model the integrated nature and three-dimensional structures that inform cell survival, proliferation, differentiation, and biological function. This approach better allows us to understand the molecular and cellular processes that mediate and affect scarring, wound healing, drug toxicity, and cell development. How do cells choose between these outcomes, and how can different cell types and their interactions with materials direct these processes? Our biologically authentic cell culture models help answer these research questions with the goal of contributing to regenerative medicine applications.

This collection can be viewed as a “Journal of Cell Culture Models”, and contains articles written following the processes and adhering to the conventions of the primary scientific literature. Each work herein was authored by undergraduate students at Worcester Polytechnic Institute (WPI) enrolled in an authentic research laboratory course, and credits the teaching assistant and instructor (as corresponding author). Generating and disseminating this collection was made possible via the generous support of the WPI Women’s Impact Network (WIN) EmpOwER program.

Foreword for Volume I

This inaugural volume reflects the contributions of the students enrolled in the undergraduate laboratory course BB 3570 Cell Culture Models for Tissue Regeneration at Worcester Polytechnic Institute. The students choose, design, build, and test their models. Subsequently, the students prepare their findings as an open-access journal article. While the research and writing are guided by the instructor and teaching assistant, the students are the scientists conceiving, executing, and disseminating their work. I hope they are as proud of their work as I am!

Volume I, 2023 contributors

Olivia Atkins, Claire Behning, Alexander Boucher, Cleo Caldwell, Katherine Corbin, Lilah Delbou, Binh Diec, John Gabelmann, Kelly Heffernan, Lia Kelly, Samantha Lopez, Grace McCarthy, Jaya Mills, Emma Smith, Yizhe Ma (teaching assistant), Louis Roberts (instructor).

Table of Contents

Fibroblast Embedded 3D Collagen as a Potential Tool for Epithelial Wound Repair.....	1
Claire Behning, Lia Kelly, Emma Smith, Yizhe Ma, Louis Roberts	
Effect of Retinoic Acid on HaCaT and NIH-3T3 cells in an in vitro 3D Collagen Cell Culture Skin Model.....	13
Samantha Lopez, Olivia Atkins, Yizhe Ma, Louis Roberts	
Anti-adhesive Hydrogel Synthesis for Post-operational Physical Barriers.....	26
Alexander Boucher, Grace McCarthy, Binh Diec, Yizhe Ma, Louis Roberts	
Interleukin-6 Cytokine Production After Wounding in NIH3T3 and HaCaT Cell 3D Tissue Models is Impacted by Wounding Method but Uninfluenced by Co-Culture Ratio.....	35
Cleo Caldwell, Lilah Delbou, John Gabelmann, Yizhe Ma, Louis Roberts	
Determining the toxicity or potential carcinogenesis of sunscreen on HaCaT and NIH-3T3 cells.....	44
Katherine Corbin, Kelly Heffernan, Jaya Mills, Yizhe Ma, Louis Roberts	

Fibroblast Embedded 3D Collagen as a Potential Tool for Epithelial Wound Repair

Claire Behning^{a1}, Lia Kelly^{a1}, Emma Smith^{b1}, Yizhe Ma^a, Louis Roberts^{a*}

^aDepartment of Biology and Biotechnology, Worcester Polytechnic Institute, Worcester, MA

^bDepartment of Biomedical Engineering, Worcester Polytechnic Institute, Worcester, MA

¹Authors contributed equal intellectual effort to this manuscript; order determined alphabetically.

*To whom correspondence should be addressed: laroberts@wpi.edu

<https://doi.org/10.33697/ajur.2020.NN>

Students: cebehning@wpi.edu, lmkelly@wpi.edu, eesmith@wpi.edu Mentor: laroberts@wpi.edu*

ABSTRACT

Collagen is a functional biomaterial with many applications including in the use of wound healing. 3D collagen hydrogels mimic an *in vivo* cell culture experience which has been used in studies of cell survival and growth. In experimentally examining human cells under contact with 3D collagen, it is possible to understand the role of collagen in human epithelial tissue repair. This study explored the growth and attachment response of human MCF-7 cells when exposed to 3D collagen by investigating if the presence of NIH/3T3 fibroblasts embedded within the collagen should produce an increased response in cell repair. 3D collagen and fibroblast presence was able to be analyzed in tandem with a “sandwich-like” configuration of the gels to determine how these variables impact or improve the tissue repair response in MCF-7 cells. Examinations in growth, attachment, viability, and migration patterns demonstrated that MCF-7 repair response may be increased when in contact with 3T3 embedded 3D collagen without impairing viability. Most notably, results from the migration assay revealed that MCF-7 cells migrate the most when covered by and adhered to cellular 3D collagen. Fibroblast embedded collagen on top of and below MCF-7 cells exceeded quantitative assessment to near confluency, whereas less than 50 counted cells per image migrated without any top collagen layering. Continuation of these methods could involve *in vivo* experiments that incorporate live animal models to determine if these results would continue to extend and apply to live tissue.

KEYWORDS

Collagen; 3D Collagen; Fibroblasts; Wound Healing; Hydrogels; Tissue Repair; Migration

INTRODUCTION

The most common cell type in connective tissue is fibroblasts, a structural mesenchymal cell type. A major function of these cells includes the production of collagen fibers, proteoglycans, fibronectin, glycosaminoglycans, and other extracellular matrix (ECM) components.¹ In the wound healing process, the body’s response phases are as follows: homeostasis, inflammation, migration, proliferation, and remodeling.² Fibroblast cells, during the proliferative phase, increase production of collagen, elastin, proteoglycans, and hyaluronic acid, and these molecules are reorganized into a new ECM during the final phase.² The presence of fibroblasts has shown increased keratinocyte migration in a 3D wound model compared to fibroblast absence, indicating the importance of these cells in tissue repair.³ The NIH/3T3 fibroblast tetraploid cell line (ATCC® CCL-1658™) isolated from Swiss albino (*Mus musculus*) murine embryos have been used in thousands of publications as a model system because of its functionality as a transfection host.

In addition to NIH/3T3 cells, MCF-7 cells (ATCC® HTB-22™) are used in cell modeling. MCF-7 cells are epithelial human breast cancer cells. The line was isolated in 1973 from a pleural effusion of a 69-year-old woman who had metastatic disease.⁴ Cancer cells have different wound healing behavior. Cancer cells hijack parts of the wound healing process to ensure their survival.⁵ When observing cancer cell behavior, 3D models can be used to more clearly identify invasive or migratory patterns compared with 2D models.⁶ When using a 3D collagen model, cell migration and degeneration of the extracellular matrix can be observed, which allows for cancer cell metastasis to be more accurately modeled.⁶ Because deregulated dynamics with the

extracellular matrix are a main characteristic associated with cancers, using a 3D model allows for more visualization of the processes and observing changes to the matrix's mechanical and structural properties to better direct treatments.⁷ This response can be paired with 3D matrices, which shows that when MCF-7 cells are cultured in hydrogels there is up-regulation of breast-specific markers than when comparing the response to a standard 2D culture. This allows for a more in-depth analysis of the cell model to be done with conditions that are in vivo.⁸

Collagen is a useful biomaterial to be used in tandem with the above cell lines. This triple helix structured protein is one of the most abundant proteins in the ECM.^{9,10} It is a fibrous protein that creates a scaffold for cells and is highly compatible with a cellular environment.⁹ Over time, collagen-based biomedical materials have been developed into effective structures that have a wide range of applications including in the food, cosmetics, pharmaceutical, and biomedical industries.¹⁰ Currently, the most common method of cell culture is conventional 2D cell culture, which provides information to understand cell pathology, physiology, and function. However, a 3D cell culture method can create an environment that more closely resembles in vivo conditions.¹¹ 3D culture allows some of the cell and matrix interactions to be captured, resulting in information about differentiation, proliferation, and cell functions being lost.¹¹ Collagen is one of the most commonly used proteins in the creation of matrices because of its ease of use, low cost, and flexibility.¹¹ Using collagen as a scaffold in a 3D culture allows for a variety of factors, such as pore size, ligand density, and stiffness, to be customized for each experiment through simple changes that alter the structural properties of the gel.¹¹ Through the use of a collagen 3D matrix, the interactions between cells are more clearly expressed, and a biologically active environment is established which allows cells to behave in a way more representative of in vivo conditions.¹¹

Different cell lines and biomaterials are used in a wide variety of medical and research applications. They can be modified to deliver drugs or cell therapy, coat medical devices, and protect against infection.¹² The use of collagen in tandem with NIH/3T3 cells in medical applications is becoming more common, as their properties are excellent for wound healing. Collagen is commonly used as a hydrogel material and is known for its biocompatibility, in addition to its ability to promote cell attachment, proliferation, and migration. Cells have been cultured on and within collagen to mimic biological microenvironments and examine their potential as a treatment for wounds.¹³ One study seeded fibroblasts into a collagen-rich hydrogel; the hydrogel formulation was thought to be a candidate for diabetic wound healing.¹⁴ Cell viability, proliferation, and migration were studied using in vitro models. These models showed fibroblast survival and proliferation increasing with a higher concentration of collagen.¹⁴ In addition, migration through, into, or out of the hydrogel could not be detected, likely due to a lack of chemotactic factors.¹⁴ This study indicated that the formulation of this particular 3T3/collagen hydrogel would be useful in wound healing applications.¹⁴

Another study used a hydrogel made of recombinant human collagen as a skin graft overlay.¹⁵ This hydrogel was made from recombinant human collagen type III and sodium alginate, where the final solution was 10% collagen.¹⁵ Once hydrogels were formed from this solution, they were subjected to a variety of tests to determine their biological properties. To determine the biological properties, both cell lines and live animals, rat subjects, were used. HaCaTs, HUVECs, and primary human fibroblasts were used in cytotoxicity and migration studies.¹⁵ The cytotoxicity study indicated that the collagen extract had slight cytotoxicity, particularly for the HUVECs.¹⁵ The migration study indicated that the ability of each cell line to migrate was increased following six to 24 hours of culture.¹⁵ Live animals were used to test the hydrogel's ability to aid wound healing. These experiments indicated that the hydrogel promoted wound healing, dermis formation, basement membrane formation, angiogenesis, and proliferation.¹⁵ Following these experiments, the researchers determined that this hydrogel has the potential to aid in wound healing as a graft overlay.¹⁵ Collagen hydrogels with and without cells seeded within them have the potential to aid in the treatment of wounds, but further research and modeling are needed.

Much of the work described previously utilized 2D culture models and animal models to test a material's wound healing properties. Some work has been done to assess these materials on 3D culture models. There is more to be done in the development of 3D culture models to assess these properties. Because of the biochemical healing properties naturally expressed by fibroblasts, we proposed that a hydrogel, constructed from 3D collagen embedded with NIH/3T3 cells, has the potential to increase the wound repair response in MCF-7 epithelial tissue. Repair response was measured using physical and quantitative values of cell attachment, growth, viability, and migration. In seeing a consistency in cell viability and increase in attachment and migration, cellular collagen hydrogels have the potential for being used as a tool for tissue repair.

METHODS AND PROCEDURES

Cell Maintenance

NIH/3T3 (ATCC® CCL-1658™) and MCF-7 (ATCC® HTB-22™) cell lines from the American Type Culture Collection

(ATCC) were maintained in complete medium containing Dulbecco's Modified Eagle Medium (DMEM) with 10% Fetal Bovine Serum (FBS) and 1% Penicillin/Streptomycin (PS). Cells were incubated at 37°C and 5% CO₂ in T25 and T75 flasks. Cells were passaged between every 48-72 hours, occurring as needed or when nearing confluency.

Cell Counting

Cells were trypsinized and diluted in complete medium. 100 µL of the cell suspension were aliquoted and 100 µL of 0.4% Trypan Blue was added. When manual cell counting, 10 µL of the cell-dye mixture was loaded on a hemacytometer and analyzed using a 10x objective microscope. Cells within one mm² squares were counted, and the average of four squares was calculated. The total cell density was calculated using the following formula: average number of cells per square * 2 * 10⁴.

Cell Suspension in 3D Collagen

Nearly confluent NIH/3T3 cells were trypsinized and resuspended in complete medium. For the attachment, proliferation, and alamarBlue™ assay, a 3D collagen (Sigma-Aldrich® C4243™) mixture was prepared using 300 µL of cell suspension and 1.2 mL of collagen to create a final concentration of 2.02 * 10³ cells per mL. For the migration experiment, the same method was used with different volumes- 360 µL and 240 µL of cell suspension and 1.44 mL and 960 µL of collagen mixture for the 300 µL and 200 µL aliquots, respectively. The final concentrations were 3.9 * 10³ cells per mL for the 300 µL and 4.6 * 10³ cells per mL for the 200 µL aliquots. For the acellular collagen mixture, complete medium was added in place of a cell suspension. The collagen mixture was resuspended evenly. 300 µL and 200 µL aliquots were placed into the allotted collagen wells for 12- and 24-well plates, respectively. The collagen was left to firm in a 37°C incubator for two-to-three hours. Following gelation, MCF-7 cells were trypsinized for placing on the set collagen gel. Medium was added to wells without cells seeded on top.

Attachment and Proliferation Assay

Attachment and proliferation were assessed by plating a 12-well plate of MCF-7 cells on acellular and cellular 3D collagen (**Table 1**). MCF-7 cells were seeded at equal concentrations on top of collagen either embedded with 3T3 cells (Cell Col) or not embedded (Acell Col). Negative controls consisted of wells with collagen or on its surface. Positive controls consisted of wells with MCF-7 cells adhered and no collagen (No Col). One mL of complete medium was added to each well to ensure collagen hydration and cell maintenance. Observations were made after 24, 72, and 120 hours. At 120 hours, cell counts were performed and the remaining cells from representative conditions were transferred to a 96 well plate to perform an alamarBlue™ assay.

	1	2	3	4
A	MCF-7 Cells Only	MCF-7 Cells Only	Acellular Collagen with MCF-7s Seeded on Top	Cellular Collagen with MCF-7s Seeded on Top
B	Acellular Collagen	Acellular Collagen	Acellular Collagen with MCF-7s Seeded on Top	Cellular Collagen with MCF-7s Seeded on Top
C	Cellular Collagen	Cellular Collagen	Acellular Collagen with MCF-7s Seeded on Top	Cellular Collagen with MCF-7s Seeded on Top

Table 1. Design conditions for the attachment and proliferation assay in a 12-well plate.

AlamarBlue™ Assay

To assess viability of the MCF-7 cells in response to collagen exposure, an alamarBlue™ Assay (BIOSOURCE® Cat. No. DAL1025) was performed using samples from a cellular control well, an acellular collagen well, and a cellular collagen well from the attachment assay. Each well was trypsinized and a cell count was performed with hemocytometry. The cell counts were found and used as a reference when setting up the assay. A 96-well plate was set up using three different samples: control MCF-7 cells grown in only medium (control), MCF-7 cells grown on acellular collagen, and MCF-7 cells grown on cellular collagen. A two-fold dilution series ranging from undiluted to 1:64 was performed, with a final volume of cell solution in each well of 125 µL. 125 µL of medium was added to wells to serve as a blank. After incubating the plate for 72 hours, 12.5 µL alamarBlue™ Cell Viability Reagent was added to each well and incubated for two hours. A Biotek Synergy H1 Hybrid Multi-Mode Reader was used to read the fluorescence of the wells using excitation and emission values of 540 nm and 590 nm, respectively. The average of blank wells was calculated and used to find the blank-subtracted values of each well. Averages of the conditions (control, acellular collagen, cellular collagen) for each well dilution were calculated and used in statistical analysis using two-sample t-tests (*p*<0.05).

Microscopy/Imaging

Each well was observed at 0, 24, 72, and 120 hours. Cells were assessed for attachment and growth through visual analysis. Shape of the cells, confluency, and other visually apparent changes were noted at each observation point. Images were taken through an Olympus IMT-2 Inverted Research Microscope at 100x magnification to record the qualitative data.

Migration Assay

Migration was assessed by plating two 12-well plates of MCF-7 cells on acellular and cellular 3D collagen (**Table 2**). Alongside the 12-well plates, a 24-well plate was used to plate 200 μ L collagen gels to be transferred on top of the scratch once firmed. MCF-7 cells were seeded on top of collagen either embedded with 3T3 cells or not embedded. Two wells with MCF-7 cells adhered to the well bottom were scratched without layering collagen on top for positive controls. One mL of complete medium was added to each well to ensure collagen hydration and cell maintenance. Each well was then lightly scratched with a 1000 μ L pipette tip to simulate a wound. An hour after scratching, the collagen gels were transferred to the 12-well plates and placed on top of the scratch. Plates were incubated at 37°C and 5% CO₂. Following 24 hours, observations were conducted of each well, and images were taken using a Biotek Cytation 5 Cell Imaging Multimode Reader at 10x brightfield. Image recoloring was performed in Google. Scratch images were divided into three fields of view (FOVs) acting as three technical replicates per condition, and the number of cells migrated within the scratch were counted per FOV. The average and standard deviation was calculated for each condition, and two-sample t-tests ($p < 0.05$) were performed to determine significance between groups.

	1	2	3	4
A	MCF-7 Cells Only with Acellular Collagen on Top	MCF-7 Cells Only with Acellular Collagen on Top	MCF-7 Cells Only with Cellular Collagen on Top	MCF-7 Cells Only with Cellular Collagen on Top
B	Acellular Collagen with MCF-7s Seeded on Top (Acellular Collagen on Top)	Acellular Collagen with MCF-7s Seeded on Top (Acellular Collagen on Top)	Acellular Collagen with MCF-7s Seeded on Top (Cellular Collagen on Top)	Acellular Collagen with MCF-7s Seeded on Top (Cellular Collagen on Top)
C	Cellular Collagen with MCF-7s Seeded on Top (Acellular Collagen on Top)	Cellular Collagen with MCF-7s Seeded on Top (Acellular Collagen on Top)	Cellular Collagen with MCF-7s Seeded on Top (Cellular Collagen on Top)	Cellular Collagen with MCF-7s Seeded on Top (Cellular Collagen on Top)

	1	2	3	4
A	MCF-7 Cells Only With No Collagen on Top	MCF-7 Cells Only with No Collagen on Top	EMPTY	EMPTY
B	Acellular Collagen with MCF-7s Seeded on Top (No Collagen on Top)	Acellular Collagen with MCF-7s Seeded on Top (No Collagen on Top)	EMPTY	EMPTY
C	Cellular Collagen with MCF-7s Seeded on Top (No Collagen on Top)	Cellular Collagen with MCF-7s Seeded on Top (No Collagen on Top)	EMPTY	EMPTY

Table 2. Design conditions for the migration assay in two 12-well plates. Wells contained a bottom layer of collagen, top layer of collagen, both layers, or neither. MCF-7 cells were seeded in all experimental wells.

RESULTS

Cellular 3D Collagen increases MCF-7 attachment and does not decrease cell viability.

Visual confirmation of gel conformation and cell attachment was completed prior to and immediately following cell seeding. **Figure 1** depicts the visual confirmation of cells being present following seeding. Immediately following seeding, cells maintain a rounded shape, indicating potential lack of attachment and spreading on the bottom of the well. This assay ran for 120 hours

total. At the 24-hour time point of the assay, the MCF-7 cells seeded on top of the collagen had become partially attached. In all wells, a significant number of rounded cells remained, indicating a lack of attachment and spreading on the collagen gel. When examining for visual confirmation of attachment, cells appeared to be viable with typical conformation and growth patterns. The attempted monolayer creation of MCF-7 cells on the top of the collagen gel was successful, as all of the cells were visually noted to be in one layer and had not migrated or fallen into the gel layer. When observing the wells with NIH/3T3 cells embedded in the collagen, they were not easily visible, leaving only the MCF-7 cells to be viewed with a high level of certainty. A significant number of cells in every well remained unattached or partially attached and lacked spreading. Although medium was changed through pipette aspiration followed by addition of new media, many of the rounded cells remained which suggests partial attachment rather than complete unattachment as aspiration would have removed fully unattached cells.

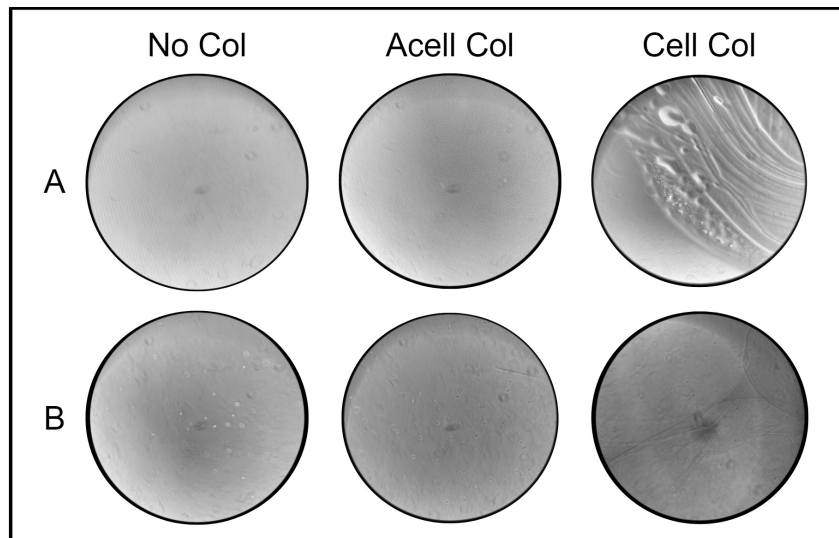


Figure 1. Attachment and Proliferation Assay, before **(A)** and after **(B)** cell seeding, (From top left to right: No Collagen (No Col) prior to cell seeding, Acellular Collagen (Acell Col) prior to seeding, Cellular Collagen (Cell Col) prior to seeding, No Col following cell seeding, Acell Col following cell seeding, and Cell Col following cell seeding)

At the 72-hour time point (**Figure 2B**), each well was observed for cell conformation, attachment, viability, and growth. Based on visual observations, cells in the cell-only (No Col) well and on top of the acellular collagen (Acell Col) and cellular collagen (Cell Col), were all growing at an expected rate, reaching 40% confluency (**Figure 2B**). Some cells in every well continued to maintain a rounded shape indicative of lack of attachment or partial attachment, and spreading. At the end of observations, each well was given fresh media.

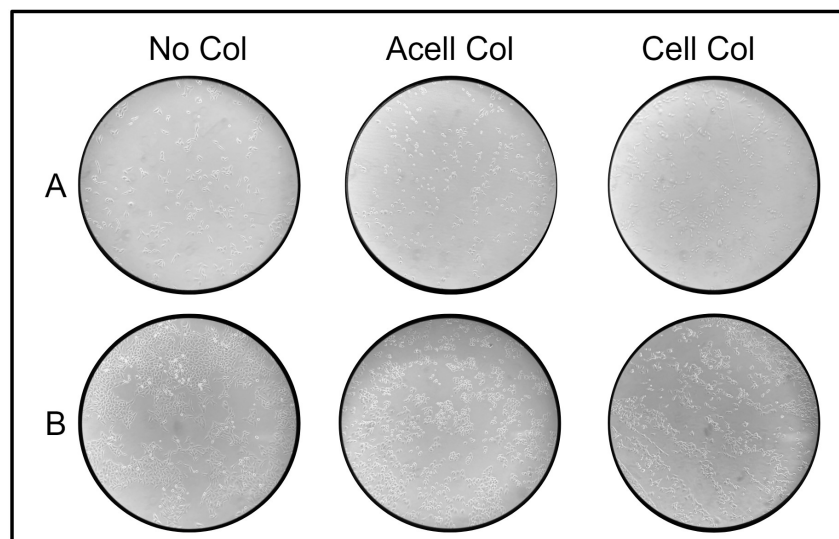


Figure 2. Attachment and Proliferation Assay, 24 (A) and 72 (B) hour time point, (From top left to right: No Collagen (No Col) after 24 hours, Acellular Collagen (Acell Col) after 24 hours, Cellular Collagen (Cell Col) after 24 hours, No Col after 72 hours, Acell Col after 72 hours, and Cell Col after 72 hours)

Cells were again observed at the 120-hour time point for cell conformation, attachment, viability, and growth. Cells in all wells appeared to be more attached and spread than at the 72-hour time point. In wells with collagen that had MCF-7 cells seeded on top, distinct clusters of cells had been created. These areas, visually, separated highly confluent areas of cells from those with less confluence. This was noted on the wells with unseeded collagen and MCF-7 cells on top of the gel (**Figure 3A**). The wells that appeared to have the highest confluency of MCF-7 cells were of the Cell Col condition. All cells appeared to be more attached than at previous time points and had less rounded conformation. Throughout each well, conformation and shape of cells was consistent with each other and with what is expected of the cell line. The average number of cells was 3.4×10^4 cells/mL in No Col control wells, 3.2×10^4 cells/mL in Cell Col wells, and 1.0×10^4 cells/mL in Acell Col wells. Cell counts revealed that there was no significant increase nor decrease in growth from the control condition compared to cellular collagen attachment. Interestingly, the decrease in cell concentration for acellular collagen conditions was remarkable. It appeared as though cellular attachment and, most notably, confluency increased in collagen wells. In contrast, MCF-7 proliferation rates did not seem to improve as supported by the cell counts.

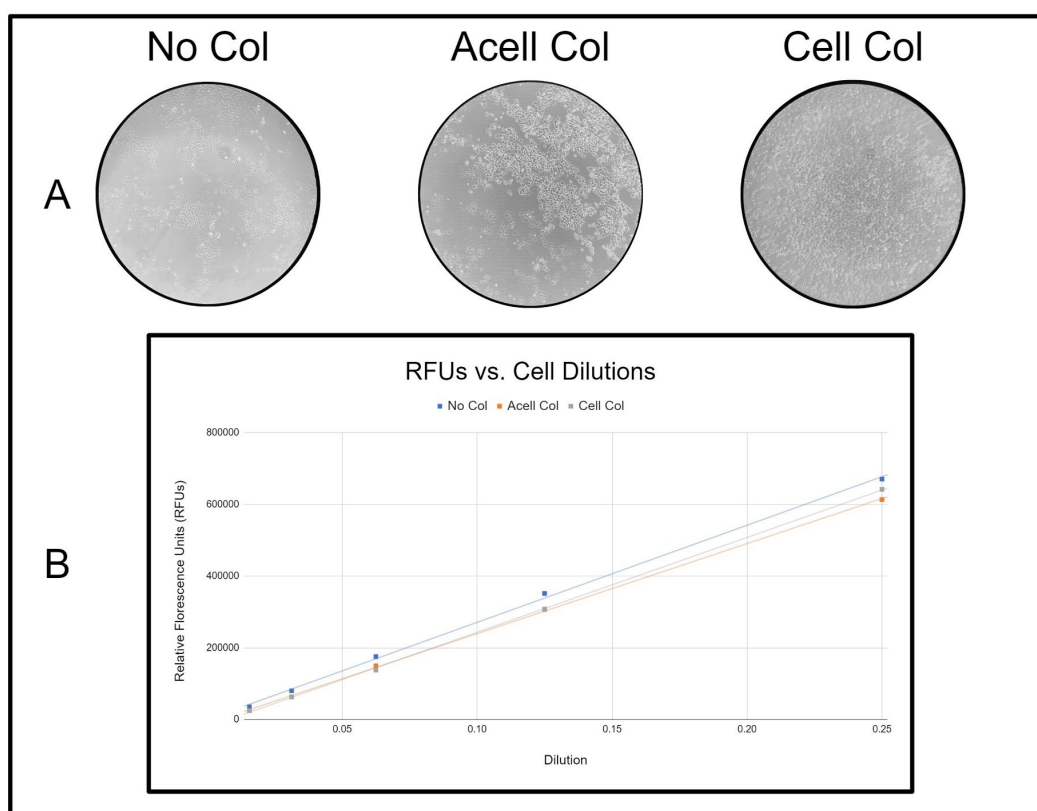


Figure 3. (A) Attachment and Proliferation Assay, 120 hour time point. From top left to right: No Collagen (No Col) after 120 hours, Acellular Collagen (Acell Col) after 120 hours, Cellular Collagen (Cell Col) after 120 hours, Proliferation Assay Results. (B) Graph of fluorescence plotted against dilution for each condition of the previous attachment and proliferation assay.

The alamarBlue™ assay using a resazurin solution measured MCF-7 viability after no collagen exposure, exposure to 3D collagen, and exposure to fibroblast-embedded 3D collagen. When relative fluorescence units (RFUs) were graphed over dilutions, all three conditions showed a consistent linear growth across the dilutions 0.02 to 0.25 with R^2 values approaching 1 (**Figure 3B**). More concentrated dilutions (1.0 and 0.5) decreased the linear trend for each category, indicating that the concentration of cells in these wells exceeded detectable fluorescence levels. Therefore, data points from dilutions up to 0.25 were analyzed. Statistical analysis using two-sample t-tests comparing conditions in the 0.25 diluted wells revealed no significant differences ($p < 0.05$) suggesting that contact to collagen does not affect cell viability.

MCF-7 cells migrate the most when covered by and adhered to cellular 3D collagen.

The migration assay began with plating MCF-7 cells onto either acellular or cellular collagen and incubating for 24 hours. At this time, cells not adhered to collagen were 30% confluent, cells adhered to acellular collagen were 75% confluent, and cells adhered to cellular collagen were 95% confluent (**Figure 4A**). After 24 hours of incubation, each well was scratched with a 1000 μ L pipette tip (**Figure 4B**). Each scratch was made in the center of a well and did not puncture through the collagen gel, if present. After the scratches were made, collagen gels were added on top of designated scratches to represent a wound repair aid.

After a 24 hour incubation period, representative images of each scratched condition were taken to assess the proliferation and migration of MCF-7 cells in response to an artificial wound when treated with 3D collagen (**Figure 5**). Using three fields of view along the scratch (**Figure 6A**), the averages for each condition were calculated. Cell counts varied between conditions depending on the presence of collagen on top or bottom and whether fibroblasts had been embedded. Wells with acellular collagen on the bottom produced the highest attainable MCF-7 count (**Figure 6B**) when acellular collagen was placed on top, with an average of 78 migrated cells. Other wells contained more than 78 migrated cells, but due to an abundance of cells, could not be counted accurately. All fields of view with cellular collagen on the bottom and top were too confluent to accurately count the number of migrated cells.

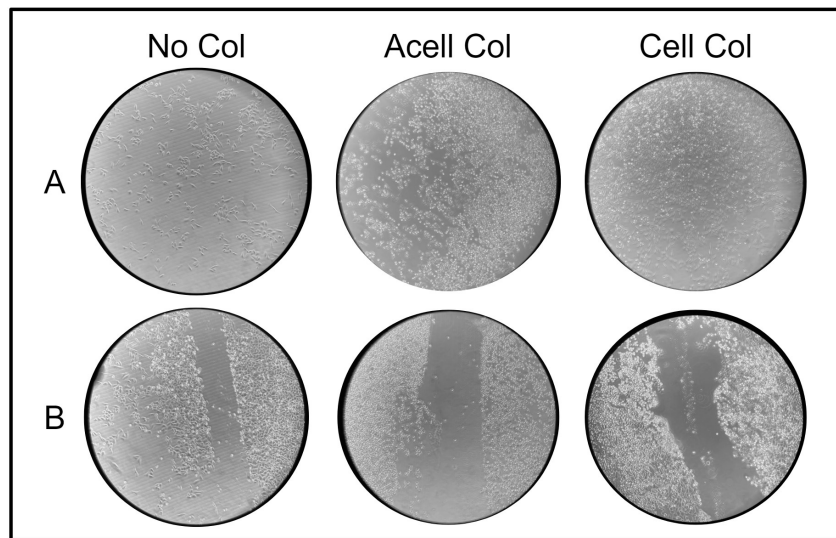


Figure 4. (A) 3T3 Collagen base #2 MCF-7 cells before scratching. From left to right: Cells on No Collagen (No Col), MCF-7 cells on Acellular Collagen (Acell Col), MCF-7 cells on Cellular Collagen (Cell Col). (B) Initial scratches of MCF-7 cells. From left to right: No Collagen (No Col), Acellular Collagen (Acell Col), Cellular Collagen (Cell Col).

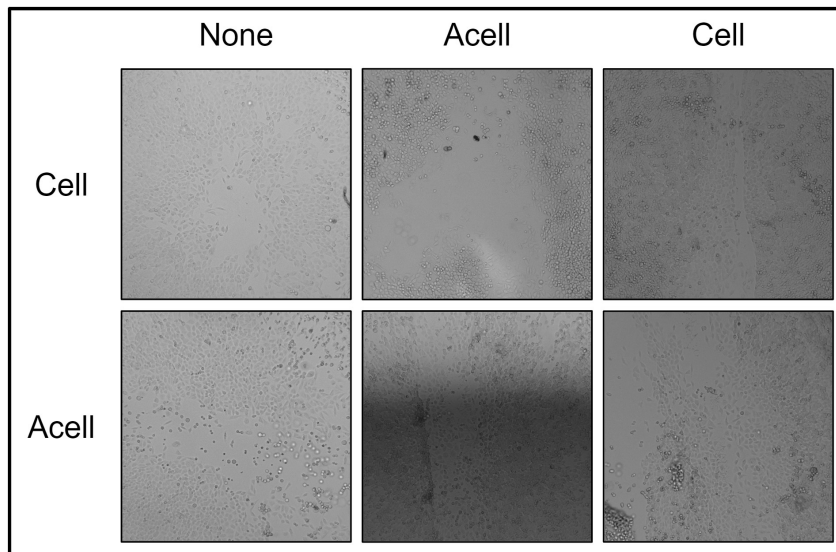


Figure 5. Scratches of MCF-7 cells following 24 hours (None - No Collagen on Bottom, Acell - Acellular Collagen on Bottom/Top, Cell - Cellular Collagen on

Bottom/Top)

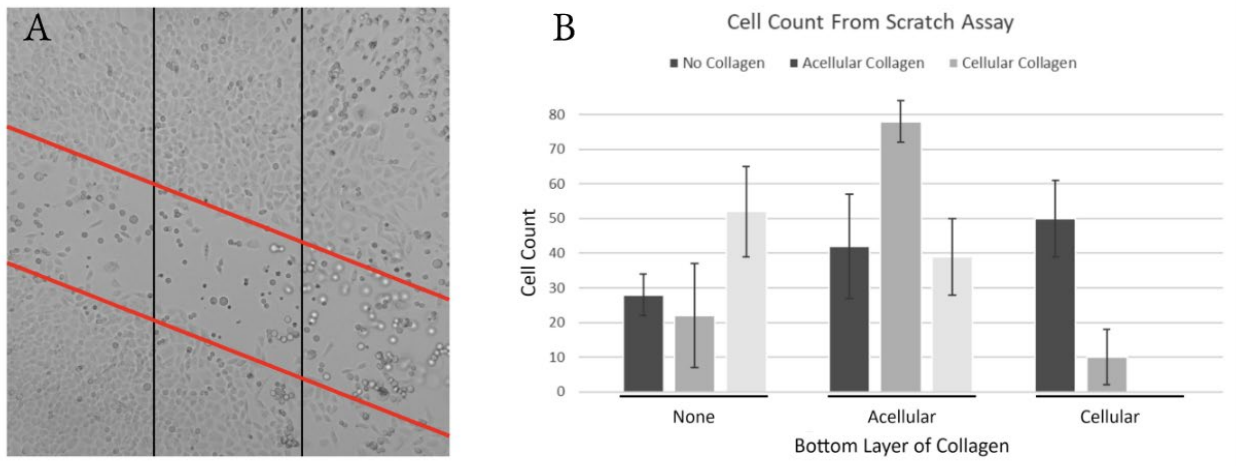


Figure 6. (A) Fields of View (FOV) for Cell Count, the black lines indicate the field of view and red lines indicate the scratch location. Image taken at 100x magnification. (B) Results of Scratch Assay Cell Count Averages (None - No Collagen on Top, Acellular- Acellular Collagen on Bottom/Top, Cellular - Cellular Collagen on Bottom/Top, MCF-7s Only - No Collagen on Bottom). Error bars represent standard deviations replicates. A cell count for Cellular Collagen on Top/Bottom was unattainable because there were too many cells to count.

The cells were examined using a microscope and images were taken after 24 hours (Figure 5). The images were used to perform a cell count of the scratched region. The wells with no collagen on the bottom had average cell counts of 28 ± 6 , 22 ± 15 , and 52 ± 13 cells for the conditions with no collagen on top, acellular collagen on top, and cellular collagen on top (Figure 6B). Of the conditions with no collagen on the bottom, the cellular collagen on top resulted in the largest number of migratory cells. The wells that had acellular collagen on the bottom had average cell counts of 42 ± 15 , 78 ± 6 , and 39 ± 13 cells for the conditions with no collagen on top, acellular collagen on top, and cellular collagen on top, respectively (Figure 6B). The largest cell count was found in the well with acellular collagen on top and the bottom. Finally, in the wells with cellular collagen on the bottom, the average cell counts were 10 ± 8 and 50 ± 11 cells for the conditions with no collagen on top and acellular collagen on top, respectively (Figure 6B). The condition where cellular collagen was present on the bottom and top of a cell monolayer was unable to be counted due to the density within the scratch.

Overall, the conditions in which no collagen was placed on top of the scratch wound were associated with the least amount of cell migration. The conditions with the highest visible migration and wound healing rate were wells which had collagen placed on both the top and bottom which matched variables. The wells with cellular collagen on both top and bottom or wells with acellular collagen on both top and bottom had the most growth success when compared to wells with no collagen placed on top of the wound or collagen that had mismatched cellular states. It is important to note that mere presence of collagen tended to increase migration rate, as the average counts for conditions without collagen on top were below 50 cells per FOV.

After performing a two-sample t-test ($p < 0.05$) on the cell counts from the scratch assay in Figure 6B, the wells were compared to one another to determine significance of migration in the scratch wound healing. When comparing the control condition with no collagen on the bottom of the well to conditions that had acellular collagen placed on top of the MCF-7 cell scratch, the migration of the MCF-7 cells was found to be larger and statistically significant for the acellular on top collagen conditions, regardless of the cellular state of the collagen on the bottom of the wells when compared to controls. When comparing the control condition with only MCF-7 cells and no collagen on the bottom of the well to conditions that had cellular collagen placed on top of the MCF-7 cell scratch, the migration of the MCF-7 cells was found to be larger and statistically significant for the cellular collagen on top conditions, regardless of the cellular state of the collagen on the bottom of the wells, when compared to controls. Finally, when comparing the condition that had acellular collagen placed on top of the MCF-7 cell scratch to the condition that had cellular collagen placed on top of the MCF-7 cell scratch, the migration of the MCF-7 cells was found to be larger and statistically significant for the acellular on top collagen conditions, regardless of the cellular state of the collagen on the bottom of the wells, when compared to the cellular on top collagen conditions.

DISCUSSION

This study aimed to explore the growth and attachment response of human MCF-7 cells when exposed to 3D collagen by

investigating if the presence of NIH/3T3 fibroblasts embedded within the collagen should produce an increased response in cell repair. 3D collagen and fibroblast presence was able to be analyzed in tandem with a “sandwich-like” configuration of the gels to determine how these variables impact or improve the tissue repair response in MCF-7 cells. Through the use of physical and quantitative values of cell attachment, growth, viability, and migration assay techniques, the wound repair response was measured and assessed. Examinations in growth, attachment, viability, and migration patterns demonstrated that MCF-7 repair response may be increased when in contact with 3T3 embedded 3D collagen without impairing viability.

Based on the experimental plate set up with the collagen being unevenly distributed, there could have been growth patterns of cells that were distributed or organized in a different orientation. This could have caused some of the stark lines or grouping of cell growth that we observed or the slower rate of attachment. Additionally, this environment and transfer likely caused a significant amount of cell stress which could have influenced the slowed attachment rate, more rounded epithelial shape, and decrease in proliferation for Acell Col wells. Overall, based on the repair pattern of the MCF-7 cells over time, the wells with the highest attachment rates were those with collagen gels that were seeded with 3T3 cells. Despite this, conditions with cellular collagen were expected to have increased MCF-7 growth and replication due to the function that 3T3 cells serve during wound healing. Fibroblast cells increase production of collagen, elastin, proteoglycans, and hyaluronic acid which promote new extracellular matrices to be developed. Further investigation should be done to confirm the absence in improved growth response from the cellular collagen attached cells.

It is important that wound treatments do not impact cell viability nor cause increased cell death. Because collagen conditions did not impact viability compared to the control, we can infer that a collagen hydrogel does not produce any cytotoxic effects to live tissue cells. Trends for the three conditions remained linear for a majority of the dilution wells with high values for R^2 showing consistency in the viabilities. An ideal healing model would not only be safe and nontoxic to cells but also increase tissue regeneration. While improved proliferation was not witnessed in these results using a constant cellular concentration, exploration of varying NIH/3T3 density within collagen can be done to further address this aspect.

When setting up the attachment and viability assay, multiple wells had collagen bases that did not set evenly through the entirety of the well. This was a factor that had to be considered through the whole assay as the inconsistency of the gel width could cause data discrepancies. Additionally, the collagen appeared to have pockets of air when observed with a microscope before seeding cells (**Figure 7**). These bubble pockets existed in both cellular and acellular collagen. This was also seen in the migration/scratch assay. When the wells were scratched with the 1000 μ L pipette tip, some of the cells were lifted up from the collagen, and there was additional movement and folds added to the collagen.

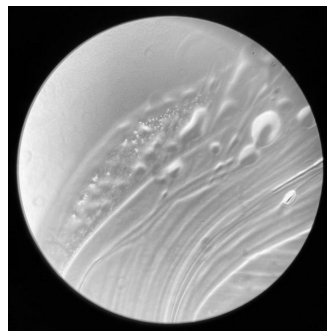


Figure 7. Example of a collagen layer with 3T3 cells embedded which has bubbles from air pockets in the collagen and the uneven width of the gel.

The scratch-migration assay demonstrated that the most successful wound healing occurs when the cellular state of the top and bottom collagen agreed. The highest growth rate for all conditions was seen in the well with cellular collagen gels on both the top and bottom of the MCF-7 cells. However, the cellular state of the collagen only benefited the wound healing progression when both of the gels were cellular. When one collagen gel was cellular and one was acellular, this resulted in worse wound healing than the condition which had matching acellular collagen gels on the top and bottom of the scratch. This data shows that it is important to prioritize matching the collagen gel states to generate the most successful wound healing. Because cellular collagen is able to be used as a representative model of human skin, this makes the well conditions with cellular collagen on the bottom most relevant to human application.

When cellular collagen was added to the top of scratch wounds in MCF-7 cells, the growth of the cells was too confluent in the

scratch fields to count accurately. This results indicates that the addition of the cellular collagen layer on top of the wound rendered the scratch completely healed after 24 hours from a visual assessment standpoint. Additionally, it is important to recognize that even though when this condition had acellular collagen gels added to the top of the scratch wound, the healing was not as significant when compared to the cellular condition; however, the cell growth with the acellular gel was higher than the condition in which no collagen was added to the top of the scratch. This recommends that in situations in which a cellular collagen gel is not available, an acellular gel for wound healing would be more beneficial than not having one at all. Overall, these results support the hypothesis that cell migration increases when exposed to cellular collagen, indicating a potential for applications of fibroblast based wound healing mechanisms.

CONCLUSIONS

The cell attachment and viability assays showed that cellular collagen gels that are seeded with 3T3 cells are able to promote higher levels of growth of cells than acellular collagen. To add to this finding, both cellular and acellular collagen gels resulted in more successful wound healing when collagen was added to the top of the scratch wound. Specifically, wound healing based on migration occurred most successfully for the cellular collagen conditions, but it was also noted that matching cellular states of the gels was important as well. This data supports our hypothesis that cellular collagen will promote wound healing because of its ability to model human epithelial cells and wound healing mechanisms. Our work provides a novel approach to explore the applications of collagen gels in wound healing. By creating a nontoxic model that placed collagen on both top and bottom of a scratch, we were able to more closely resemble a model of human epithelial tissue. This work is significant as it provides data on the benefits of using cellular collagen as a model for epithelial tissue and as a method for wound healing, as well as developing a novel method of testing layered collagen gels for cell growth. Future directions to continue these methods would be to vary cellular concentrations within this experiment and to conduct *in vivo* experiments that incorporate live animals models to determine if the results would continue to extend and apply to live tissue.

ACKNOWLEDGMENTS

We thank the WPI Department of Biology and Biotechnology, as well as the EmpOwER grant awarded by the Women's Impact Network, for funding these research initiatives. We acknowledge and thank the Cell Engineering Research Equipment Suite (CERES) for allowing us to utilize their imaging and plate reading equipment to examine our experiments at a higher level. We also would like to thank Dr. Catherine Whittington and Dr. Jeanine Coburn from the WPI Department of Biomedical Engineering for consultation regarding materials and model construction.

REFERENCES

1. Dick, M. K., Miao, J. H., & Limaïem, F. (2022). *Histology, Fibroblast*. StatsPearls. Retrieved January 22, 2023, from <https://www.ncbi.nlm.nih.gov/books/NBK541065/>
2. Xue, M., & Jackson, C. J. (2015). Extracellular Matrix Reorganization During Wound Healing and Its Impact on Abnormal Scarring. *Adv Wound Care*, 4(3), 119–136. <https://doi.org/10.1089/wound.2013.0485>
3. Iyer, K., Chen, Z., Ganapa, T., Wu, B. M., Tawil, B., & Linsley, C. S. (2018). Keratinocyte Migration in a Three-Dimensional In Vitro Wound Healing Model Co-Cultured with Fibroblasts. *Tissue Eng Regen Med*, 15(6), 721–733. <https://doi.org/10.1007/s13770-018-0145-7>
4. Comsa, Servan, Cimpean, Anca Maria, Raica, Marius. (2015). The Story of MCF-7 Breast Cancer Cell Line: 40 years of Experience in Research. *Anticancer Res*, 35, 3147–3154.
5. Foster, D. S., Jones, R. E., Ransom, R. C., Longaker, M. T., & Norton, J. A. (2018). The evolving relationship of wound healing and tumor stroma. *JCI insight*, 3(18), e99911. <https://doi.org/10.1172/jci.insight.99911>
6. Campbell, Jonathan J., Husmann, Anke, Hume, Robert D., Watson, Christine J., Cameron, Ruth E. (2017). Development of three-dimensional collagen scaffolds with controlled architecture for cell migration studies using breast cancer cell lines. *Biomaterials*. 114, 34–43. <https://doi.org/10.1016/j.biomaterials.2016.10.048>
7. Leibiger, C., Kosyakova, N., Mkrtchyan, H., Gleï, M., Trifonov, V., & Liehr, T. (2013). First molecular cytogenetic high resolution characterization of the NIH 3T3 cell line by murine multicolor banding. *J Histochem Cytochem*, 61(4), 306–312. <https://doi.org/10.1369/0022155413476868>
8. Vantangoli MM, Madnick SJ, Huse SM, Weston P, Boekelheide K (2015) MCF-7 Human Breast Cancer Cells Form Differentiated Microtissues in Scaffold-Free Hydrogels. *PLoS ONE*, 10(8): e0135426. <https://doi.org/10.1371/journal.pone.0135426>
9. Meyer M. (2019). Processing of collagen based biomaterials and the resulting materials properties. *Biomed Eng Online*, 18(1):24. <https://www.ncbi.nlm.nih.gov/pmc/articles/PMC6423854/>
10. Ramshaw, J. A. M.. (2016). Biomedical Applications of collagens. *J Biomed Mater Res*, 104(4), 665–675 <https://doi.org/10.1002/jbm.b.33541>
11. Ravi, Maddaly, Paramesh, V., Anuradha, Kaviya E., Solomon, F.D. Paul. (2014). 3D Cell Culture Systems: Advantages and

- Applications. *J Cell Physiol*, 230(1), 16–26. <https://doi.org/10.1002/jcp.24683>
12. Correa, S., Grosskopf, A. K., Lopez Hernandez, H., Chan, D., Yu, A. C., Stapleton, L. M., & Appel, E. A. (2021). Translational applications of Hydrogels. *Chem Rev*, 121(18), 11385–11457. <https://doi.org/10.1021/acs.chemrev.0c01177>
 13. Artym, V. V., & Matsumoto, K. (2010). Imaging cells in three-dimensional collagen matrix. *Curr Protoc Cell Biol*, 48(1). <https://doi.org/10.1002/0471143030.cb1018s48>
 14. Sotelo Leon, D., Williams, T., Wang, Z., Leyden, J., Franklin, A., Kaizawa, Y., Chang, J., & Fox, P. M. (2020). Analysis of cell-seeded, collagen-rich hydrogel for wound healing. *Plast Reconstr Surg Glob Open*, Publish Ahead of Print. <https://doi.org/10.1097/gox.0000000000003049>
 15. Liu, T., Qiu, C., Lu, H., Li, H., Zhu, S., & Ma, L. (2023). A novel recombinant human collagen hydrogel as minced split-thickness skin graft overlay to promote full-thickness skin defect reconstruction. *Burns*, 49(1), 169–181. <https://doi.org/10.1016/j.burns.2022.02.015>

ABOUT STUDENT AUTHORS

Claire Behning will graduate from Worcester Polytechnic Institute in the Spring of 2023 with a Bachelor of Science in Biology and Biotechnology and Bachelor of Science in Psychology. She enjoyed being able to expand her laboratory skills in cell culture while also being able to engage in the research process. As of 2023, she is applying to jobs as a high school biology teacher in public school districts, with the goal of applying her love of science and education to develop the next generation of scientists and lifelong learners.

Lia Kelly will graduate from Worcester Polytechnic Institute in the Spring of 2023 with a Bachelor of Science in Biology and Biotechnology. She enjoyed developing her cell culture skills and learning how to utilize biomaterials while experiencing the research process. As of 2023, she is applying to and gaining experience for veterinary school with the hopes of continuing her involvement in research to improve human and animal health and medicine.

Emma Smith will graduate from Worcester Polytechnic Institute in the Spring of 2023 with a Bachelor of Science in Biomedical Engineering. They enjoyed being able to apply knowledge from their materials courses in a setting focused on biologics. As of 2023, they will be starting their MS in Biomedical Engineering at Worcester Polytechnic Institute in the Fall Semester, with the goal of completing a research-based project to further their knowledge in functionalizing biomaterials, allowing them to utilize their knowledge to improve our understanding of disease and disease treatment.

Effect of Retinoic Acid on HaCaT and NIH-3T3 cells in an *in vitro* 3D Collagen Cell Culture Skin Model

Samantha Lopez^a, Olivia Atkins^b, Yizhe Ma^b & Louis Roberts^{*b}

^aDepartment of Biomedical Engineering, Worcester Polytechnic Institute, Worcester, MA

^bDepartment of Biology & Biotechnology, Worcester Polytechnic Institute, Worcester, MA

<https://doi.org/>

Students: splopez@wpi.edu, omatkins@wpi.edu

Mentor: lroberts@wpi.edu*

ABSTRACT

Human skin aging is characterized by epidermal and dermal thinning, loss of elasticity, and wrinkles. Keratinocytes, the most common type of skin cell and fibroblasts, present in the cellular stroma beneath the skin's surface, each play a role in aging. Using these cell lines in *in vitro* research can reveal a deeper understanding of the dermatological function and cellular changes in aged skin. 3D cell culture techniques provide an opportunity to use these cell lines in a model that can more accurately mimic human skin. Treatment of aging skin is of interest to both medical and consumer communities. Retinoic acid (RA) is a metabolite of vitamin A and retinol that assists in cell proliferation, differentiation, and immune functions. Over the counter (OTC) and prescription retinoids are common topical products used for anti-aging and acne treatments. This study seeks to determine the impact of topical retinoid creams on keratinocyte proliferation and morphology in 3D cell culture models of aged and unaged human skin. NIH-3T3 fibroblasts were embedded in a 3D collagen matrix of varying thickness, and HaCaT keratinocytes were seeded on top of the matrix at varying seeding densities to mimic aging skin. 0.1 μ M 0.025% tretinoin and 0.1 μ M 0.1% adapalene topical creams were prepared in culture medium and used to treat cells daily, on alternate days, or just once during a week-long period. AlamarBlue assays and microscopy showed that tretinoin treatment was cytotoxic at this concentration, with a single treatment reducing cell viability by ~43% compared to the untreated control. Adapalene treatment, while showing significantly better cell proliferation than tretinoin, did not exceed the proliferation of the untreated control. It is understood that retinol increases cell turnover by killing cells rapidly, so it is proposed that in our model, the rate of proliferation does not overcome the rate of cell death. Cell viability trends remain similar between young and old skin model treatments. Future studies should focus on creating a 3D model more accurately representing the aging *in vivo* skin environment where keratinocytes can be readily differentiated from epidermal stem cells.

KEYWORDS

HaCaTs; NIH-3T3; Retinoids; Retinoic Acid; Tretinoin; Adapalene; 3D Collagen Gel; Proliferation

INTRODUCTION

Epithelial cells are polygonal-shaped cells with regular, consistent dimensions. In two-dimensional culture, they grow in patches, form a monolayer, and tend not to migrate. Keratinocytes are the most common type of skin cell and function as the structural and barrier components of the epidermis, the outermost layer of the skin. Keratinocytes differentiate from epidermal stem cells and originate from the stratum basale, the deepest layer of the epidermis. As they age, grow, and differentiate into keratinocytes, they make their way to the epidermis, where they stay until they reach the final layer of the stratum corneum as corneocytes, where they die and are eventually shed by the body. Through differentiation, they produce keratin, the protein that strengthens the skin, hair, and nails.¹ Molecularly, these cells can be used to study the release of inflammatory and repair mediators. These cells can be used as a method to study the molecular mechanisms of epidermal regulation, homeostasis, pathophysiology, wound healing, and dermatologic diseases in *in vitro* models.³ HaCaT cells are a nontumorigenic monoclonal cell line of spontaneously immortalized keratinocytes derived from human skin. HaCaTs are epithelial in nature and fully differentiate under culture conditions.³ After stimulation from different calcium concentrations in the medium, HaCaT cells can form stratified layers, differentiate, and express differentiation markers. In addition, they can revert back and forth between differentiated and basal states.²

NIH-3T3 cells are fibroblasts derived from mouse embryos.⁴ Fibroblasts are a key component of the stroma and, more specifically, the extracellular matrix (ECM). In connective tissue stroma, fibroblasts make several important products, including collagen, glycans, and prostaglandins. Commonly characterized by their plasticity, fibroblasts can differentiate to have many distinct functions. In the skin, for example, superficial fibroblasts hold a role in follicle formation and wound healing, while deeper cells are involved in ECM reorganization.⁵ These cells are in constant communication with their surroundings and respond to both autocrine and paracrine signaling. Fibroblasts can interpret these signals and synthesize or remodel the ECM with regulation from various growth factors and pathways. Fibroblast structure is characterized by a star-like shape with several cytoplasmic projections.⁵ In culture, the live cells are adherent and migratory. This specific 3T3 cell line was established in the 1960s, and since then, it has advanced the scientific understanding of fibroblast biology and lineage.⁶ Fibroblasts are a valuable component of many cell culture models. In 3D models specifically, fibroblast-collagen matrices provide cell cultures that more closely represent the *in vivo* environment than traditional 2D cultures. Aspects such as cell-to-cell signaling and cell migration in a 3D fibroblast-collagen matrix more closely mimic those physiological conditions in the extracellular matrix.⁷

Collagen is the most abundant protein in animals and is the primary component of the extracellular matrix, with 90% of the 29 identified types of collagens being fibrillar. This protein has a highly complex and hierarchical conformation with a recognizable triple helix secondary structure of amino acids.⁸ Collagen I is the most common fibrillar collagen for cell culture, makes up the major structural component of many tissues, and can be found in skin, bone, tendons, and other connective tissues.⁹ Collagen is the most used naturally derived hydrogel and coating for tissue engineering.¹⁰ Collagen I is used in 2D cell culture as a coating or base and in 3D cell culture as a neutralized hydrogel to replicate the *in-vivo* environment of the body. 3D collagen hydrogels are used widely in cell culture, biotechnology, and medicine due to their polymer network and high-water content. As defined by Andersen et al., a three-dimensional cell culture involves cells embedded in a 3D matrix where cell and ECM signaling can be sent and received in all directions.¹¹ Cells can be embedded in the 3D collagen hydrogels or seeded on top of the hydrogel, serving as a 2D surface.⁶ For example, a commonly used concentration of collagen is 2 mg/mL, a low concentration, specifically used for embedding cells as the hydrogel is less stiff and gives cells higher motility and higher cell migration velocity.¹² Collagen is advantageous for cell culture because of its biometric cytocompatibility, ability to assist cell adhesion, promote cell growth and differentiation, and can provide a similar viscoelastic environment.⁷

Retinoic acid (RA) is a metabolite of vitamin A that assists in the vitamin's related biological activities. RA is also a natural metabolite of retinol that assists in cell proliferation, differentiation, and immune functions.¹³ Researchers have studied the growth and differentiation of human keratinocytes (HaCaTs) in response to RA *in vivo* and *in vitro* by evaluating differentiation through keratin synthesis and production; they found that RA was correlated to cell proliferation *in vitro*.¹⁴ In addition, they discovered that HaCaT cells expressed specific keratins dependent on RA and calcium levels in the media.¹⁴ When compared to untreated keratinocytes, HaCaTs treated with retinoic acid showed a mild increase in cell proliferation at certain doses.¹⁴

When skin ages, it undergoes structural changes such as thinning of its epidermal and dermal layers as well as weakening of the junction between these layers.¹⁵ In a study with women aged 18-69, it was found that there is progressive and significant thinning, 6.4% per decade, of the epidermis beginning at age 30.¹² Mimicking these changes *in vitro* can be achieved by obtaining skin explants from elderly donors or treating cells with age-inducing chemicals. Researchers have developed a 3D model of aging skin to replicate the phenotypic changes observed in aging human skin using a collagen-based matrix seeded with normal human fibroblasts and then seeded healthy human skin cells from young subjects on top.¹⁶ They found that in these prolonged cultures, epidermal thickness decreased over time.¹⁶ Further analysis also indicated similarities to naturally aging skin, such as the thickening of the lamina densa, a part of the skin between the epidermis and dermis.¹⁶ Another study used human skin models, to represent aging by manipulating the seeding concentration of senescent and normal fibroblasts in the matrix while monitoring keratinocyte proliferation and differentiation.¹⁷ In their aged models they used specific keratinocyte seeding densities and fibroblast densities to more accurately represent *in vivo* skin.

Human skin needs to be examined experimentally to understand how different types of retinoic acid help its rejuvenation. Investigating this topic using a 3D cell culture more accurately models the *in vivo* skin environment. Topical Vitamin A treatments, such as retinol, retinoid, tretinoin, and adapalene, are used to treat acne by unclogging pores and providing anti-aging effects by increasing collagen production and cell proliferation while exfoliating and removing dead skin cells.¹⁸ Tretinoin is a prescription retinoid whereas adapalene is sold over the counter. Since tretinoin is more concentrated it is used for different purposes like treatment of cystic acne and to assist in the healing of acne scars. Adapalene is used for skin rejuvenation, prevention and removal of wrinkles and fine lines.¹⁹ The concentration of each drug, adapalene and tretinoin, is determined by several factors such as potency, effectiveness, and safety profile. Tretinoin and adapalene's concentration are also related to their mechanisms of action. Tretinoin is a highly potent retinoid that binds to nuclear retinoic acid receptors and regulates gene expression and leads to changes in cellular differentiation, proliferation, and apoptosis.²⁰ The effectiveness of tretinoin is dose-dependent and higher concentrations of the drug can lead to greater therapeutic effects. However, tretinoin can also be highly irritating and cause side

effects such as redness, peeling, and dryness of the skin.²⁰ On the other hand, adapalene is a less potent retinoid that acts by binding to specific retinoic acid receptors in the skin and regulating sebocyte differentiation and proliferation.¹⁹ Adapalene is generally less irritating and handled better by users than tretinoin.¹⁹ Therefore, lower concentrations of adapalene can still achieve similar therapeutic effects while minimizing the harmful side effects.

Previous studies have investigated the molecular basis of retinoids *in vivo* for cosmetic purposes.²¹ Tretinoin and other FDA-approved retinoids are more thoroughly studied, with the mechanisms of action, genomic and nongenomic, well defined.²² They also have clinical evidence to support their efficacy.²² More must be understood about the comparative efficacy of over-the-counter (OTC) retinoids, like adapalene, which are readily available and popular for cosmetic use. As previously mentioned, retinoids show anti-aging effects, however, there need to be more studies surrounding these effects *in vitro*, specifically in 3D skin models. Our study begins to address this gap by creating a 3D model of human aging skin to investigate the proliferation rate of human epidermal tissue cells after treatment with prescription tretinoin and OTC adapalene creams. In this study, we show how HaCaTs (human epithelial cells), proliferate and behave in the presence of topical vitamin A treatments in *in vitro* 3D cell culture.

METHODS AND PROCEDURES

Cells and Culture Conditions

NIH-3T3 (ATCC, Catalog No. CRL-1658) and HaCaT (AddexBio, Catalog No. T0020001) cells were obtained. These cell lines were cultured at 37°C and 5% CO₂ in complete medium that contains Dulbecco's Modified Eagle Medium (DMEM) (Corning, Catalog No. 10-013-CV) with 1x penicillin-streptomycin and 10% fetal bovine serum (FBS). Dulbecco's Modified Eagle Medium (DMEM) has a calcium concentration of 1.8 mM.²³ Cells were routinely passaged with 5% trypsin every two days prior to seeding in the 3D model.

3D Gel Model

To embed NIH-3T3 fibroblasts in a 3D collagen gel with a layer of HaCaTs on top of the gel a multi-step procedure was performed; a schematic can be found in **Figure 1** below. To mimic aged skin, the layer of fibroblasts embedded in collagen was 1 mm thick, as this was the smallest thickness that would cover a 24-well plate and be correlated to skin age. Since there is a 6.4% decrease in epidermis thickness every 10 years, younger skin was chosen to be 2 mm thick.²⁴ To seed 2 mm thick collagen gel, 0.2 mL of the fibroblast embedded collagen gel solution was needed to create this thickness, and 1 mm thick collagen gel required 0.1 mL of the fibroblast embedded collagen gel solution. The fibroblast-embedded collagen gel solution was 20% cell suspension and 80% 3D collagen. The gels were seeded with a fibroblast density of 0.55 x 10⁶ cells/mL. So, a T75 flask of confluent NIH3T3 cells, at a concentration of approximately 0.7x10⁶ cells/mL, was trypsinized with 1 mL of 5% trypsin and centrifuged for 5 minutes in a clinical centrifuge at 3000 rpm. The cell pellet was resuspended into 1 mL into complete media, counted, and resuspended again in 0.9 mL of complete media to create the 20% of 4.5 mL needed for the cell suspension. To make the fibroblast-embedded collagen gel solution, 3.6 mL of 3 mg/mL 3D collagen gel (Sigma Aldrich Catalog No. C4243) was mixed with 0.9 mL of the cell suspension was added.²⁵ To add the control gels to the plate, 0.2 mL, or 0.1 mL of 3D collagen gel without fibroblast cells was added to non-fibroblast control wells. To add the remaining control and treatment gels to the plate, 0.2 mL or 0.1 mL of the fibroblast-embedded collagen gel solution was added to the wells. The plate was incubated for 1 hour for the gel to harden. A schematic of the plate can be found in **Table 1** below.

To mimic skin, a layer of HaCaTs were seeded on top of the fibroblast-embedded collagen gel with a density of 3500 cells/cm² to mimic aged skin and 7000 cells/cm² to mimic younger skin.¹⁷ The surface area of a 24-well plate is 1.9 cm² with 0.75 mL of complete media. The cell density needed for the aged skin model was 6650 cells per well with 0.75 mL of media, and 10 mL of this cell suspension was needed to add to the top of 13 wells; the math can be seen in **Equation 1** below. Therefore, the cell density for the younger skin model was 13,300 cells per well in 0.75 mL media. To seed this layer of HaCaTs on top of the fibroblast collagen gel, a confluent T75 flask of HaCaT cells was trypsinized with 1 mL of trypsin, resuspended in 1 mL of complete media, counted, and resuspended in the correct amount of media to make the needed cell densities for each treatment group. After the fibroblast-embedded collagen gel solidified, 0.75 mL of the correct cell suspensions were added to the respective wells according to the schematic in **Table 1**. Finally, the plate was incubated at 37°C with 5% CO₂ in a humid environment.

$$\begin{aligned}
 & \begin{array}{l} 3500 \text{ cells/cm}^2 \text{ with } 0.75 \text{ mL media} \\ 24 \text{ well plate} = 1.9 \text{ cm}^2 \text{ surface area} \end{array} \\
 & \frac{3500 \text{ cells}}{\text{cm}^2} \times 1.92 \text{ cm}^2 = 6.650 \text{ cells per well with } 0.75 \text{ mL media} \\
 & \frac{6.650 \text{ cells}}{0.75 \text{ mL media}} \times \frac{\text{cells per } 1 \text{ mL}}{1 \text{ mL media}} = 8867 \text{ cells/mL}
 \end{aligned}$$

Equation 1.

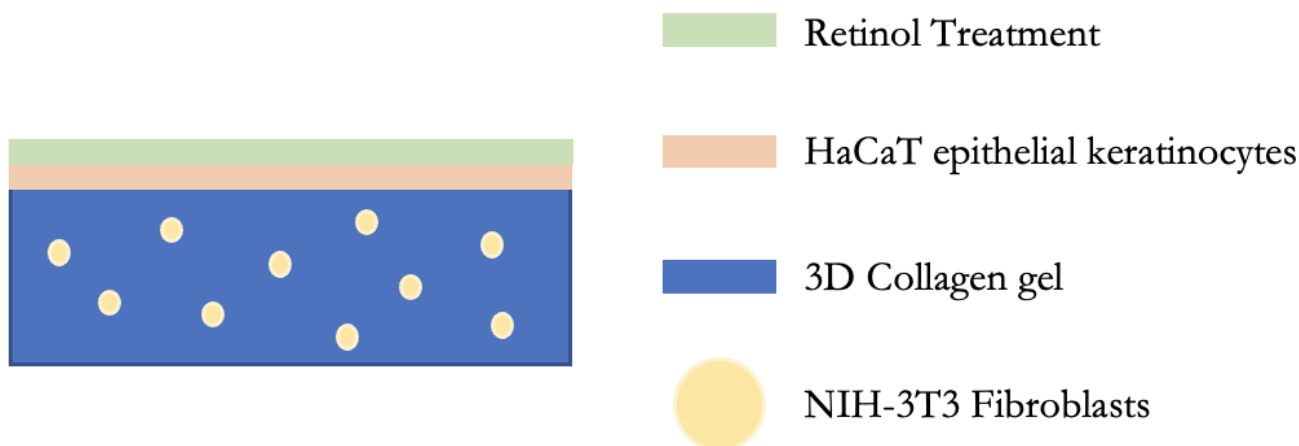


Figure 1. This Figure shows the collagen-cell matrix design. NIH-3T3 fibroblasts are embedded in a 3D collagen gel with a thickness of either 2 mm (0.2 mL) or 1 mm (0.1 mL) and HaCaT epithelial cells are seeded on top of the gel.

Table 1. Retinoid Treatment Plate Set up
This Table shows the original treatment plate set up.

	1	2	3	4	5	6
A	2 mm CG + H + M	2 mm CG(F) + H + M	1 mm CG(F) + H + M	2 mm CG + M	1 mm CG + M	M only
B	2 mm CG(F) + H + T daily treatment	2 mm CG(F) + H + T alternating treatment	2 mm CG(F) + H + T single treatment	1 mm CG(F) + H + T daily treatment	1 mm CG(F) + H + T alternating treatment	1 mm CG(F) + H + T single treatment
C	2 mm CG(F) + H + A daily treatment			1 mm CG(F) + H + A daily treatment	1 mm CG(F) + H + A alternating treatment	1 mm CG(F) + H + A single treatment
D		2 mm CG(F) + H + A alternating treatment	2 mm CG(F) + H + A single treatment			

M = Complete DMEM
CG = Collagen Gel
CG(F) = Collagen Gel with NIH-3T3
fibroblast cells embedded
H = HaCaT cells
A = Adapalene treatment
T = Tretinoin treatment

Retinoid-Media Preparation

Perrigo Tretinoin Cream, USP 0.025% and Differin Gel Adapalene 0.1% were used. Due to retinoid sensitivity to both light and heat, these sterilization methods were not possible without altering the potency of the creams. Tretinoin and adapalene creams were streaked on LB agar plates and incubated for two days at 37°C to assess sterility. No growth was visible on any of the plates. 1 μM retinoid-media solutions were prepared by first massing specified amounts of 0.025% tretinoin cream and 0.1% adapalene cream according to the calculations in **Equations 2, 3, and 4** below for a final media volume of 20 mL. **Equation 2** shows the calculation of the desired 1 μM concentration in moles. **Equation 3** calculates the mass required for 1 μM 0.025% Tretinoin in 20 mL media. **Equation 4** calculates the mass required for 1 μM 0.1% Adapalene in 20 mL media. After measuring the appropriate retinoid weight, the cream was resuspended in 20 mL complete DMEM, 10% FBS as used in culturing described above. The solutions were filter sterilized using a 50 mL Steriflip filter unit (Millipore Sigma, Catalog No. C3238). Once prepared, the retinoid-media solutions were stored at 4°C and equilibrated to room temperature prior to cell treatment.

$$1 \mu\text{M} \times 20 \text{ mL} = 20 \times 10^{-9} \text{ mol}$$

Equation 2.

$$1 \mu\text{M} \text{ 0.025\% Tretinoin} \\ (300.44\text{g/mol} / (20 \times 10^{-9} \text{mol})) / 0.00025 = 2.4 \times 10^{-2} \text{g in 20 mL media}$$

Equation 3.

$$1 \mu\text{M } 0.1\% \text{ Adapalene} \\ (412.52\text{g/mol}(20 \times 10^{-9}\text{mol}))/0.001 = 8.25 \times 10^{-3}\text{g in } 20 \text{ mL media}$$

Equation 4.

Retinoid Treatments

After the plate was prepared and incubated for the cells to reach the correct confluence, the wells were treated with the 1 μM adapalene and tretinoin media prepared above. DMEM was removed from the wells and replaced with the respective treatment media. In the original treatment plate, control models were treated with complete DMEM every other day. For testing the impact of tretinoin on cells, young and old skin models were treated with either consecutive 5 days, 3 alternating days, or a single first day treatment of 0.1 μM 0.025% tretinoin. Young and old skin models were treated with 0.1 μM 0.1% adapalene in the same manner. Each well was observed daily, with a final imaging and proliferation assay readout on the 9th day after treatment.

Microscopy

During treatment, each well was imaged every day the media was changed on days 1, 2, 3, 4, 7, and 9 with the Olympus IMT-2 inverted microscope at 100X magnification, under 10X objective with a 10X eyepiece. After treatment concluded, HaCaT cells were imaged using a Cytation Gen 5 microscope under brightfield at 10X objective magnification.

AlamarBlue Resazurin Proliferation Assay

To assess cellular activity dependent on retinoid treatment conditions, a cell proliferation assay was completed with alamarBlue Cell Viability Reagent (Invitrogen, Catalog No. DAL1025). For T=0 data, wells with 2 mm collagen-cell model, 1 mm collagen-cell model, and media only were treated 72 hours after seeding with alamarBlue reagent at 10% of the gel and media volume in the well. For example, the wells with 0.2 mL collagen gel and 0.75 mL of media had 95 μL of alamarBlue added. The plate was incubated at 37°C and 5% CO_2 for 40 hours. The fluorescence of each well was measured using an excitation wavelength of 540 nm and an emission wavelength of 590 nm. This fluorescence intensity was measured in relative fluorescence units (RFU). Each measurement had an associated blank measurement without cells which was used to determine the baseline fluorescence of the media and collagen gel. The blank measurement value was subtracted from the cell dilution measurements to obtain fluorescence values from the cellular activity.²⁶ This procedure was repeated 72 hours after completion of the treatment plate.

RESULTS

Proliferation Imaging Results

The wells were imaged every time the media were changed to observe HaCaT confluency and cell morphology. Models without cells were not imaged. Through visual observations, the HaCaTs proliferated normally in control models, treated with complete media. Controls included HaCaTs seeded on top of 2 mm thick 3D collagen gel with no fibroblasts embedded inside the gel and HaCaTs seeded on top of 2 mm and 1 mm thick 3D collagen gel with fibroblasts embedded inside the gel. Throughout the experiment, these models maintained a healthy cell morphology, with the cells being very confluent by the end of the experiment on day 9, as shown in **Figure 2**. As the experiment goes on the cells become more confluent as expected with very few floaters every day. The few floaters were removed with media changes every other day. The first day after seeding the HaCaTs seeded on top of the gel with fibroblasts embedded were more confluent than the HaCaTs seeded without fibroblasts embedded.

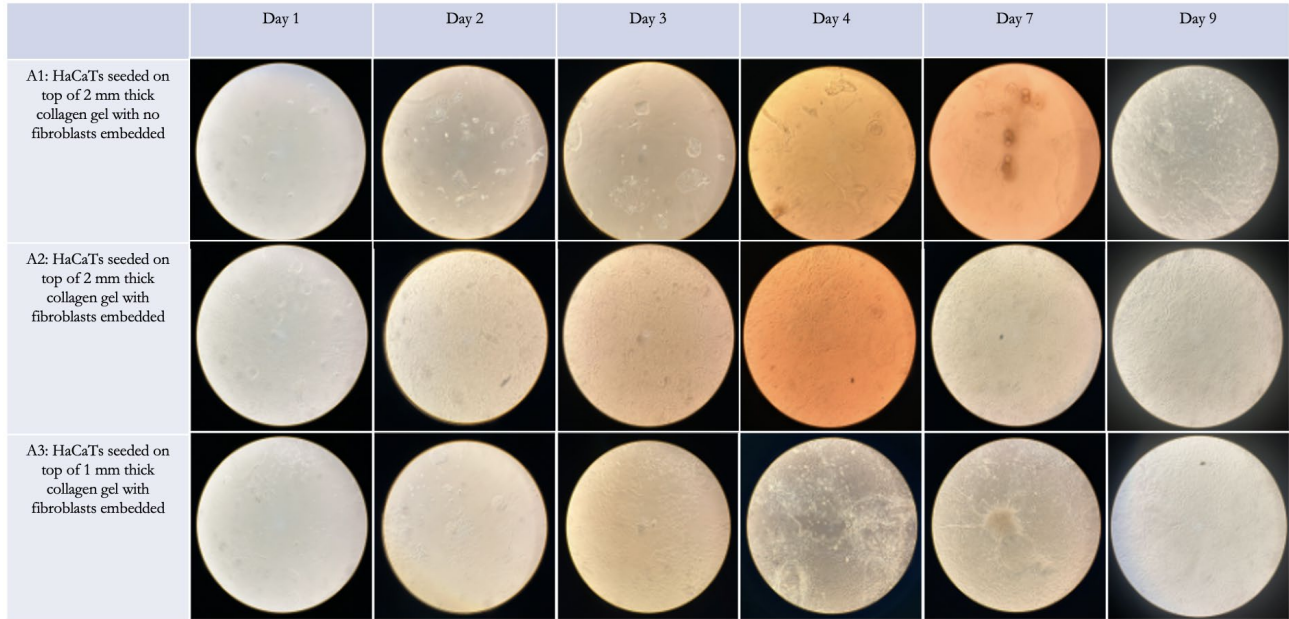


Figure 2. This Figure shows the daily imaging of the HaCaT control wells A1, A2, and A3. Well A1 has HaCaTs seeded on top of 2 mm thick collagen gel with no fibroblasts embedded and wells A2 and A3 have HaCaTs seeded on top of 2 mm and 1 mm thick collagen gel with fibroblasts embedded, respectively. The confluency of each well increases daily as expected and by day 9 all wells are very confluent with healthy cells with a healthy morphology.

The tretinoin treatments produced cells that balled up, detached from the gels, and floated. Images correlating to tretinoin treatment wells can be found in **Figures 3** and **Figure 4** for the younger and aged treatments respectively. Throughout the course of the tretinoin treatment, the wells with less treatment frequency had healthier-looking and more confluent cells. The wells treated with tretinoin every day were losing cells when the media was replaced; the remaining cells were circular and not attached to the gel and by day 9 the well had lost most of its cells and was not very confluent; this may be due to tretinoin's mechanisms of action.

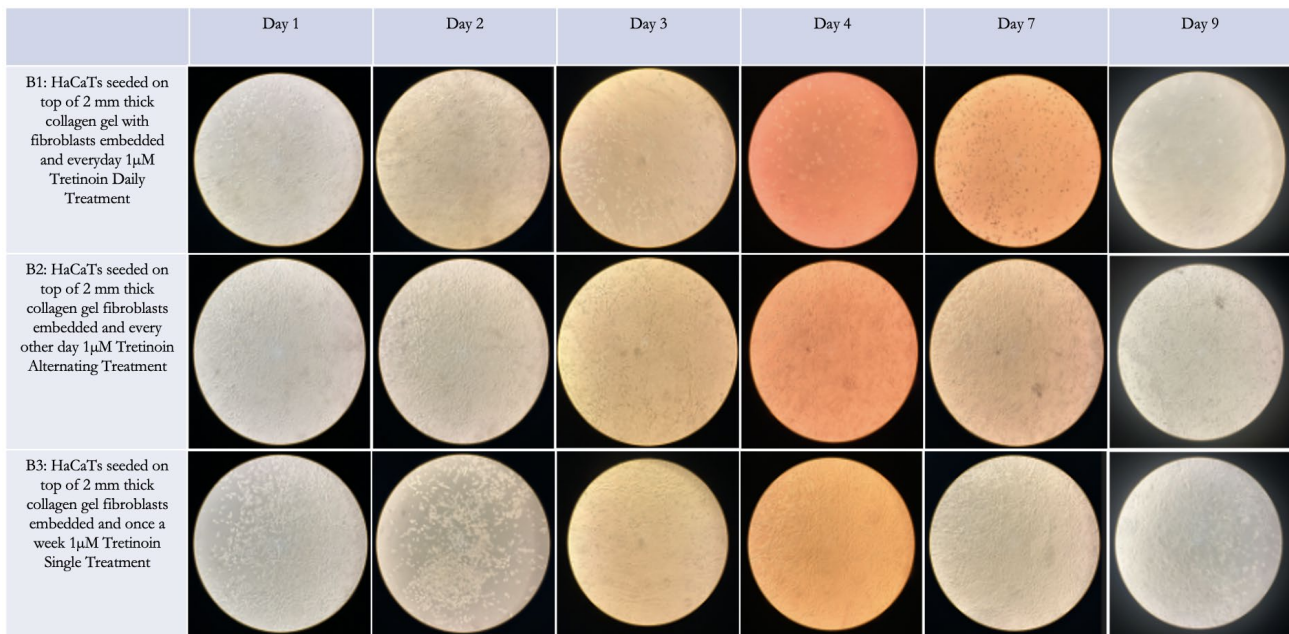


Figure 3. This Figure shows the daily imaging of HaCaT cells seeded on top of 2 mm thick collagen gel with fibroblasts embedded inside the gel. Well B1 was treated everyday with 1 μ M tretinoin media, B2 was treated every other day, and B1 was treated once a week with complete media changes every other day. The confluency of B1 decreased as the experiment went on, in B2 and B3 the confluency increased daily. The cells produced from this section of the experiment looked healthy by day 9, with an exception in B2.

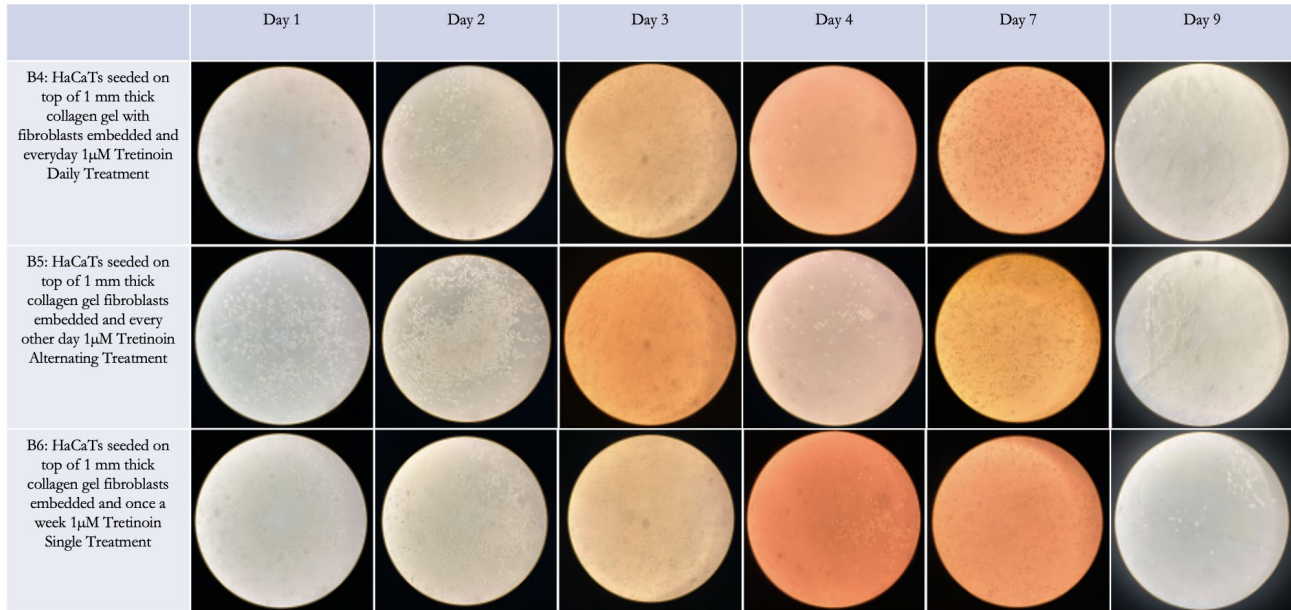


Figure 4. This Figure shows the daily imaging of HaCaT cells seeded on top of 1 mm thick collagen gel with fibroblasts embedded inside the gel. Well B4 was treated everyday with 1 μ M tretinoin media, B5 was treated every other day, and B6 was treated once a week with complete media changes every other day. The confluency of B4 and B6 decreased as the experiment went on, in B5 the confluency increased daily. By the end of the experiment the cells produced from this section of the experiment looked unhealthy as they were bubbled with a strange morphology and not attached to the gel well.

The adapalene treatments produced much healthier cells with better morphology and higher proliferation rates. The images that correlate to the adapalene treatment wells can be found in **Figure 5** and **Figure 6** for the younger and aged treatments respectively. Again, the wells treated less frequently with adapalene were more confluent and healthier. The confluency of younger treatments is significantly more confluent than the older treatments, but the seeding density of the older treatments was lower than the younger treatments. This may be because there was more room for the cells to proliferate and grow since the seeding density was lower.

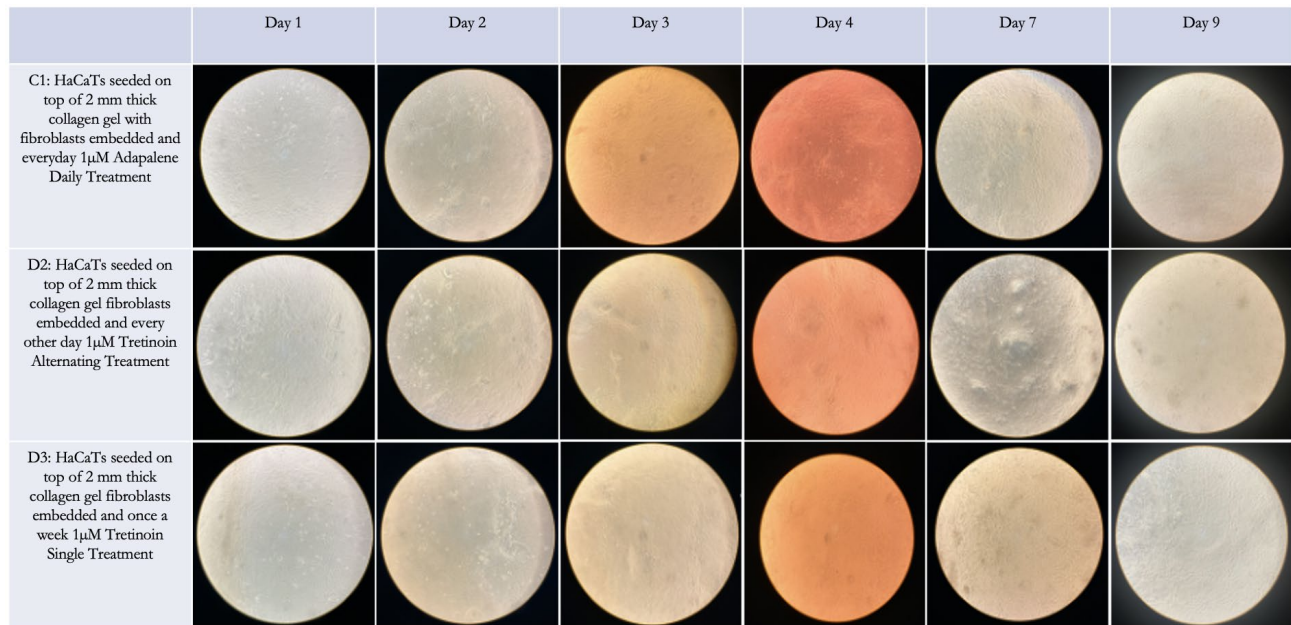


Figure 5. This Figure shows the daily imaging of HaCaTs seeded on top of 2 mm thick collagen gel with fibroblasts embedded inside. Well C1 was treated every day 1 μ M adapalene, D2 was treated every other day, and D3 was treated once a week with every other day complete media replacements. On the first day, all wells had healthy and confluent cells. Throughout treatment the well was confluent with healthy HaCaT cells with very few floaters. By the end of the experiment, all wells were healthy and very confluent.

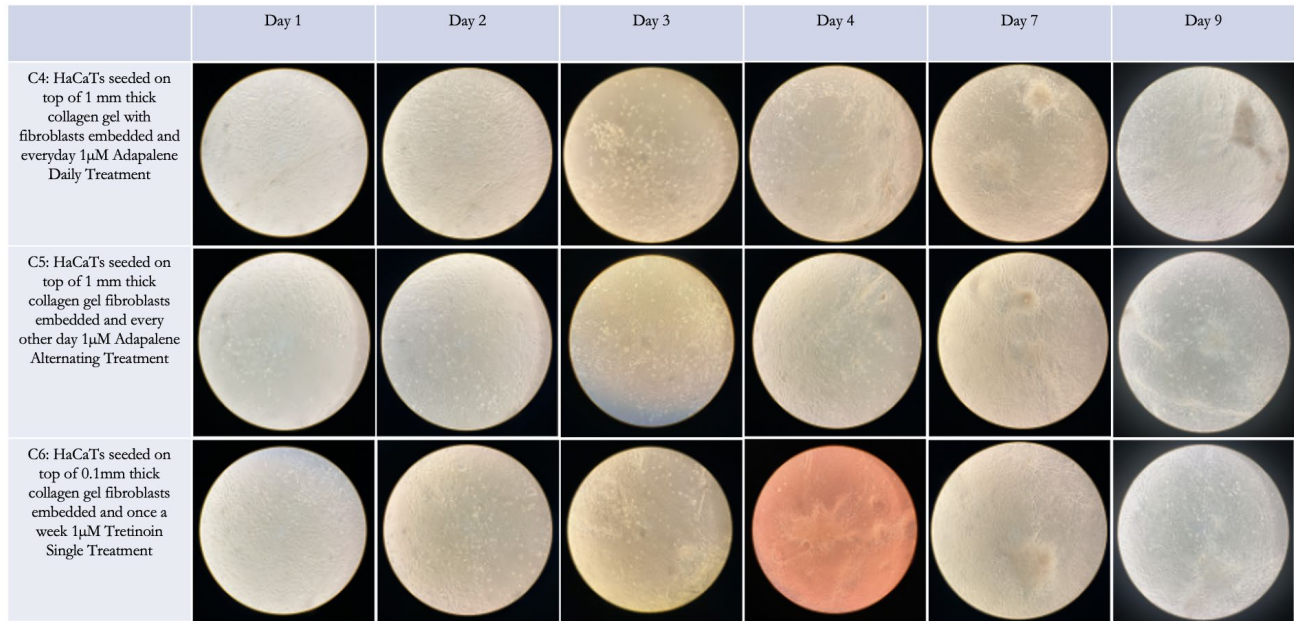


Figure 6. This Figure shows the daily imaging of HaCaTs seeded on top of 2 mm thick collagen gel with fibroblasts embedded inside. Well C4 was treated every day 1 μ M adapalene, C5 was treated every other day, and C6 was treated once a week with every other day complete media replacements. On the first day there were no floaters, but the wells were less confluent than their younger counterparts in wells C1 and D2-D3, because they were seeded at a lower density. Throughout treatment the well was confluent with healthy HaCaT cells and few floaters. By the end of the experiment, all wells were healthy and confluent.

On the final day, the wells were imaged to assess the health of the cells, and the images can be found in **Figure 7**. Overall, the cells from the control model of HaCaTs with no retinoid treatments, were healthy and confluent. Control models with fibroblasts embedded were more confluent than those without, indicating a possible relationship between fibroblast and HaCaT proliferation. The models treated with tretinoin had relatively healthy cells but were less confluent than those treated with adapalene. Tretinoin is more concentrated than adapalene, so the effects are stronger. Overall, the adapalene treatment, no matter the treatment frequency or younger or aged model, had healthy and very confluent cells. For the younger adapalene treatments, as the treatment frequency decreased, the cell confluency increased. However, for the aged adapalene treatments, as the treatment frequency decreased, the cell confluency decreased.

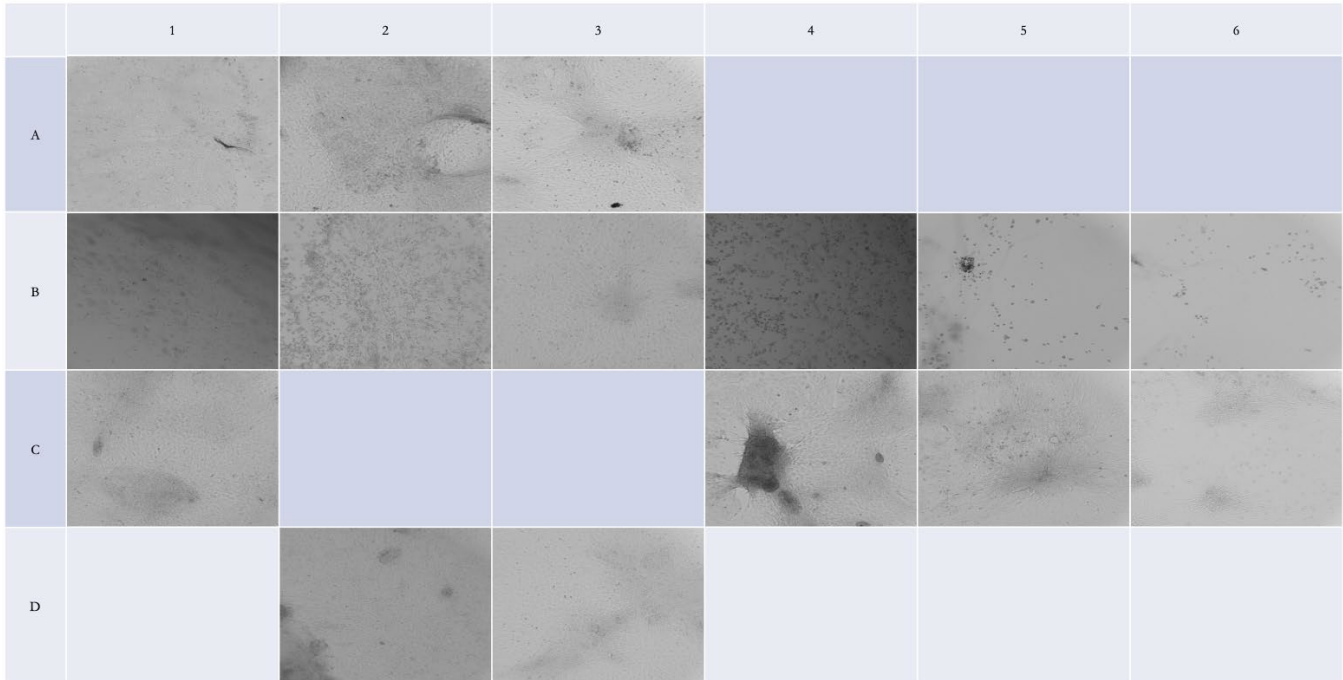


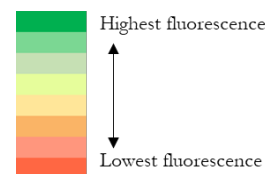
Figure 7. Final day images of the whole plate with wells that had HaCaT's seeded on top of the 3D collagen gel. In well A1, the cells look healthy and confluent. The cells in wells A2 and A3 look healthy but more confluent than in A1. Though the cell density in A3 was lower than in A2, they are similarly confluent when visually assessed. The everyday tretinoin treatment for the younger model, in well B1, had healthy cells, and they were less confluent than the other young tretinoin treatments. For the aged everyday tretinoin treatment model, in well B4, there were more cells than in the other aged tretinoin treatments, but they had a strange morphology. In the every-other-day tretinoin treatment for the younger model, in well B2, the cells appeared more confluent than in B1 but appeared unhealthy with strange morphology. For the aged every other day tretinoin treatment model, in well B5, there were fewer cells than in B4, and the few cells that were found did not look healthy and had strange morphology. In the once-a-week tretinoin treatment for the younger model, in well B3, the cells were much more confluent than B2 and more confluent than B1 and were healthy. For the aged once-a-week tretinoin treatment model, in well B6, there were fewer cells than in B4 and B5, and the few cells that were found did not look healthy and had strange morphology.

Effects on Cell Proliferation

The alamarBlue resazurin assay provided a quantitative reflection of cell metabolism for each condition, which correlates to proliferation of live cells. **Table 2** shows the contents of the alamarBlue plate along with the associated reference-subtracted fluorescence readouts. Numbers under each description represent these reference-subtracted fluorescence values obtained for the well. 2 mm gel models used the 2 mm controls for reference subtraction, while 1 mm gel wells used the controls with 1 mm gels. Media only wells were self-subtracted. Wells are color coded according to fluorescence values, with the brightest red color representing the lowest reference-subtracted fluorescence, associated with the least number of live cells, while the brightest green color representing the highest reference-subtracted fluorescence, associated with the greatest number of live cells. A detailed key for the color code is included to the right of the table. Control wells present in both the T=0 and treatment plate included gels with and without embedded fibroblasts. The presence of fibroblasts in the collagen gel matrix correlated to greater proliferation and subsequently greater HaCaT cell proliferation. A fluorescence of 649,675 RFU was recorded with embedded fibroblasts in the 2 mm gel, and only 176,057 RFU for the same gel thickness without fibroblasts (A1).

Table 2. AlamarBlue Well Contents and Associated Reference-Subtracted Fluorescence values

	1	2	3	4	5	6
A	2mm CG + H + M 176057	2mm CG(F) + H + M 649675	1mm CG(F) + H + M 477158	2mm CG + M 0	1mm CG + M 0	M only 0
B	x	x	x	x	x	x
C	2mm CG + H + M 1132518	2mm CG(F) + H + M 2083877	1mm CG(F) + H + M 2085823	2mm CG + M 0	1mm CG + M 0	M only 0
D	2mm CG(F) + H + T daily 197042	2mm CG(F) + H + T alternating 740699	2mm CG(F) + H + T single 1180820	1mm CG(F) + H + T daily 98911	1mm CG(F) + H + T alternate 631870	1mm CG(F) + H + T single 1186139
E	2mm CG(F) + H + A daily 1983226	2mm CG(F) + H + A alternating 8319	2mm CG(F) + H + A single 1780495	1mm CG(F) + H + A daily 864618	1mm CG(F) + H + A alternating 2053607	1mm CG(F) + H + A single 1910548



M = Complete DMEM
 CG = Collagen Gel
 CG(F) = Collagen Gel with NIH-3T3 fibroblast cells embedded
 H = HaCaT cells
 A = Adapalene treatment
 T = Tretinoin treatment

Table 2 shows the well contents for the alamarBlue assay from the T=0 control plate, in row A, and the original treatment plate, in rows C through E. Numbers under each description represent the reference-subtracted fluorescence values obtained for the well. 2 mm gel wells used the controls in wells A4 and C4 for reference subtraction, while 1 mm gel wells used the controls in wells A5 and C5. Wells are color coded according to fluorescence values, with the brightest red color representing the lowest reference-subtracted fluorescence, associated with the least number of live cells, while the brightest green color representing the highest reference-subtracted fluorescence, associated with the greatest number of live cells. A detailed key for the color code and abbreviations is included to the right of the Table.

To better visualize and compare fluorescence values for the different control and treatment conditions, data was graphed in **Figures 8 and 9**. The graphed values are referenced subtracted in the same manner as previously described. **Figure 8** depicts the primary T=0 controls, 2 mm (young) and 1 mm (old) collagen gels embedded with fibroblasts, seeded with HaCaTs on top, and DMEM media treatment. This assay was completed prior to treatment and after 3 days of seeding. The young skin model was seeded with higher HaCaT density and shows a significantly higher fluorescence, correlating with higher cell viability. Conversely the old skin model shows lower fluorescence, and less cells. These controls act as a basis for the following young and old skin models that were treated. **Figure 9** includes data for the treated models with HaCaT proliferation based on an alamarBlue assay fluorescence readout plotted against frequency of tretinoin or adapalene treatment for young (2 mm) skin in the left panel and old (1 mm) skin in the right panel. 5 days indicates 5 consecutive days of treatment, 3 days indicates alternate days of treatment, and 1 day indicates a single first day of treatment during the course of 5 days. The well for alternate day adapalene treatment for the young skin dried causing cell death and an inaccurate readout, so this data point is not representative of the true effects of the treatment, so it was removed from **Figure 9a**; however, these data correlate with the microscopy results which show very few viable cells after the well dried. Ignoring this data point, the adapalene appears to increase proliferation with increased treatment frequency for young skin, but it does not meet or surpass the fluorescence measured for the untreated control. Adapalene with the old skin model shows alternate day treatment to have the greatest fluorescence with a value nearly equivalent to the untreated control (2,053,607 RFU and 2,085,823 RFU, respectively). Tretinoin treatment in both young and old skin shows an interesting linear trend. When a simple linear regression is made for these points, there is a nearly perfect fit in both the young and old skin, with R² values of 0.9963 and 0.9999, respectively. Tretinoin performed better when only treated once a week, but in both models this single treatment reduces cell viability by about 43% compared to the untreated control. More significant toxicity was observed if treated more than once per week.

Fluorescence Detected at T=0 for Young and Old Skin Models

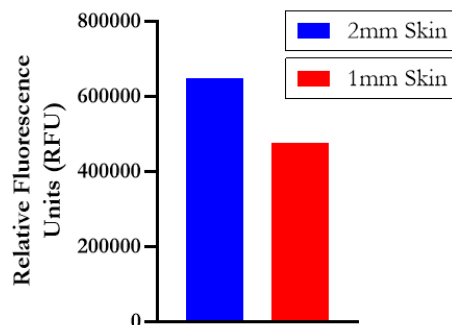


Figure 8. This Figure shows the fluorescence detected using an alamarBlue assay for the young (2 mm) and old (1 mm) skin models at T=0, prior to treatment and 3 days after seeding. Cell metabolism was more active at the higher seeding density, as expected.

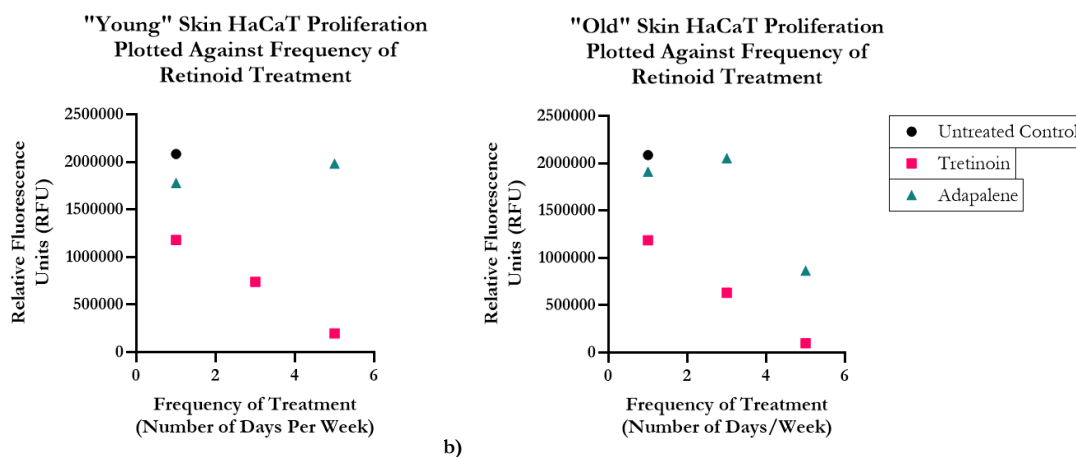


Figure 9. These Figures show HaCaT proliferation, based on an alamarBlue assay fluorescence readout, plotted against frequency of tretinoin or adapalene treatment for **a)** young (2 mm) skin and **b)** old (1 mm) skin in the right panel. Alternate day adapalene treatment (3 days/week) for the young skin data point was not obtained due to the well drying out.

DISCUSSION

As human skin ages, it has been shown the epidermal and dermal layers thin due to the weakening of the junction between those layers.¹⁵ It is also known that different types of retinoic acid help human skin rejuvenation and providing anti-aging effects by increasing collagen production and cell proliferation while exfoliating and removing dead skin cells. It is necessary to understand the proliferation rate provided by differing treatment frequencies with retinol products in 3D cell culture that mimics human skin.¹⁸ The data gathered for this paper shows the proliferation rates of different treatment frequencies of retinol products through an alamarBlue proliferation assay and visual observations during and after treatment on HaCaT cells.

The results show the frequency of treatment, and the type of treatment affects the proliferation rate of the HaCaT cells. Retinoids like adapalene and tretinoin are known to increase cell turnover by promoting differentiation of skin cells, which can lead to shedding of dead skin cells and the growth of new ones.¹⁸ Adapalene and tretinoin are known to cause differentiation in HaCaT cells, differentiation of cells can lead to a slower rate of cell division and an overall decrease in cell proliferation; however, the treatment may also have induced apoptosis. When looking at the data of the untreated control wells, they have a much higher proliferation rate than those of the adapalene or tretinoin treated wells. Throughout the daily images, it can also be seen how the tretinoin treatment causes the cells to change their morphology. This may be because tretinoin is inherently more concentrated and thus more toxic to the cells than adapalene.

In addition, the side effects and safety profiles of each treatment should be considered when assessing the results. Tretinoin is known to cause skin irritation and sensitivity, while adapalene is generally better tolerated.¹⁸ The effects of retinoids on cell turnover and proliferation depend on the concentration of the treatment and duration of treatment. When the cells were treated with adapalene they had a healthier, more confluent appearance than when treated with tretinoin. Again, since tretinoin is more

concentrated, it probably leads to higher rates of cell turnover, resulting in more dead cells that were lifted from the gel and were removed, without new cells being turned over in the skin cycle. The higher number of dead cells through more concentrated and more frequent treatments can be seen quantitatively in **Figure 9a** and **Figure 9b**. In this figure, tretinoin-treated models are significantly less confluent than the adapalene and control counterparts. When treated once a week and supplemented with a complete medium, more nutrients and growth factors were introduced to the cells to help the surviving cells heal and proliferate. This led to an increase in cell number over time in the once-a-week treatment.

Further studies need to be done to obtain proliferation data that incorporates HaCaT production instead of purely HaCaT growth from a set cell density. Recommendations for future experiments would be to perform a viability assay to determine the percentage of live and dead cells as well as immunostaining to assess the effects on cell differentiation between the two treatments. For future experiments, observing the healthy proliferation rate of HaCaTs and supplementing additional HaCaTs into the treatment wells to mimic cell turnover during treatment would help make the experiment and skin model more accurate. Another aspect that can be considered is the elasticity of the model since loss in elasticity is a sign of aging skin.

CONCLUSIONS

When looked at in tandem, the data from the alamarBlue proliferation assay and the daily visual observations indicate the proliferation of HaCaTs under retinoic acid conditions is not improved. However, this is due to the set-up of the model. It has been shown that retinoic acid does increase the proliferation of cells in *in vivo* conditions because the body is producing more HaCaT cells underneath the layer that retinoic acid removes. When used on human skin, retinol products exfoliate and remove the top layer of skin to bring the bottom layers of skin to the surface faster to increase cell turnover. Since there is nothing in the model that allows new HaCaTs to be brought up from below the surface, proliferation could not be measured precisely. From this experiment design, the optimal frequency and duration of retinoid treatment cannot be concluded as there were errors in the treatment that were not consistent between each treatment well. Regardless, this study addressed the gap by creating a 3D model of human aging skin while investigating the proliferation rate of human epidermal tissue cells and the retinoic acid effects.

ACKNOWLEDGMENTS

Samantha Lopez and Olivia Atkins thank the WPI Biology and Biotechnology department, the EmpOwER grant awarded by the Women's Impact Network for funding these research initiatives, Dr. Catherine Whittington, and Dr. Jeannine Coburn (WPI Department of Biomedical Engineering) for consultation regarding materials and model construction, as well as the Cell Engineering Equipment Suite (CERES) at WPI for allowing access to fluorescence and imaging instrumentation.

REFERENCES

1. ATCC. (2022). NIH/3T3. Retrieved January 20, 2023 from <https://www.atcc.org/products/crl-1658>
2. Colombo, I., Sangiovanni, E., Maggio, R., Mattozzi, C., Zava, S., Corbett, Y., Fumagalli, M., Carlino, C., Corsetto, P. A., Scaccabarozzi, D., Calvieri, S., Gismondi, A., Taramelli, D., & Dell'Agli, M. (2017). HaCaT Cells as a Reliable In Vitro Differentiation Model to Dissect the Inflammatory/Repair Response of Human Keratinocytes. *Mediators of inflammation*, 2017, 7435621. <https://doi.org/10.1155/2017/7435621>
3. Wilson V. G. (2014). Growth and differentiation of HaCaT keratinocytes. *Methods in molecular biology (Clifton, N.J.)*, 1195, 33–41. https://doi.org/10.1007/7651_2013_42
4. ATCC. (2022). Keratinocytes. Retrieved January 22, 2023, from <https://www.atcc.org/cell-products/primary-cells/keratinocytes#t=productTab&numberOfResults=24>
5. Dick, M. K., Miao, J. H., & Limaem, F. (2022). Histology, Fibroblast. In *StatPearls*. StatPearls Publishing. <http://www.ncbi.nlm.nih.gov/books/NBK541065/>
6. Plikus, M. V., Wang, X., Sinha, S., Forte, E., Thompson, S. M., Herzog, E. L., Driskell, R. R., Rosenthal, N., Biernaskie, J., & Horsley, V. (2021). Fibroblasts: Origins, definitions, and functions in health and disease. *Cell*, 184(15), 3852–3872. <https://doi.org/10.1016/j.cell.2021.06.024>
7. Rhee, S. (2009). Fibroblasts in three dimensional matrices: Cell migration and matrix remodeling. *Experimental & Molecular Medicine*, 41(12), Article 12. <https://doi.org/10.3858/emm.2009.41.12.096>
8. Chen, H., Xue, L., Gong, G. *et al.* (2022). Collagen-based materials in reproductive medicine and engineered reproductive tissues. *J Leather Sci Eng* 4, 3. <https://doi.org/10.1186/s42825-021-00075-y>
9. Caliani, S., Burdick, J. (2016) A practical guide to hydrogels for cell culture. *Nat Methods* 13, 405–414. <https://doi.org/10.1038/nmeth.3839>
10. Alamán-Diez, P, García-Gareta, E, Arruebo, M, Pérez, María Ángeles. (2023) A bone-on-a-chip collagen hydrogel-based model using pre-differentiated adipose-derived stem cells for personalized bone tissue engineering. *J Biomed Mater Res*. 2023; 111(1): 88- 105. doi:10.1002/jbm.a.37448
11. Andersen, T., Auk-Emblem, P., & Dornish, M. (2015). 3D Cell Culture in Alginate Hydrogels. *Microarrays*, 4(2), 133–161. <https://doi.org/10.3390/microarrays4020133>

12. Yao, L., Tran, K., & Nguyen, D. (2022). *Collagen Matrices Mediate Glioma Cell Migration Induced by an Electrical Signal*. *Gels*, 8(9), 545. <https://doi.org/10.3390/gels8090545>
13. Chen, Q., & Ross, A. C. (2004). Retinoic acid regulates cell cycle progression and cell differentiation in human monocytic THP-1 cells. *Experimental cell research*, 297(1), 68–81. <https://doi.org/10.1016/j.yexcr.2004.02.017>
14. Breitkreutz, D., Stark, H. J., Plein, P., Baur, M., & Fusenig, N. E. (1993). Differential modulation of epidermal keratinization in immortalized (HaCaT) and tumorigenic human skin keratinocytes (HaCaT-ras) by retinoic acid and extracellular Ca²⁺. *Differentiation; research in biological diversity*, 54(3), 201–217. <https://doi.org/10.1111/j.1432-0436.1993.tb01602.x>
15. Yokoshiki, S., Maeda, M., & Saijo Y., (2017). High resolution facial skin imaging with three-dimensional ultrasound microscope. *Proc. Mtgs. Acoust.* 32, 020015 <https://doi.org/10.1121/2.000>
16. Dos Santos, M., Metral, E., Boher, A., Rousselle, P., Thepot, A., Damour, O. (2015). In vitro 3-D model based on extending time of culture for studying chronological epidermis aging, *Matrix Biology*, 47, 85-97. <https://doi.org/10.1016/j.matbio.2015.03.009>.
17. Weinmüller, R., Zbiral, B., Becirovic, A., Stelzer, E. M., Nagelreiter, F., Schosserer, M., Lämmermann, I., Liendl, L., Lang, M., Terlecki-Zaniewicz, L., Andriotis, O., Mildner, M., Golabi, B., Waidhofer-Söllner, P., Schedle, K., Emsenhuber, G., Thurner, P. J., Tschachler, E., Gruber, F., & Grillari, J. (2020). Organotypic human skin culture models constructed with senescent fibroblasts show hallmarks of skin aging. *Npj Aging and Mechanisms of Disease*, 6(1), Article 1. <https://doi.org/10.1038/s41514-020-0042-x>
18. Cleveland Clinic medical professional. (2022, June 17). *Retinol: Cream, serum, what it is, benefits, how to use*. Cleveland Clinic. Retrieved February 6, 2023, from <https://my.clevelandclinic.org/health/treatments/23293-retinol>
19. Tolaymat L., Dearborn H., Zito PM. (2022) Adapalene. *StatPearls*.
20. Yoham, A., Casadesus D., (2022). Tretinoin. *StatPearls*.
21. Shao, Y., He, T., Fisher, G. J., Voorhees, J. J., & Quan, T. (2017). Molecular basis of retinol anti-ageing properties in naturally aged human skin in vivo. *International Journal of Cosmetic Science*, 39(1), 56–65. <https://doi.org/10.1111/ics.12348>
22. Babamiri, K., & Nassab, R. (2010). Cosmeceuticals: The Evidence Behind the Retinoids. *Aesthetic Surgery Journal*, 30(1), 74–77. <https://doi.org/10.1177/1090820X09360704>
23. Fujisaki, H., Futaki, S., Yamada, M., Sekiguchi, K., Hayashi, T., Ikejima, T., & Hattori, S. (2018). Respective optimal calcium concentrations for proliferation on type I collagen fibrils in two keratinocyte line cells, HaCaT and FEPE1L-8. *Regenerative therapy*, 8, 73–79. <https://doi.org/10.1016/j.reth.2018.04.001>
24. Farage, M. A., Miller, K. W., Elsner, P., & Maibach, H. I. (2013). Characteristics of the Aging Skin. *Advances in Wound Care*, 2(1), 5. <https://doi.org/10.1089/wound.2011.0356>
25. Roberts, L. (n.d.). *Seeding Cells in Collagen Gels*. Word Document.
26. Roberts, L. (n.d.). *Resazurin Assay protocol*. Word Document.

ABOUT STUDENT AUTHORS

Samantha Lopez and Olivia Atkins will graduate in May 2023 with a Bachelor of Science in Biomedical Engineering and Biology and Biotechnology, respectively. They both plan on furthering their education and pursuing a master's degree in their respective fields.

PRESS SUMMARY

Human skin aging is characterized by thinning, loss of elasticity, and wrinkles. Keratinocytes, the most common type of skin cell, and fibroblasts, cells present in the stroma beneath the skin's surface, both play a role in aging. Using these cell lines in research can reveal a deeper understanding of skin function and changes in aging. 3D cell culture techniques provide an opportunity to use these cell lines in a model that can more accurately mimic human skin compared to 2D models. Treatment of aging skin is of interest to both medical and consumer communities. Retinoic acid (RA) is a derivative of both vitamin A and retinol that assists in cell growth and immune functions. Over the counter (OTC) and prescription retinoids are common topical products used for anti-aging and acne treatments. This study seeks to determine the impact of topical retinoid creams on skin cell growth and characteristics in 3D cell culture models mimicking aged and unaged human skin. NIH-3T3 fibroblasts were embedded in a 3D collagen matrix of varying thickness, and HaCaT keratinocytes were seeded on top of the matrix at varying seeding densities. Equivalent concentrations of 0.025% tretinoin and 0.1% adapalene topical creams were prepared in cell medium and used to treat cells daily, on alternate days, or just once during a week-long period. AlamarBlue proliferation assays and microscopy provided quantitative and qualitative data regarding the effects of the retinoid products on the skin models. Tretinoin treatment killed the cells, and adapalene treatment, while resulting in significantly more live cells than tretinoin, did not exceed the proliferation of the untreated control. It is understood that retinol increases cell turnover by killing cells rapidly, so it is proposed that in this model, the rate of proliferation does not overcome the rate of cell death. Future studies should focus on creating a 3D model that can more accurately represent the skin environment in the human body where cells can be readily grown.

Anti-adhesive Hydrogel Synthesis for Post-operational Physical Barriers

Alexander Boucher^a, Grace McCarthy,^a Binh Diec^b, Yizhe Ma^a, & Louis Roberts^{a*}

^aDepartment of Biology and Biotechnology, Worcester Polytechnic Institute, Worcester, MA

^bDepartment of Biomedical Engineering, Worcester Polytechnic Institute, Worcester, MA

<https://doi.org/>

Students: arbocher@wpi.edu, bdiec@wpi.edu, gpmccarthy@wpi.edu, yma12@wpi.edu

Mentor: laroberts@wpi.edu*

ABSTRACT

Post-operative cell adhesion can lead to a number of issues for surgical patients during internal healing, motivating new research towards preventative treatments that can be imposed during surgeries to decrease the likelihood of cell adhesion during wound healing. Biocompatible hydrogels offer a potential strategy to combat this issue due to the availability of both natural and synthetic polymers/ molecules that can be implemented into a hydrogel matrix. These materials can be used to create pure or functionalized hydrogels from single polymers being treated with a chemical/drug, or composite hydrogels that combine features of the different biomaterials. Our approach was to create a viable hydrogel with a mechanical strength that allows it to be held in place with sutures that minimizes cell adhesion and degradation when applied to a wounded cell surface. The two synthetic polymers polyethylene glycol (PEG) and polyvinyl alcohol (PVA) were added to two base materials commonly used in hydrogel synthesis- collagen and alginate. Testing revealed that novel hydrogel synthesis is inherently difficult, as crosslinking a material requires a great deal of revision when it comes to the deciding composition of the hydrogels and the additives that will produce a solid and manipulatable hydrogel. We demonstrate the possibility of physically crosslinking a synthetic polymer to sodium alginate; we observed the healing of a wound that the hydrogel is sheathing. Several of the created hydrogels were unable to be tested due to their physical instability. Our results suggest further optimization of the hydrogel/biocompatible molecule compositions is required to create physical barriers that would be able to withstand post-operative implementation. Cellular adhesion was observed on our physical barriers which is non-ideal, however the experimentation with the different natural and synthetic biomaterials has provided insight on future directions that will hopefully bear more promising, and mechanically strong hydrogels.

KEYWORDS

NIH-3T3 cells; alginate; collagen; anti-adhesion; hydrogel; cross-link; polyethylene glycol; polyvinyl alcohol

INTRODUCTION

Post-operational cell adhesion is a serious issue facing not only patients having invasive or traumatic surgeries, but all patients left with internal tissue wounds contacting other internal membranous tissue surfaces after a surgical operation. These adhesions are fibrous bands of tissue produced during recovery of internal wounds after 50-90% of all surgeries no matter the anatomical position (Fatehi Hassanabad et al., 2021)¹. Many of these adhesions require further surgery resulting in a larger financial burden and longer recovery time (Sikirica et al., 2011)². There are a number of current products to combat this issue, none of which are perfect and require serious improvisation to create a simpler, less stressful surgical experience for patients worldwide.

Known for their elongated shape, fibroblasts can be either bipolar or multipolar, and grow attached to a substrate. Fibroblasts are the most important cell type in connective tissues, producing extracellular matrix components like collagen, while also playing a part in wound healing due to their abilities to contract and produce replacement tissue material (Piipponen, Li, & Landén, 2020)³. A common type of fibroblast, NIH-3T3 cells, are derived from NIH/Swiss mice embryos. The NIH-3T3 line is widely used in research as they are easy to maintain and are suitable for a wide range of applications within both cell and molecular research. They can be grown in normal culture flasks in complete medium and have a doubling time of about 1 day, ~20-24 hours (Rahimi, Cai, & Hoyer-Fender, 2022)⁴.

Keratinocytes are skin cells that have roles in a number of bodily and tissue system processes such as wound-repair, organ structure, immune system function, and most importantly keratin production. Being skin cells, keratinocytes are native to the stratum basal and stratum spinosum layers of the skin. HaCaT²⁶ cells are spontaneously transformed human skin cells, specifically

keratinocytes. The HaCaT cell line is derived from a 62 year old caucasian male (Somaiah et al., 2015)⁵. Outside the skin, keratinocytes form an adherent monolayer of cells when grown in a culture flask in complete medium; they have a doubling time of ~1 day, closer to 26 hours (Somaiah et al., 2015)⁵.

Alginate is a natural anionic polymer that is extracted from brown seaweed, a biomaterial that has good biocompatibility and low toxicity allowing it to interface with biological systems. It has a similar structure as an extracellular matrix and can be formed into hydrogels through different cross-linking methods (Woo, Kim, & Kim, 2011)⁶. One method of cross-linking that can be used is ionic crosslinking, where the aqueous alginate solution is combined with divalent cations, most commonly Ca^{2+} . The divalent cations allow for guluronate blocks within the alginate chains to form junctions with other guluronate blocks on other polymer chains, resulting in a gel structure (Woo, Kim, & Kim, 2011)⁶. This is possible due to alginate's native hydrophilic and negatively charged surface. Cross-linking the alginate enhances the mechanical properties, but they can vary depending on gelation rate and temperature (Woo, Kim, & Kim, 2011)⁶. Alginate can also be functionalized to increase properties such as cell-adhesion by chemical modification or adding functional groups, proteins/peptides, or growth factors (Yong Lee & Mooney, 2012)⁷. These characteristics of alginate allow for applications in wound healing, drug delivery, and cell transplantation.

Collagen is a fibrous, structural protein that is found in animals and it is the most prevalent component of the extracellular matrix within humans as it comprises one-third of the total protein within the body. The structure of collagen is a 3-dimensional helix that consists of three parallel polypeptide strands. It is essential to tissue formation, structural integrity, and repair (Yang, Chen, & Wang, 2014)⁸. Collagen is an ideal material to use in cell culture as cells natively recognize it, and it has been seen to promote adhesion, survival, and proliferation. The matrix provides space for the cells to create microenvironments and regulate necessary gene expression in a cultured environment (Yang, Chen, & Wang, 2014)⁸. There are five main types of collagen; collagen 1 from bovine skin (COL1A1) is utilized in this model because it is the major structural protein for bone, tendon, skin, and tendon. Also, it plays an important role in growth and maintenance of organs and tissues. Experimentally, collagen matrices can be prepared both two and three dimensionally and they each have their benefits depending on the needs for a specific experiment (Yang, Chen, & Wang, 2014)⁸. 3D collagen requires a scaffold to be introduced, cells to be seeded within the collagen mixture, and the collagen to be filtered sterilely instead of denatured when prepared. 2D collagen is more conventional, where it is used to grow cells on top of a layer of collagen, and can be sterilized in an autoclave because denaturing the collagen only affects its 3D structure abilities (Yang, Chen, & Wang, 2014)⁸. All the properties outlined of collagen allow for applications in wound healing and tissue regeneration because it can be used as a drug/treatment delivery method, cell scaffold, hydrogel, and more.

Polyethylene glycol (PEG) is a hydrophilic synthetic biocompatible polymer that is non-toxic and can be cross-linked with other biomaterials to manipulate surface properties whether it be adhesion, repulsion, etc. PEG solidifies through free-radical polymerization, and the viscosity and surface pore size will depend on the molecular weight or PEG chain size. Functionalizing peptides and other protein or biomaterial modifications can also be performed to change the interaction between specific molecules, cells, or surfaces and the PEG chains. PEG can be coupled with functional groups to change its interactive properties such as hyaluronic acid, or RGD peptides that can promote anti-adhesion in physical barrier settings. These properties can vary drastically depending on the molecular weight/PEG-arm size, where in most cases the larger armed PEG derivatives have increased gelation and are more viscous (Xu et al., 2022)⁹. The diverse functionality of PEG makes it a good candidate for crosslinking in different applications whether it be postoperative barriers or other cellular interaction models.

Polyvinyl Alcohol (PVA) is another hydrophilic synthetic biocompatible polymer that has increased mechanical strength depending on molecular weight, comparatively to other biocompatible hydrogels. PVA is able to form a cryogel, thus can be solidified from liquid via freeze-thaw cycles. The PVA will form a hydrogel after repeating this process by forming strong hydrogen bonds. The amount of cycles depends on the application, molecular weight, and composition of the PVA solution. The cryogel properties of PVA allow for the encapsulation of non-synthetic biomaterials and natural extracellular matrix molecules but also decreases the abilities of the hydrogel to chemically react with other biomaterials (Xu et al., 2022)⁹. Its innate strength makes PVA a potentially ideal crosslinked molecule for producing a postoperative cell adhesion barrier that can be held in place with sutures or other common medical devices.

Our model is inspired by a study using NIH-3T3 fibroblasts to demonstrate the adhesion properties of a chitin-based hydrogel, in hopes of combating the issue of injuries caused by cell adhesion to improper surfaces after a surgical operation (Zou et al, 2023)¹⁰. The researchers set a goal to create an improved physical barrier that would inhibit cell adhesion to be used during wound healing in-between a healing organ and the surface it would normally be in-contact with (Zou et al, 2023)¹⁰. Currently, there are physical barriers used in industry, but they are prone to undesirable side effects. One of the most commonly used physical barriers in surgery is known as SepraFilm™, a hydrogel produced by Baxter Advanced Surgeries. Although this hydrogel does prevent some

cell adhesion, it has also been observed to cause abscesses, pulmonary embolisms, and fevers in patients with the barrier. The hydrogel tested in this paper is a cross-linked chitin based gel crosslinked with BDDE, which is an ether in the glycidyl family, commonly used for reducing the viscosity of resins (Zou et al, 2023)¹⁰. The researchers obtained promising results when implementing this hydrogel into a rat-based experiment, creating a wound in the rat's abdomen and testing this experimental hydrogel against an industry standard, as well as against a control of no physical barrier. The results were positive as no healing abnormalities were observed, the rats were able to live without experiencing toxicity from the hydrogel during the healing period, and no cell adhesion was observed in the abdomen of the chitin gel samples (Zou et al, 2023)¹⁰.

In this article, a model was designed to test cell adhesion to hydrogels made from and crosslinked with various natural and synthetic biocompatible polymers. These experiments will help to identify a possible starting material to further develop into an anti-adhesive hydrogel that can be implemented into surgical procedures to reduce fibrous adhesions between healing wounds and other internal membranous surfaces.

METHODS AND PROCEDURES

Cell line maintenance and conditions

Cell cultures were grown at 37°C in a humidified 5% CO₂ atmosphere. T25 flasks containing NIH3T3 fibroblast cells (ATCC CRL-1658) or HaCaT cells (T0020001), were checked under a 100x bifocal light microscope to determine confluency. To prepare for cell passaging, complete medium containing Dulbecco's Modified Eagle Medium (DMEM) with 10% Fetal Bovine Serum (FBS) and 1% Penicillin/Streptomycin (PS), PBS, and trypsin were utilized for routine passaging. Any excess liquids and biohazard wastes are disposed of properly and the hood is wiped down using 70% ethanol.

Cell proliferation assay

This assay was completed to understand proliferative characteristics of the different cell types at varying seeding and growth densities. To prepare for the cell proliferation assay, cells that had been cultured to about 100% confluency were trypsinized and counted via hemocytometry. After counting the cells, they were diluted to a concentration of 1*10⁵ cells/mL. These cells were seeded into 32 wells of a 96 well plate through a two-fold serial dilution ranging from undiluted to a 1:64 dilution with a well volume of 125 µL. One additional well was plated with undiluted cells for hemacytometry; three wells were filled with 125 µL complete medium to serve as a blank for the assay. The cells were then left to incubate at 37°C in a humidified 5% CO₂ atmosphere for 48 hours. The plate was observed under a microscope, and the cells in one undiluted well were counted using a hemocytometer. An alamarBlue™ Cell Viability assay (Invitrogen® DAL1025™) was performed, where 12.5µL of alamarBlue™ resazurin reagent was added to all utilized wells. The plate was incubated for 4 hours at 37°C in a humidified 5% CO₂ atmosphere. When the plate was ready (signified by color change), the plate was read by in a Biotek Synergy H1 Hybrid Multi-Mode Reader for fluorescence using excitation and emission values of 540 nm and 590 nm, respectively.

Synthetic tissue generation

A prepared 3D collagen solution was used to create NIH-3T3-fibroblast 3D cultures following the Sigma-Aldrich protocol for collagen solution from bovine skin (Sigma, C4243). The cold (4°C) 2 mg/mL 3D collagen solution (1.5 mL) was combined 1:1 with NIH/3T3-Fibroblasts in complete growth medium at 2*10⁶ cells/mL (1.5 mL). A total of 3 mLs of the 3D Collagen/Fibroblast mixture was created and pipetted into a clear 24-well plate at 1.0 mL, 0.75 mL and 0.5 mL volumes. The plate was incubated at 37°C until solidified, approximately 30 minutes or until noticeably solid. 200 uL complete growth media was added on top of the cell/collagen matrix, which was incubated for six days with media changes every 2 days.

A second culture of NIH/3T3-Fibroblast cells at 80% confluency in a T75 flask was trypsinized and resuspended in complete medium, where the total volume was 10mL. These cells were then transferred into a conical tube and placed in a centrifuge for 10 minutes at 3000 rpm. The excess complete medium was aspirated until only the cell pellet was left within the tube. The cells were resuspended in 6mL of new complete medium (~1.1*10⁶ cells/mL) and 1mL of cells was added to each of the six collagen wounded wells. The plate was incubated at 37°C in a humidified 5% CO₂ atmosphere for 48 hours and then observed under a microscope to confirm monolayer development.

Alginate hydrogel synthesis

To create the alginate-based hydrogels, three 200 mL Erlenmeyer flasks were filled with 30 mL of dH₂O and 1.5% by weight of sodium alginate (Sigma, W201502). Into one sample 1% by weight of PVA MW: 70,000-100,000 (Sigma, P-1763) was added; into a second sample 1% by weight of PEG3550 (VWR Life Science, 0955) was added; a third sample was kept as a pure sodium alginate solution. The three solutions were heated to 65°C and stirred with a stir bar until the powdered reagents were fully dissolved. Once dissolved, the samples were transferred into three 50 mL conical tubes and heat pasteurized in a 100°C water bath for 30 minutes. After pasteurization, the samples were stored at 4°C until gelation was required. In order to gel the alginate +

PEG/PVA mixtures two methods were used: the first was mixing the alginate samples with equal parts 50 mM CaCl₂ in a syringe (“syringe method”) and dispensing the mixture into a 24-well plate, then freezing the thin gel mixture at -20°C for 24 hrs; the second method (“slab method”) was dispensing a 4 mL droplet of the alginate solution into a petri dish and pouring 50 mM CaCl₂ atop them and soaking until solid. Only the slab method was used for generating the two pure alginate gels.

2D collagen hydrogels coupled with PEG and PVA

To create the collagen-based hydrogels Type I 2D collagen from rat tail (Sigma-Aldrich, C3867) at 4 mg/mL was diluted 1:1 with sterile dH₂O and aliquoted into three conical tubes with 10 mLs in each. To physically cross-link PEG3350 (VWR Life Science, 0955) and PVA (Sigma, P-1763) to the collagen, both were added at 13.5% by weight to 10 mLs of 1M NaCl in dH₂O and stirred with a stir-bar at 80°C until fully dissolved. The 10 mL PEG and PVA solutions, respectively, were added 1:1 individually to different 2 mg/mL 10 mL collagen aliquots, which creates final solutions of 1 mg/mL 2D collagen at 6.25% by weight PEG or PVA in 0.5M sodium chloride. In order to use these solutions in a cell culture setting they needed to be pasteurized, so they were heated to 100°C in a water bath for 30 minutes and stored at 4°C until ready to pour. The aliquot without PEG or PVA was kept at 2 mg/mL and was already sterile so pasteurization was unnecessary.

To keep similar size to the 3D collagen tissue matrices and induce gelation, freezing the hydrogels was tested by dispensing 1.5 mL of each collagen solution into a well of a 24-well plate, to, and placing them at -20°C for two days. A larger surface was also tested by pouring just enough of each solution to cover the entire bottom of a petri dish and freezing it with the goal of cutting the gels to size after gelation.

3D tissue wounding and hydrogel barrier application

In order to wound the 3D collagen, a sterile 26 ½ gauge needle was used to create an intersecting wound on the surface of the collagen matrix. When wounding the collagen only the surface of the collagen was cut, as shown in **Figure 1** below.

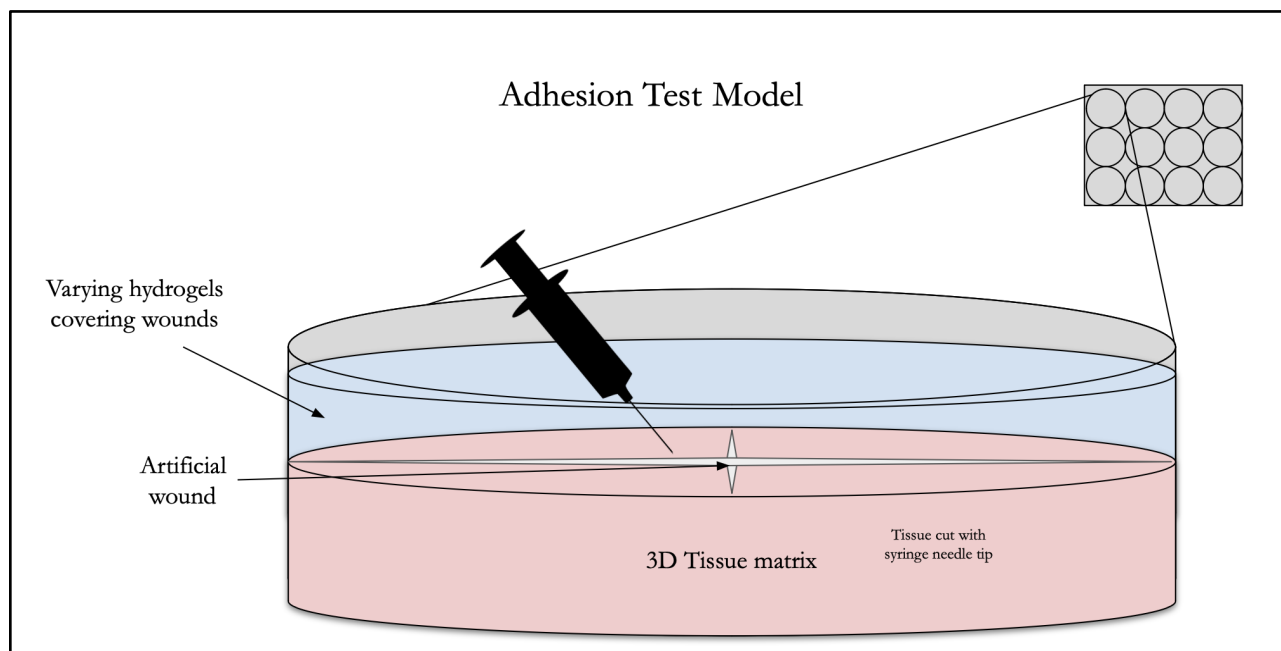


Figure 1. Visualization of the Adhesion Test Model. This was the method used to show how the varying hydrogels will be applied to the healing wound matrices.

To remove the hydrogels from their mold-wells, 10 uL microbiology inoculation loops were used to carefully scoop around the perimeter and then sweep beneath the hydrogel and balanced in the middle of the loop. The hydrogel was then placed on top of the wounded collagen, ensuring that the wound was fully covered.

The hydrogel organization for which was covering which of the near identical wound surfaces is outlined in **Figure 2** below, as shown only alginate-based hydrogels. After covering the wounds, each well received 1mL of new complete medium and incubated at 37°C in a humidified 5% CO₂ atmosphere for 48 hours. After this incubation period, the hydrogels were removed from the collagen with 10 uL microbiology inoculation loops, and both the collagen wound surface and hydrogel barriers were observed for cell adhesion as described in the sections below. To remove the hydrogels from the 3D matrix, 10 uL microbiology inoculation loops were used to carefully scoop around the perimeter and then sweeping beneath the hydrogel, above the 3D tissue

matrix, and balancing it in the middle of the loop.

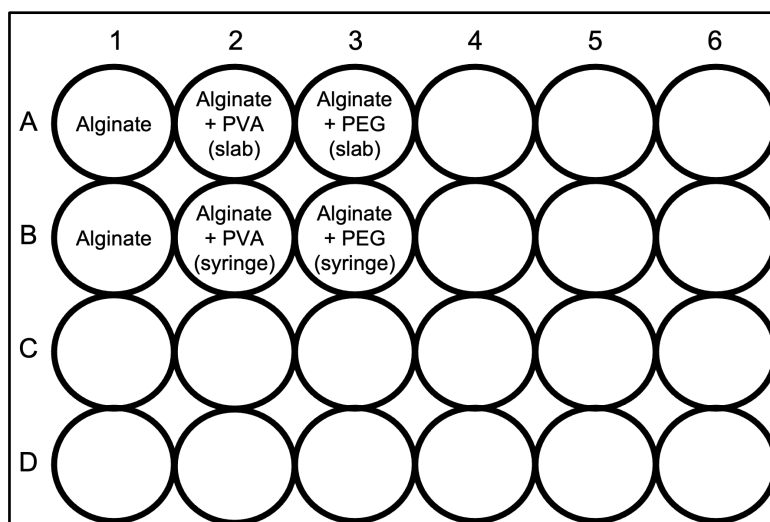


Figure 2. This image shows the layout of hydrogels in the 24-well plate atop of a wounded collagen tissue/fibroblast matrix.

Fixing and staining cells on hydrogels

The hydrogels were removed from the wounded collagen surface gently with 10 μ L microbiology inoculation loops and placed in a new 6-well plate. They were rinsed twice with 4 mL of 1X PBS to clean off excess complete medium. The cells were fixed into place on the hydrogel using 2 mL of 3.7% paraformaldehyde in each well and left for 30 minutes. The paraformaldehyde was removed and the hydrogels were rinsed with another 4 mL of 1X PBS. The cells were stained with 500 μ L of 0.5% crystal violet by ensuring full coverage of hydrogel via rocking the plate. Once fully covered the hydrogels were left for 20 minutes and washed 2 more times with 4 mL of 1X PBS. One unused well in the plate was filled with 2 mL of 1X PBS to ensure the gels did not dry out when parafiled and stored at 4°C until imaging was conducted.

Imaging healing tissues and hydrogels

The hydrogels and collagen 3D tissues were placed under a 100x bifocal light microscope to visualize any cell adhesion that may have occurred from the monolayer-wound surface of the collagen onto the respective hydrogel's contact surfaces. Groupings of cells were searched for on the contact surface of the hydrogels where they were directly touching the wound surface of the 3D tissue matrices. Different focus fields were viewed to observe migration deeper into the hydrogels, as well as multiple fields of view on the contact surfaces to ensure that any cell adhesion was detected. This data collection method is purely observational and qualitative to understand a baseline of cell adhesion to the biomaterials composing the hydrogels.

RESULTS

Cell Proliferation assay: Understanding the proliferative behaviors/ characteristics of cell lines at varying seeding densities

The cell proliferation assay was performed in order to determine the growth rate of the cells that will be used throughout the experiments mentioned in this paper. The analyzed results of the resazurin assay are shown in **Table 2** below, where it was observed that the average relative fluorescence unit (RFU) for the wells decreased as the dilution factor of cells decreased. The cell count was calculated based on the dilution factor and cell count of control well D1 which contained 160,000 cells. This data was plotted to create **Figure 3 (below)**, with an x-axis of \log_2 to stabilize the data variance between the cell counts.

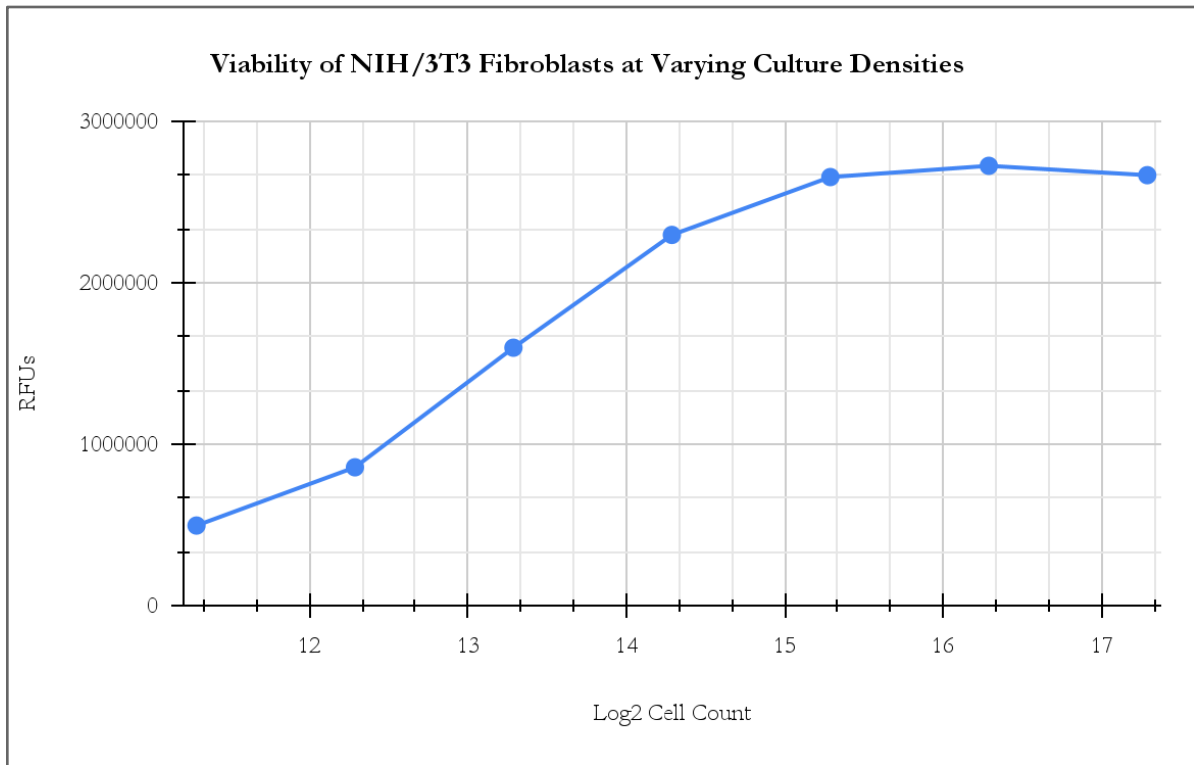


Figure 3. This graph shows a proliferative characterization of NIH/3T3-Fibroblasts based on metabolic conversion of resazurin (non-fluorescent) to its metabolite, resorufin (fluorescent), at different culture densities.

Healing assessment (adhered cell counting, and wound migratory analysis)

The process and results of the healing assessment are shown in **Figures 4-6**. Created using a sterile 26 ½ gauge needle, the intersections cut into the collagen are visible in **Figure 4**. It is to be noted that **Figure 4** shows five out of the six wells with an intersection cut into them, but all six wells were wounded with an intersection prior to hydrogels being placed on top. **Figure 5** shows the 6 wounded wells after hydrogels were placed on top. The alginate-only hydrogels are the most opaque and the wounded collagen is not visible below these hydrogels. The alginate and PVA hydrogels are the most transparent with the wound intersection being completely visible under these hydrogels. The alginate and PEG hydrogels are both slightly opaque which is why the wounds become less visible in **Figure 5** since they are covering the wounds.

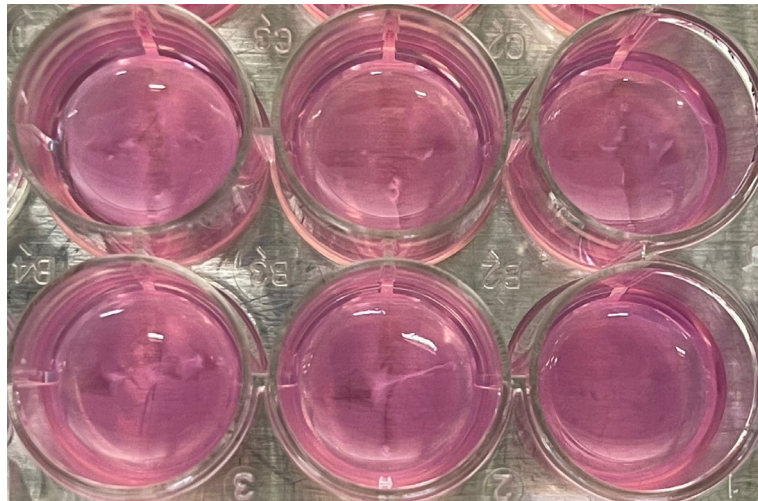


Figure 4. This image shows the wounds made on the collagen before the hydrogels were applied. Note: Before hydrogel application a wound was created in the sixth well (bottom right).

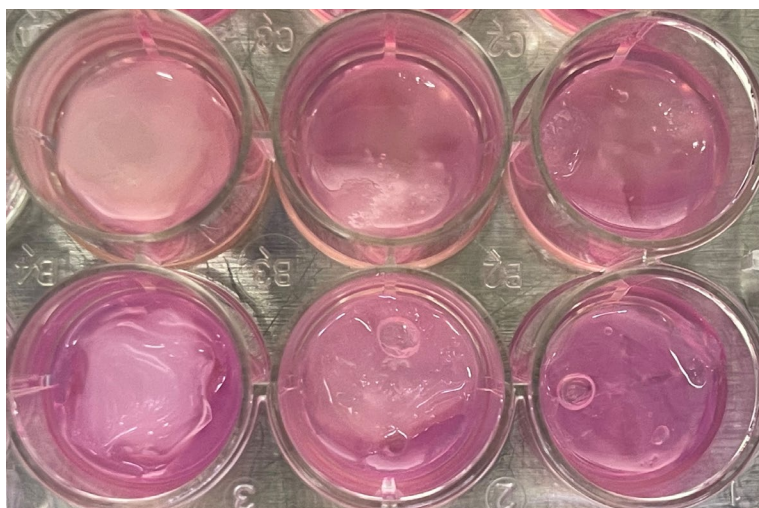


Figure 5. This image shows the wounds made on the collagen after the hydrogels were applied. Left hydrogels (top and bottom) are alginate. Middle hydrogels (top and bottom) are alginate and PVA. Right hydrogels (top and bottom) are alginate and PVA.

The results of the wound migration assay are shown below in **Figure 6**. The wound migration assay performed to see if healthy cells would migrate back into wounded areas of collagen. **Figure 6** shows a close-up view of wound intersections for alginate, alginate and PVA, and alginate and PEG after a 48 hour incubation period.

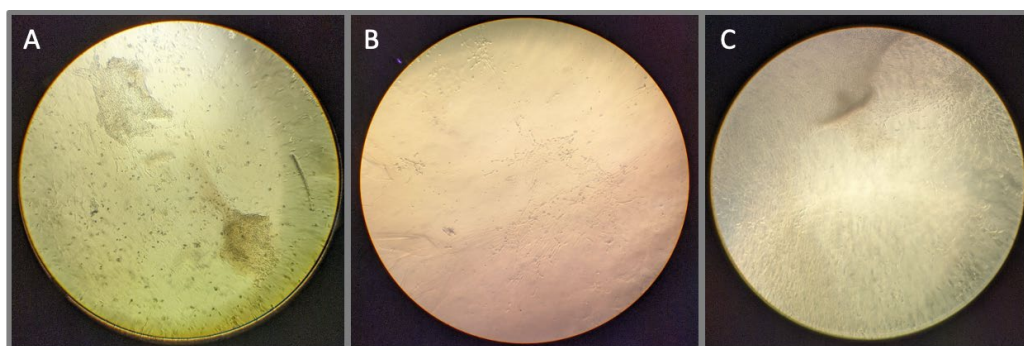


Figure 6. The figure depicts the contact surface of 3 of the wounded collagen wells in the following order: Alginate (Panel A), Alginate and PVA (Panel B), and Alginate and PEG (Panel C).

In **Figure 6**, clumps of fibroblasts are shown in/ near the edge of the wound in all three panels. These cells have migrated from the “healthy” collagen into the wounded area.

Cell Adhesion Assessment

The results from the fixing and staining of the hydrogels are shown below in **Figure 7**. The staining of the hydrogels made cells present on the hydrogels post removal from the wounded collagen visible. Cells are represented by the deep purple coloring and can be seen in each of the images grouped below. All of the hydrogels observed did in fact have cells adhered to their respective contact surfaces. Qualitatively, it seems like there was more general adhesion from the monolayers in contact with the alginate + PVA, whereas the alginate controls look like adhesion is happening in linear columns resembling the wound surfaces.

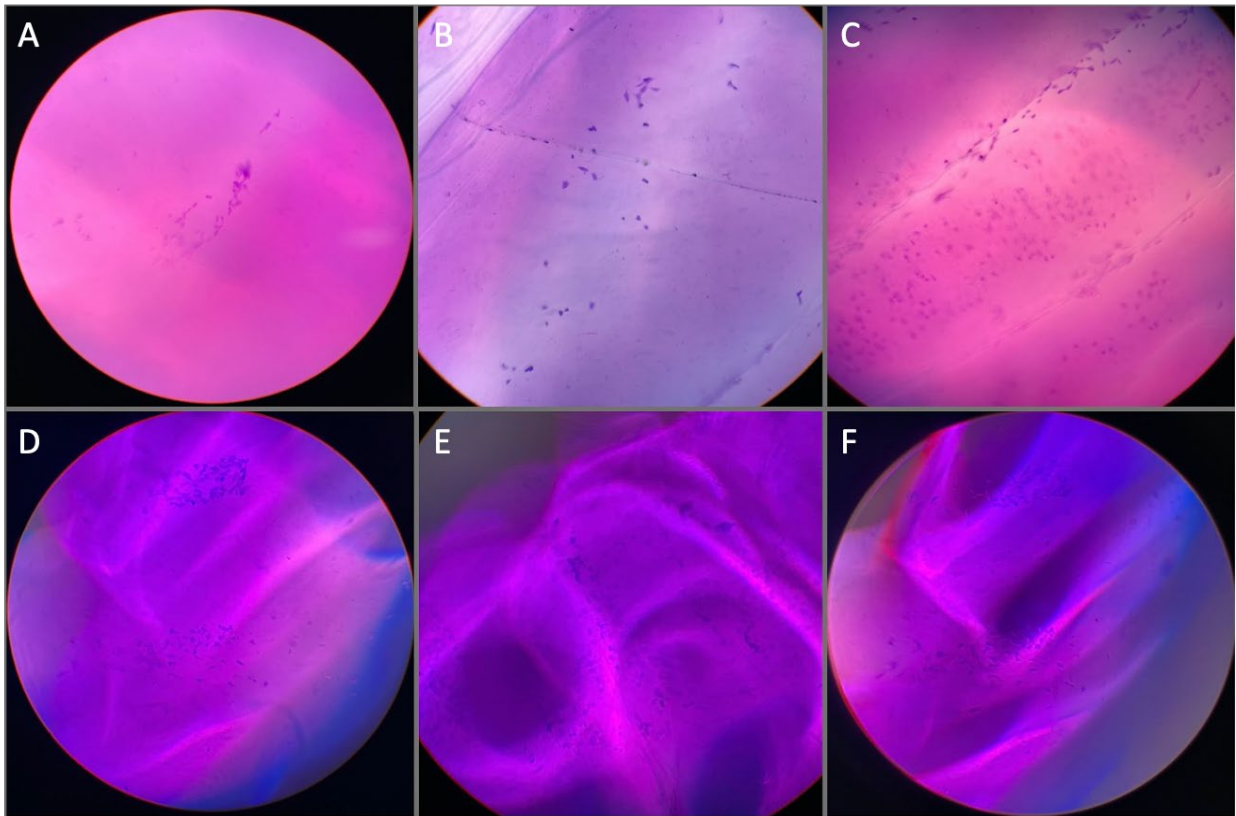


Figure 7. This figure depicts the fixing and staining of cells present on the hydrogels after removal from the collagen. On the top row, Panel A shows the contact surface side of alginate control 1 (slab method) field of view (FOV) with the only grouping of fibroblasts, Panel B shows alginate control 2 (slab method) FOV 1 with a small grouping of divided cells on the outer ring of the hydrogel's contact surface, and Panel C shows alginate control 2 (slab method) center of wound surface with cells dispersed and suspended within the gel. On the bottom row, Panel D shows alginate+PVA (slab method) FOV 1 two surface groups of cells left of wound surface, Panel E shows alginate+PVA (slab method) FOV 2 direct wound surface contact suspended within gel, and Panel F shows alginate+PVA (slab method) FOV 3 top right of wound surface with large groupings of cells.

DISCUSSION

Post-operational cell adhesion can cause an extreme amount of discomfort for recovering patients and can require correction surgeries and side effects, depending on the types of adhesions, like internal or abdominal bleeding, blood in stool, etc. Current solutions for this issue like SeptraFilm™ and CoSeal™ by Baxter Advanced Surgeries have been implemented into current surgical practice, but have not shown consistent abilities to reduce or prevent adhesions for varying reasons (Fujita et al., 2021)¹¹. Hydrogel synthesis can be complicated due to the properties of the biomaterials that compose them, which is why different hydrogel compositions were researched aimed towards improving the current post-operative barriers being used currently in surgical operations. To do so, 2D collagen and alginate were selected as bases for the newly designed barriers, which were physically crosslinked with PEG and PVA to test anti-adhesive abilities when exposed to an artificial wound surface (i.e., 3D collagen seeded with NIH-3T3 fibroblasts). Synthesis of solid hydrogels composed of these natural and synthetic polymer-based biomaterials proved difficult with somewhat limited research available. Determining the correct proportions and concentrations of these materials was likely the underlying issue in solidifying the hydrogels enough for mechanical manipulation onto the artificial wound surfaces.

Of the two hydrogel bases planned to test, 2D collagen and sodium alginate, only the alginate hydrogels were able to be successfully synthesized to be solid enough to be imparted onto the artificial wound surfaces. The pure alginate, alginate + PVA, and alginate + PEG were all placed upon wounds, but only the pure alginate and alginate + PVA were successfully removed and imaged, as seen in **Figure 7**. The alginate + PEG dissolved during the staining process after being exposed to the paraformaldehyde and thus, its anti-adhesiveness was unable to be analyzed. The 2D collagen hydrogels, both pure and crosslinked, after numerous trials with increasing amounts of crosslinked PEG and PVA were still liquid after attempting numerous methods to induce gelation so they could not be used as barriers atop the wounded synthetic tissues. Nevertheless, the alginate gels were incubated atop the recovering wounded synthetic 3D collagen tissues and the results were surprising. Alginate is usually believed to be anti-adhesive when not functionalized nor treated with another polymer or additive, but all the hydrogels imaged had cells adhered to them, two of which were composed of purely 1.5% sodium alginate solidified in 50 mM calcium chloride. More sporadic adhesion outside of the wound zone occurred on the alginate + PVA hydrogel, which seemed to come from even the unwounded monolayer, whereas the pure alginate was seen to only have cells adhered in a pattern similar to the wounded area of the tissue the gel was covering. The combination of two relatively non-adhesive biomaterials through a single test did not appear to reduce adhesion in comparison to the pure alginate, which is opposite of expected results.

The preliminary research performed through these experiments have sparked new ideas on how to further close the gap in knowledge about the synthesis of hydrogels with the purpose of inserting them in during a surgical procedure, in which case increased viscosity or mechanical rigidity is of utmost importance. The ability to remain fixed with sutures or internal surgical adhesives to a wound surface is a necessity to ensure the correct area is being protected from cellular adhesion while recovering from a surgical procedure. To do so, future work would consist of increasing concentrations of PEG and PVA being crosslinked to the hydrogel bases as preliminary tests showed that too high concentrations created issues with homogenization of ingredients because of the thickness of the dissolved PEG and PVA solutions. A larger armed PEG may also be tried in comparison to the PEG 3350 used in the experiments shown in this article because polymers with larger molecular weights tend to form longer polymer chains and branching molecular structures that promote interconnected polymer networks and increased crosslinking sites. Another area with possible improvement would be selecting another hydrogel base material to try crosslinking with PEG and PVA that has more innate, or reliable, gelation abilities. 3D collagen is of interest to test as a hydrogel base as it becomes viscous in an incubated environment which could be increased by the crosslinking of another polymer. This base would be ideal as the synthetic wounds are incubated during their “recovery” process so ensuring the hydrogel stays solid during incubation is essential. This may serve as an improvement to the 2D collagen as it is a denatured collagen product which was seen to congeal at lower temperatures, such as in the refrigerator, but these are only inclinations as to improving the mechanical strength of the physical barriers being designed.

Overall, this research can serve as a starting point for synthesis of new and better hydrogels that can act as physical barriers to prevent internal cellular adhesion. Certainly, more testing is required to improve the anti-adhesive properties of the hydrogels, but increasing their viscosity and ensuring they do not degrade to even be able to assess their effectiveness.

ACKNOWLEDGMENTS

The authors thank the WPI Department of Biology and Biotechnology and the EmpOwER grant awarded by the Women's Impact Network for funding their research initiatives. They also thank the Cell Engineering Research Equipment Suite (CERES) for attempting to use their imaging and plate reading instrumentation. We also thank Dr. Catherine Whittington and Dr. Jeannine Coburn (WPI Department of Biomedical Engineering) for consultation regarding materials and model construction throughout our research process.

REFERENCES

1. Fatehi Hassanabad, A., Zarzycki, A. N., Jeon, K., Dundas, J. A., Vasanthan, V., Deniset, J. F., & Fedak, P. W. M. (2021). Prevention of Post-Operative Adhesions: A Comprehensive Review of Present and Emerging Strategies. *Biomolecules*, *11*(7), 1027. <https://doi.org/10.3390/biom11071027>
2. Sikirica, V., Bapat, B., Candrilli, S. D., Davis, K. L., Wilson, M., & Johns, A. (2011). The inpatient burden of abdominal and gynecological adhesiolysis in the US. *BMC surgery*, *11*, 13. <https://doi.org/10.1186/1471-2482-11-13>
3. Piipponen, M., Li, D., & Landén, N. (2020, November). The Immune Functions of Keratinocytes in Skin Wound Healing. *International Journal of Molecular Sciences*, *21*(22), 8790.
4. Rahimi, A. M., Cai, M., & Hoyer-Fender, S. (2022, August 28). Heterogeneity of the NIH3T3 fibroblast cell line. *Cells*. *21*(22): 8790.
5. Somaiah, C., Kumar, A., Mawrie, D., Sharma, A., Dasharath Patil, S., Bhattacharyya, J., . . . Grace Jaganathan, B. (2015). Collagen Promotes Higher Adhesion, Survival, and Proliferation of Mesenchymal Stem Cells. *PLoS One*, *10*(12).
6. Woo, S.L., Kim, J.W., Kim, Y.K., & Biomater. Sci. Polym. Ed. (2011). Functionalization of Alginate Hydrogels for Cell Encapsulation and Tissue Engineering. *Journal of Biomaterials Science, Polymer Edition*, *22*, 1599-1619.
7. Xu, F., Dawson, C., Lamb, M., Mueller, E., Stefanek, E., Akbari, M., & Hoare, T. (2022). Hydrogels for Tissue Engineering: Addressing Key Design Needs Toward Clinical Translation. *Frontiers in bioengineering and biotechnology*, *10*, 849831. <https://doi.org/10.3389/fbioe.2022.849831>
8. Yong Lee, K., & Mooney, D. J. (2012, January). Alginate: properties and biomedical applications. *Progress in Polymer Science*, *37*(1), 106-126.
9. Yang, J., Chen, X., & Wang, Y. (2014). Collagen-Based Scaffolds for Tissue Engineering. *International Journal of Molecular Sciences*, *15*(1), 921-938. <https://doi.org/10.3390/ijms1500921>
10. Zou, Y., Yue, P., Cao, H., Wu, L., Xu, L., Liu, Z., . . . Ye, Q. (2023, January). Biocompatible and biodegradable chitin-based hydrogels crosslinked by BDDE with excellent mechanical properties for effective prevention of postoperative peritoneal adhesion. *Carbohydrate Polymers*, *305*.
11. Fujita, M., Policastro, G.M., Burdick, A. *et al.* Preventing post-surgical cardiac adhesions with a catechol-functionalized oxime hydrogel. *Nat Commun* *12*, 3764 (2021). <https://doi.org/10.1038/s41467-021-24104-w>

ABOUT STUDENT AUTHORS

Alexander Boucher Jr., and Binh Diec will graduate in May of 2023, and Grace McCarthy will graduate the following May of 2024 - each with their Bachelors' degree from WPI.

Interleukin-6 Cytokine Production After Wounding in NIH3T3 and HaCaT Cell 3D Tissue Models is Impacted by Wounding Method but Uninfluenced by Co-Culture Ratio

^aCleo Caldwell, ^aLilah Delbou ^aJohn Gabelmann ^aYizhe Ma ^aLouis Roberts

^aDepartment of Biology and Biotechnology, Worcester Polytechnic Institute, Worcester, MA

<https://doi.org/10.33697/ajur.2020.NN>

Students: cgcaldwell@wpi.edu, ltdelbou@wpi.edu*, jrgabelmann@wpi.edu**

Mentor: yma12@wpi.edu, laroberts@wpi.edu**

ABSTRACT

Investigating experimental designs in order to determine an ideal tissue model domain has the potential of isolating favorable environments to cultivate advancements in the medical field and the exploration of other prospective applications. Exploring cytokine production via Human-Interleukin-6 ELISA kit post-wound infliction exposed a developing method of observing inflammatory response when NIH3T3 and HaCaT cells are co-cultured in a 3D tissue model environment. This experiment was executed through the routine passaging of cells, generation of collagen gel microenvironment and air-media interface, and wounding of tissue models to determine cytokine production. Cytokine production was analyzed using an ELISA assay which displayed that the cytokine production was highest in the puncture samples and lowest in the scrape model samples, contrary to intensity of the wound. The assay also showed that cytokine production was similar in both co-culture conditions, revealing that cell type is not the primary factor when determining cytokine production, but rather, total number of cells is a far better indicator of the potential cytokine production of a tissue model in a specific wounding period.

KEYWORDS

3D-Collagen; NIH3T3 Cells; HaCaT Cells; Cytokines; Tissue Models; Interleukin-6; Keratinocytes; Fibroblasts

INTRODUCTION

Currently there are no methods to model the inflammatory response in vitro that do not involve animal models, which can be costly and low throughput. Developing a tissue engineered skin analog would be beneficial on many fronts mainly as a way to examine skin pathologies and study the relationship between the various tissues making up the skin during these events. One step on the road to creating a functional skin analog is an understanding of the relationship between keratinocytes and fibroblast in modulating the inflammatory response. The objective of this study was to create a 3D model of the human skin using differing concentrations of keratinocytes and fibroblast. This model was then wounded using various methods and analyzed for its cytokine production to examine the interplay between the two cell types. This study will aid in the creation of a functional skin analog by characterizing which cell type has more of an effect on cytokine production and examining if the ratio of cells contributes to the cytokine output over a period of time

NIH-3T3 cells are an immortalized cell line of mouse fibroblast [1]. Specifically 3T3 cells come from the NIH/Swiss strain of mice and are harvested at the embryo stage of the mouse's development [1]. The cell line was established in 1963 and were named 3T3 cells based on 3-day transfer, inoculum 3×10^5 cells [1]. During their initial development the cells were observed to go from diploid to tetraploid meaning they developed four homologous chromosomes as opposed to two. Fibroblast are a form of adherent cell they primarily are found in the connective tissue of the body and produce vital components responsible for making up the extracellular matrix (ECM) and dictating organ structure [2]. Despite being somewhat ubiquitous through the body they differ in their morphology based on the organ ECM they inhabit. 3T3 cells specifically are used in studies on cell cycle control [2]. 3T3 cells are also utilized to study skin synthesis and mechanics especially in coculture with keratinocytes. Such studies often investigate how 3T3 cells contribute to the ECM and help define tissues like the basement membrane and dermal epidermal junction.

HaCat cells are an immortalized line of keratinocytes. HaCat cells were derived from normal human skin specifically from a 62 year old male patient. These cells are mainly used in skin pathology and homeostasis studies [3]. Primary keratinocytes have the tendency to die if they are led into differentiating. HaCaT however are able to be cultured for extended periods of time and will express the same makers of differentiation such as keratin K10, which inhibits proliferation and tumorigenesis [3][4]. Like 3T3 cells HaCaT cells form an adherent monolayer. HaCat cells are also incredibly useful for the study of skin cancer as they harbor mutations in their p53 genes that are characteristics of UV radiation damage. Keratinocytes are the primary cells in the epidermis acting as a barrier. Keratinocytes also play a key role in modulating the inflammatory response [3]. Keratinocytes release inflammation factors such as

interleukin-1 and Interleukin-6 (IL-1, IL-6) responsible for modulating the inflammatory response. The release of these factors also causes the surrounding fibroblast to begin releasing Interleukin-6 among other tissue and vascular growth factors to upregulate cell proliferation. This creates a positive feedback loop as the skin begins to heal itself [5]. HaCat cells are especially employed for inflammation studies as they are able to be supported in cultures without repeated use of growth factors to keep them alive.

Collagen can be categorized as a fibrous protein that is the most essential component in connective tissue and is specifically present in mammalian cells. 3D Collagen can be obtained when placed in an aqueous solution and is typically derived from mammalian properties such as cartilage and bone [6]. The structure of this protein mimics a DNA double helix with three alpha chains, containing amino acid repeats, Gly-Xaa-Yaa (GXY). This collagen triple helix is crucial to maintaining stability, as the chain consists of hydroxyproline and proline imino acids by forming strong hydrogen bonds thus maintaining structure [6]. This structure in combination with polymerization provides high viscosity, producing gel-like substances. Ideal environmental factors contribute to the construction of 3D collagen. Low pH contributes to the dissociation of fibers to insoluble fibrils [7]. Similar to alginate, soluble fibrils permit 3D collagen to endure naturally occurring cross-linking. Although a similar outcome is reached, the collagen cross-linking process utilizes targeted reactive moieties within the soluble fibrils, allowing for the attachment of cells directly. This chemical process of conjoining molecules through covalent bonds only improves collagens' already strong extracellular matrix.

METHODS AND PROCEDURES

General Cell Culture Upkeep

Both NIH 3T3 and HaCaT cells were cultured according to standard protocol in an incubator set to 37°C with 20% O₂ 5% CO₂. The cells were first observed for confluency and then passaged in either a 1:4 or 1:2 split depending on their density. Cells were observed on an Olympus brand inverted microscope on 100x brightfield with 10X magnification. Briefly once observed the supernatant was aspirated and the cells were washed with 1x PBS. The cells were then treated with between one and two milliliters of trypsin and allowed to sit for five minutes for proper detachment. After the cells were found to be fully detached they were resuspended in complete medium consisting of 90% DMEM supplemented with 10% fetal bovine serum and 1% Penn Strep at a final volume of between six and twelve milliliters of medium depending on the flask type (T25-T75). To perform a 1:2 or 1:4 split cell solution at the required volume was taken and added to a new T75 flask. This flask was then brought to a final volume of 12 ml using the supplemented media. Both HaCaTs and NIH3T3 cells received the same media. The cells were grown approaching confluency until needed for the experiment. Cells counts were obtained throughout the experiment via hemocytometer on an Olympus brand light microscope at 10X magnification and 100X brightfield. When necessary to concentrate or wash trypsinized cells, centrifugation at ~3000 rpm for 10 minutes was utilized.

Creation of 3D Environment and Seeding of Cells

NIH3T3 and HaCaT cells were allowed to grow to confluency using the procedure detailed above. Once the cells appeared to be close to confluency, they were trypsinized and counted in order to ensure correct seeding densities for the 3D environment. The number of viable cells was determined by averaging cell count results from one hemocytometer square, multiplying by 1x10⁴ and finally multiplying by the number of milliliters present, which fell at six milliliters each time the cell count was executed.

HaCaT and fibroblast were harvested according to protocol from Wilkins et al. [7] the seeding density of the control was found to be 3.1 x 10⁴ml fibroblast to 1x10⁵ keratinocytes. The total number of cells was found to be 3.7 x 10⁵ cells assuming the culture dish used is a 12 well plate. Additionally the ratio of cells used in the Wilkins et al article was found to be 80/20 keratinocytes to fibroblast. Once found this ratio was iterated on to create an experimental group of 70/30. To seed the collagen gels the volume of cell solution was found to be in a 1/5 ratio with collagen used. The volume of cell solution and collagen needed was then calculated based on the number of wells per group. These values were calculated assuming the total cell number of 3.7 x 10⁵ cells would remain constant. These values can be seen in **Table 1**.

Groups	Calculated Fibroblast Concentration	Calculated Keratinocytes Concentrations
80/20	1x10 ⁵ cells/ml	8.5x10 ⁴ cells/cm ²
60/40	1.6x10 ⁵ cells/ml	7.4 x 10 ⁴ cells/cm ²

Table 1: A table displaying the calculated cell concentrations of fibroblast to keratinocyte ratios.

The fibroblasts were allowed to grow for two days in one milliliter of media before being seeded with keratinocytes on the surface of the gels. Fibroblast and keratinocytes were allowed to culture for 2 days in 1ml of media before it was changed to .15 ml to establish a media interface. This culture went on for six days before wounding [8].

Wounding of 3D Tissue Model to Induce Cytokine Production

Using a 1000 uL pipette tip, used media was aspirated from the air-media interface and discarded. Each hydrogel was washed with 900 uL of 1x PBS before being aspirated and discarded. Then, each wounding condition was applied to its respective well. One of each 60/40 and 80/20 well was punctured 4 times with a 1000 uL pipette tip, one of each 60/40 and 80/20 well was sliced using a scalpel, and one of each 60/40 and 80/20 well was scraped using a cell scraper. After this, 400 uL of complete media was added to each well, and 100 uL was collected from each sample to be tested as a zero hour time point. 100 uL was also collected four hours after wounding, and twelve hours after wounding [8].

ELISA for Interleukin-6 Cytokine

A Human IL-6(Interleukin 6) ELISA kit with 24 wells was purchased from Elabscience (Cat.No.:E-EL-H6156) . The manufacturer protocol was followed. Two separate blanks were used, one for the sample diluent used to create a standard curve and one for the complete DMEM, which was the blank used for the supernatant which the cytokine samples were suspended in. Samples tested from the tissue model were not diluted before testing. When creating the standard curve, only the 50, 12.5, 6.25 and 1.56 pg/mL standards were utilized. Ultimately, the data used from this assay was not the cytokine concentrations, but

the blank corrected OD values of each of the samples, referred to as “normalized cytokine production.”

RESULTS

The data collected is a direct result of the procedures listed above. This experiment aims to test and identify future methods to model inflammatory response in animal cells to advance therapeutic approaches in many common diseases. This data aimed to analyze a successful Human Interleukin-6 ELISA assay that provides viable data to determine cytokine production in various co-culture conditions, and diverse wounding techniques. Cell lines were observed at various points throughout this experiment and are included below to account for all experimental factors that may impact the overall results. Routine passaging and upkeep were maintained in order to avoid nonviable data and/or toxicity. Amplifying the qualitative analysis throughout the course of this experiment provides long-term investigation of culture conditions and the significance of simulated 3D tissue models.

Images shown in Figures 1, 2 and 3 were taken after aspirating and replacing media in 12 well plate. Images of wells 70/30 were not relevant in this study due to little variance from 60/40 wells

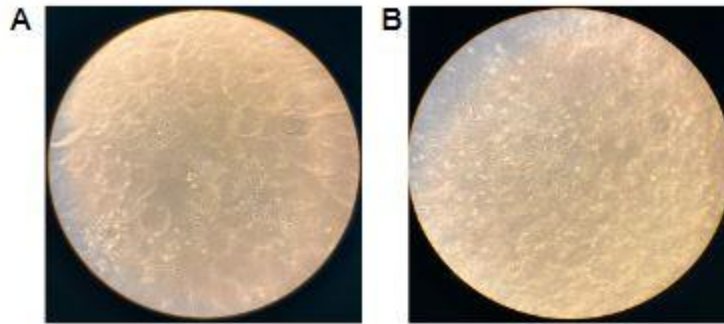


Figure 1. Image taken 2/17/23 via inverted microscope after seeding culturing fibroblasts in collagen gels for two days and seeding HaCaTs

A. 80:20 keratinocytes to fibroblast, **B.** 70:30 keratinocytes to fibroblast

The two figures above display the two day progression of the generated 3D collagen environment in combination with culturing fibroblasts after seeding HaCaTs. Co-culture conditions allowed for the determination of cytokine production to reflect the immune response initiated by different wounding methods. It is detectable that the tissue model shown in **Figure 1** contains a higher concentration of fibroblasts due to the confluency difference. Three wounding methods were deemed essential for examining variation in injury infliction and immune response. The contrast in wounding methods; puncturing, scraping, and slicing offered diverse data to examine juxtaposition.

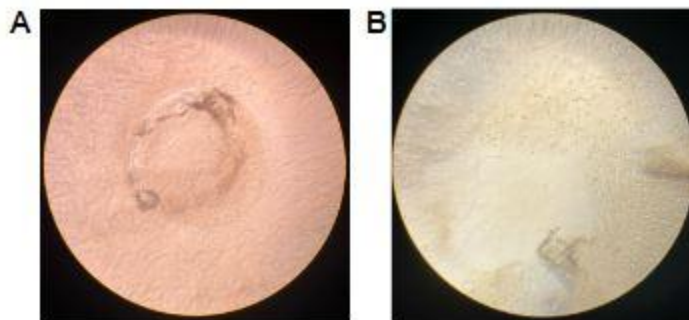


Figure 2. Image taken 2/22/23 via inverted microscope after initial wounding of the 80:20 group. **A.** collagen after four puncture wounds were inflicted on culture using a single sterile 1000 microliter pipette tip. **B.** collagen after a sterile scalpel was used to injure the culture

Wound imaging displayed above represents the impact of a puncture wound and scalpel scrape in 80:20 co-culture. This injury provides the most qualitative analysis, as the layers of collagen gel are apparent when viewed under the microscope. The scalpel wound, while considered the most intense injury in this experiment, has little visibility through the microscope. Scrape is not evident and layers of collagen are hardly qualitative. Due to complications in magnification, cell scraping wounds were not captured in this group.

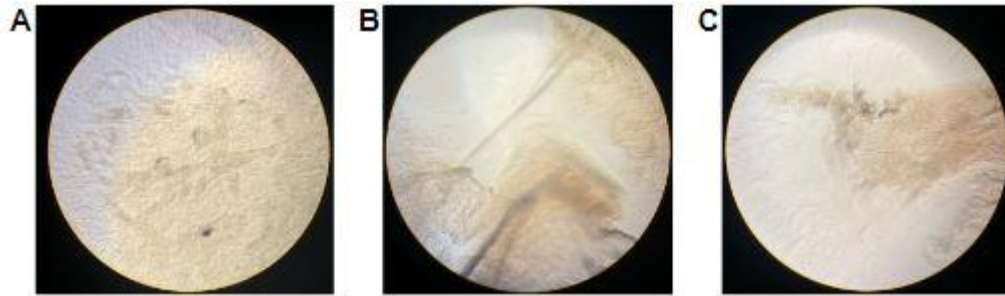


Figure 3. Image taken 2/22/23 via inverted microscope after initial wounding of the 70:30 group. **A.** culture after four puncture wounds were inflicted on well **B.** culture after a sterile scalpel was used to injure. **C.** culture after wounding with a cell scraper

Microscope images post-wound injury are displayed above to recognize the difference between the three wounding methods, and their effectiveness according to qualitative analysis. Contrary to the 80:20 puncture wound, the 70:30 puncture has minimal visibility that features the multiple layers of collagen gel. The scalpel scrape image proves to be more intense in the wounding of the 70:30, as seen in **Figure 3. B.** This set of images provides an illustration of a cell scraper, which was not observed in the 80:20 group. This injury has distinct qualities that demonstrate the impact of the wound, but is limited in showing the dimensions of the 3D environment.

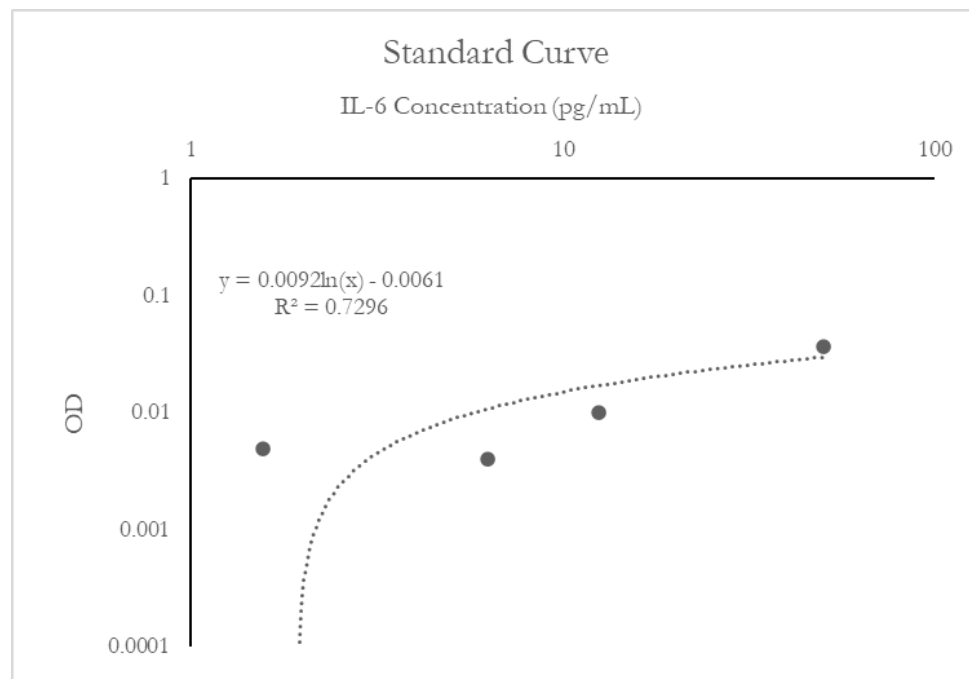


Figure 4. Standard Curve of IL-6 Production vs OD. This information was obtained from the use of the ELISA assay kit purchased from Elabscience. The equation shown represents the dotted trendline, and shows the logarithmic relationship between IL-6 concentration and OD at 450 nm when graphed on log-log axes.

Following wounding of the tissue model and execution of the ELISA assay, a standard curve was created using the 4 standards tested on the assay plate. Unfortunately, due to lack of wells in the provided assay kit, only 4 wells were able to be utilized for standard curve creation. As a result of this, the standard curve had a comparatively small range, as well as low statistical significance, contributed to by the lack of replicates. The R^2 value shown in the standard curve is 0.7296, showing that it is not a strong indicator of actual cytokine production in the samples tested. There is potential that it could be used to assign approximate values to samples up to the OD shown in the 50 pg/mL sample, however, considering that many of the collected samples fall outside that value, much of the comparison done in this section was performed based on the OD values shown in Table 1.

Table 1: Normalized Cytokine Production of Each Injury Method, Time Point and Co-Culture Ratio. This table shows the blank corrected normalized production (OD) of cytokines by each of the samples tested. Using the equation from the standard curve shown in Figure 4, it is possible to determine the concentration of cytokines by using these values as the “y” value in the equation and solving for x.

	80/20 0 Hour	80/20 4 Hour	80/20 12 Hour	70/30 0 Hour	70/30 4 Hour	70/30 12 Hour
Puncture	0.02	0.045	0.101	0.015	0.062	0.122
Scalpel	0.002	0.046	0.031	0.012	0.079	0.084
Scrape	0.038	0.022	0.064	0.005	0	0

The lack of wells for use in the creation of the standard curve not only limited the statistical significance of the curve, but also the range across which it was valid. Because of the small range, many of the samples tested had OD values outside of the range of the curve, meaning that there was no valid means to calculate the actual cytokine production in these samples. For this reason, the primary data used in analysis of these results is the blank corrected OD readings obtained from the ELISA assay. This means that the actual concentrations of cytokine production cannot be scientifically determined as a result of this experiment, but the dynamics at play between the injury methods and co-culture ratios can still be explored. For the duration of this paper, any mention of normalized cytokine production refers to the values shown in Table 1 above, as they show relative productions of cytokines by each co-culture best in light of the low R^2 value produced by the standard curve. These values effectively show the relative cytokine production of each sample relative to the other samples in the trial.

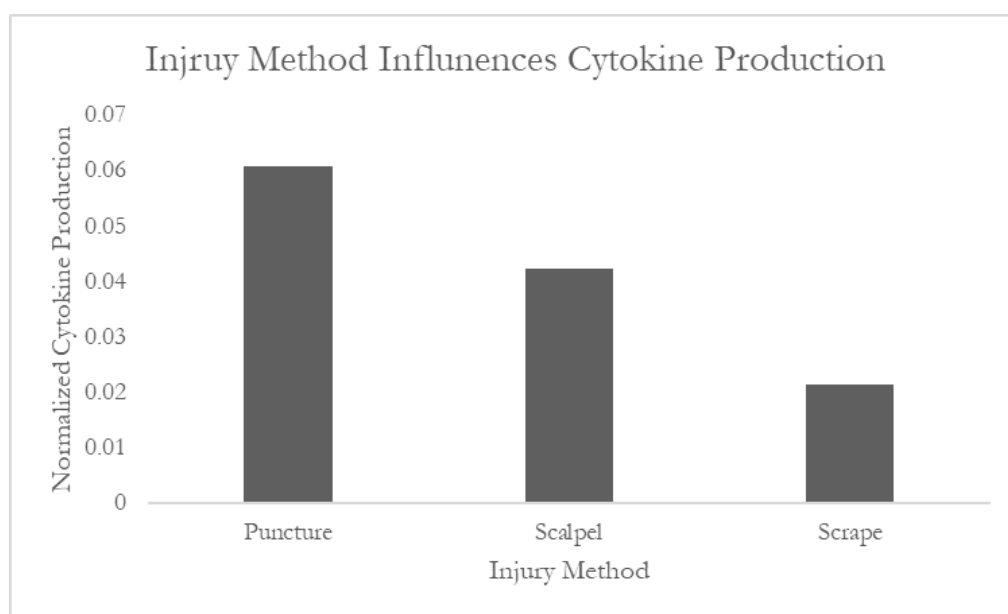


Figure 5. **Cytokine Production by Injury Method** A graph showing normalized Cytokine Production sorted by each of the injury methods, punctured with a pipette tip, slicing with a scalpel and scraping with a cell scraper. The puncture wound showed the highest cytokine production, followed by the scalpel wound then the scrape wound.

Viewing the relative cytokine production, shown in Figure 5, shows that each injury method is distinct in influencing cytokine production. Puncturing the tissue model with a 1000 uL pipette tip resulted in the highest cytokine production. Scraping with a cell scraper resulted in the lowest amount of cytokines produced, while injury with a scalpel provided a midpoint between the puncture and scrape wounds. Each wounding method showed rather distinct cytokine production relative to the others.

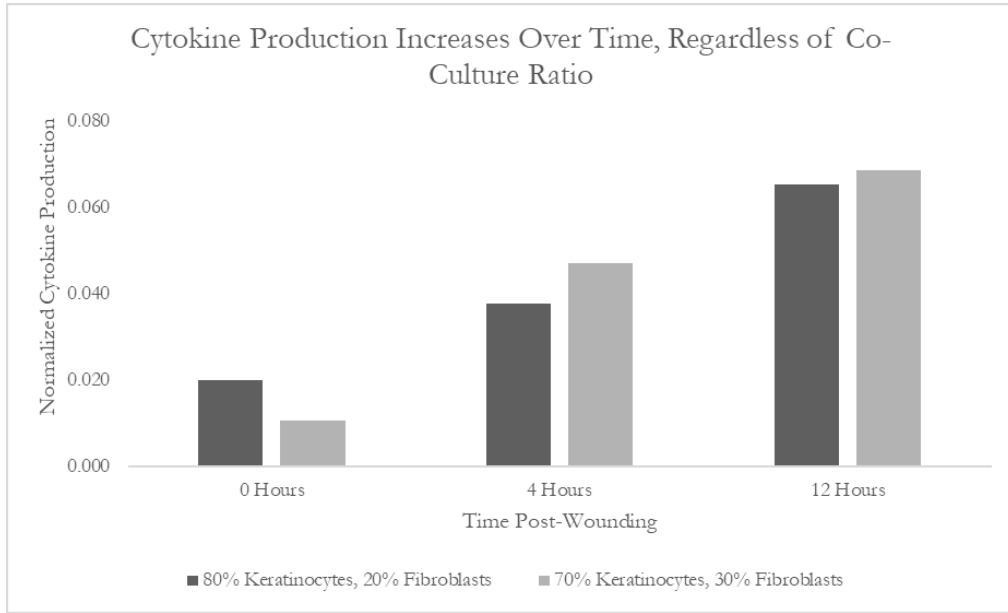


Figure 6. **Cytokine Production by Co-Culture Ratio and Time Post Wounding.** The graph shows the two different groups of co-culture ratio, the 80% keratinocyte, 20% fibroblast and 70% keratinocyte, 30% fibroblast, at each specific time point samples were taken from the tissue model post wounding. These values are charted against the normalized cytokine production in each of the categories.

Samples collected at 4 and 12 hours post wounding revealed that cytokine production increased up to 12 hours in both co-culture ratios. Although there are minute differences in each co-culture’s cytokine production when comparing time points, the two appear to increase in a relatively similar fashion.

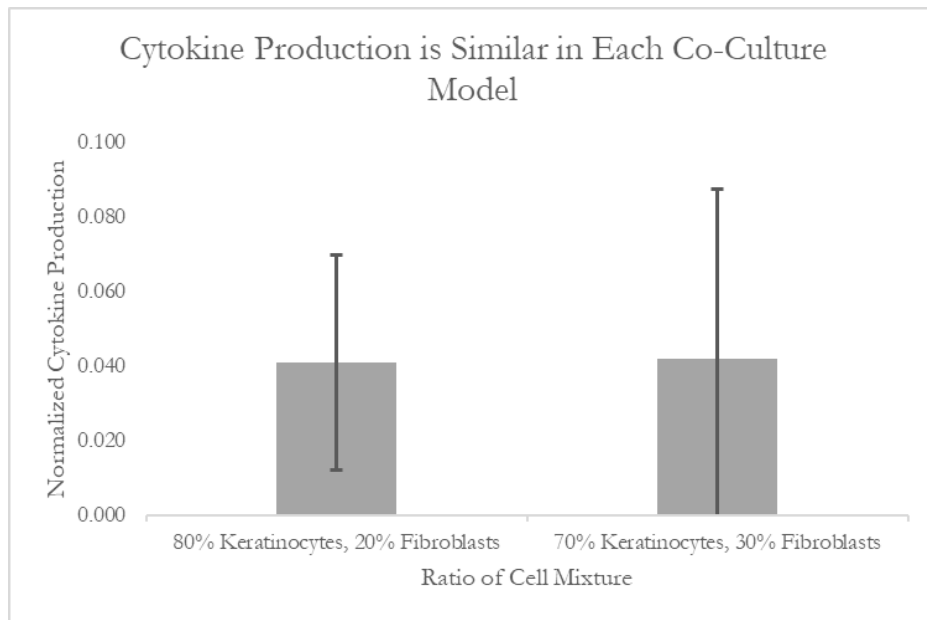


Figure 6. **Cytokine Production by Co-Culture Ratio.** A graph showing the total amount of cytokines produced by each co-culture of keratinocytes and fibroblasts. The error bars shown are standard deviations comprised of all samples in each category, and have been included to help visualize the range of cytokines produced by each of the co-cultures over the course of this experiment.

When comparing both co-cultures to each other, it becomes clear that there is no significant difference in cytokine production between the two models. The error bars shown are the standard deviation of all the samples in each co-culture. They allow the range of values assayed to be visualized, showing the relative similarity of the average cytokine production of each co-culture across all wounding methods and time points.

DISCUSSION

applications. Understanding the ways in which tissue models behave is integral to their design. Keratinocytes and fibroblasts are both very important types of cells within tissues, and understanding the ways in which alternating their proportions affects wounding patterns. This is crucial to the advancement of mapping the dynamics of how information from these tissue models can be applied to more complex organisms.

This test employed 3 different wounding methods, all ranging in intensity. The puncture wound was the most minimally invasive wound, while the scalpel cut deep across a larger area. The cell scraper was used as the most intense form of wounding, and dug deep into a large section of the tissue model. Contrary to these notions, the cytokine production was highest in the puncture samples and lowest in the scrape model, as shown in **Figure 5 above**. This may be due to the nature of the wounding, and since the samples were so small, perhaps the wounding methods which were hypothesized to be more intense killed more cells, limiting the number of cells that were left to produce cytokines. Additionally, if this test were to be repeated, a more consistent wounding method for scraping would need to be determined. Some of the wells that were subjected to scraping appeared to experience almost no visual change, while others lost hydrogel cover in 25-30% of the sample area. This inconsistency may also contribute to the magnitude of cytokine production seemingly not coordinating to wound intensity.

Interestingly, when averaging all wounding methods at each timepoint and co-culture ratio as shown in Figure 7, each of the co-culture ratios showed nearly identical cytokine production levels. This result implies that the cell type is not the primary factor when determining cytokine production, but rather, total number of cells is a far better indicator of the potential cytokine production of a tissue model in a wounding period.

CONCLUSIONS

Tissue models have great potential to provide solutions to a variety of health problems, and striving to improve their accuracy to the best possible degree will allow them to better provide answers to our questions. This experiment sought to determine potential factors when determining accurate cell signaling, such as cytokine expression, within 3D tissue models. The results of this experiment imply that cells produce the most cytokines when wounded with a puncture method, and the least when scratched with a cell scraper, allowing documentation of different wounding method's effects on cytokine production. Additionally, the results imply that the type of cell does not strongly impact cytokine production, but rather, total number of cells is a far better indicator of cytokine production. This result is supported by the seemingly small difference in cytokine production between the two different ratios of keratinocytes and fibroblasts.

There are many steps that could follow this experiment. Primarily, this research would benefit from more replicates in testing. All of the conditions tested in this experiment were only able to be assayed one time, and improving this to duplicate or triplicate testing would enhance the validity of the results drastically, and potentially allow for a more robust standard curve that could be used to comment on concentrations of cytokine production. Although this experiment provides interesting directions to explore, full conclusions cannot be drawn without more testing. Additionally, this test only applied 3 potential wounding methods. It is more than possible that there are methods which were not tested in this experiment that could inflict wounds which allowed for more robust or consistent cytokine production. For this reason, it would be wise to test other wounding methods to compare them to the ones employed in this experiment. Additionally, the wounding application may need refining. As mentioned in the paper, wounding methods such as using a cell scraper to injure the tissue model surface are difficult to standardize, and as a result may be a poor way to wound cells due to lack of consistency. If it is to be used as a wounding method in testing of tissue models, more consistent methods must be developed.

ACKNOWLEDGMENTS (Bold, all caps, no space after)

The authors thank the WPI Department of Biology and Biotechnology and the EmpOwER grant awarded by the Women's Impact Network for funding the research Initiative. Thank you to Dr. Catherine Whittington and Dr. Jeannine Coburn (WPI Department of Biomedical Engineering) for consultation regarding materials and model construction.

REFERENCES

1. Leibiger, Christine, Nadezda Kosyakova, Hasmik Mkrtchyan, Michael Gleib, Vladimir Trifonov, and Thomas Liehr. 2013. "First Molecular Cytogenetic High Resolution Characterization of the NIH 3T3 Cell Line by Murine Multicolor Banding." *Journal of Histochemistry & Cytochemistry* 61 (4): 306–12. <https://doi.org/10.1369/0022155413476868>.
2. Rahimi, Amir Mohammad, Mingfang Cai, and Sigrid Hoyer-Fender. 2022. "Heterogeneity of the NIH3T3 Fibroblast Cell Line." *Cells* 11 (17): 2677. <https://doi.org/10.3390/cells11172677>.
3. Colombo, Irma, Enrico Sangiovanni, Roberta Maggio, Carlo Mattozzi, Stefania Zava, Yolanda Corbett, Marco Fumagalli, et al. 2017. "HaCaT Cells as a Reliable In Vitro Differentiation Model to Dissect the Inflammatory/Repair Response of Human Keratinocytes." *Mediators of Inflammation* 2017: 1–12. <https://doi.org/10.1155/2017/7435621>.
4. Santos, M., Paramio, J. M., Bravo, A., Ramirez, A., & Jorcano, J. L. (2002). The expression of keratin k10 in the basal layer of the epidermis inhibits cell proliferation and prevents skin tumorigenesis. *The Journal of biological chemistry*, 277(21), 19122–19130. <https://doi.org/10.1074/jbc.M201001200>

5. Russo, B., Brembilla, N. C., & Chizzolini, C. (2020). Interplay Between Keratinocytes and Fibroblasts: A Systematic Review Providing a New Angle for Understanding Skin Fibrotic Disorders. *Frontiers in immunology*, 11, 648. <https://doi.org/10.3389/fimmu.2020.00648>
6. IBIDI:Cells in Focus. “Collagen type I, rat tail: 3D cell culture gels & coating.” Artym, Vira V, and Kazue Matsumoto. “Imaging cells in three-dimensional collagen matrix.” *Current protocols in cell biology* vol. Chapter 10 (2010): Unit 10.18.1-20. doi:10.1002/0471143030.cb1018s48
7. Wilkins, L. M., Watson, S. R., Prosky, S. J., Meunier, S. F., & Parenteau, N. L. (1994). Development of a bilayered living skin construct for clinical applications. *Biotechnology and Bioengineering*, 43(8), 747–756. <https://doi.org/10.1002/bit.260430809>
8. Falanga, V., Isaacs, C., Paquette, D., Downing, G., Koultab, N., Butmarc, J., Badiavas, E., & Hardin-Young, J. (2002). Wounding of bioengineered skin: cellular and molecular aspects after injury. *The Journal of investigative dermatology* 119(3), 653–660. <https://doi.org/10.1046/j.1523-1747.2002.01865.x>]=ning all

Determining the toxicity or potential carcinogenesis of sunscreen on HaCaT and NIH-3T3 cells

Katherine Corbin^a, Kelly Heffernan^a, Jaya Mills^b, Yizhe Ma^a, Louis Roberts^a

^aDepartment of Biology and Biotechnology, Worcester Polytechnic Institute, Worcester, MA

^bDepartment of Biomedical Engineering, Worcester Polytechnic Institute, Worcester, MA

Students: kecorbin@wpi.edu, kjheffernan@wpi.edu, jcmills@wpi.edu

Mentors: yma12@wpi.edu, laroberts@wpi.edu

ABSTRACT

The goal of this study was to test toxicity, carcinogenicity, and the UV-protective effects of commercially available sunscreen products in a three-dimensional cell culture model. A collagen and NIH-3T3 fibroblast matrix was created where HaCaT cells were seeded on top. All cells were treated with either 1 μ L of sunscreen, 3 seconds of UV ray exposure, both, or neither. A cell proliferation assay was then performed on the different cell treatment groups. Through RFU values, it was determined that sunscreen decreased cell proliferation in all groups treated with 1 μ L of sunscreen, whether or not exposed to UV. This suggests that sunscreen is toxic for both HaCaT and NIH-3T3 fibroblast cells. Interestingly, it was also determined that sunscreen appears to have a protective quality for HaCaT cells and NIH-3T3 cells grown together when exposed to UV rays, and for NIH-3T3 cells grown alone when comparing RFU values. The mechanisms for this difference remain unclear and present a new pathway to explore regarding sunscreen toxicity on different human cell types.

KEYWORDS

Fibroblasts; HaCaTs; 3D collagen; Ultraviolet radiation; Toxicity; Carcinogenesis; Sunscreen; Cancer

INTRODUCTION

There are a variety of cell types that have applications in tissue regeneration.¹ Fibroblasts account for a diverse group of cells and are the main component of connective tissues, which makes them a compelling candidate for use in tissue regeneration.¹ Studies have described fibroblasts as having a large and irregular shape that can be elongated, polygonal, or stellate. These cells have a significant amount of cytoplasm that surrounds the oval-shaped nucleus and tapers off.² Fibroblast cells are connected to nearby cells via adhesion.³ Through adhesion, different subpopulations of fibroblasts

interact with other cell types including epidermal, vascular endothelial, and immunocompetent cells. Fibroblasts hold a significant role in the healing of wounds and inflammation due to interactions with immunocompetent cells and their ability to regulate neuropeptides at the sites of wounds and inflammation, displaying their important role in the healing process.¹ Additionally, fibroblasts play a key role in the aging of specific organs and the individual. The phenotypic and functional diversity of fibroblasts displays the significance of fibroblasts in connective tissues in the body.¹

Another cell type that has applications in tissue engineering are HaCaT cells which are a spontaneously immortalized human keratinocyte cell line. HaCaTs are used frequently in studies of immunological and inflammatory responses, as they are similar enough to normal keratinocytes to be a practical model.⁴ Additionally, HaCaTs are used for studying the pathophysiology of epidermal homeostasis.⁵ HaCaT cells do not come with the complications that fresh human keratinocytes do. For example, fresh human keratinocytes need supplementary growth factors *in vitro*.⁴ When differentiation is induced in fresh human keratinocytes, the cells die rapidly. The plating efficiency, proliferation, and differentiation differ between keratinocyte cells from different donors, which causes increased complications in passaging⁴. All of the above complications can be minimized with the use of HaCaT cells, which makes them an excellent candidate for experiments testing compounds on epidermal tissue.⁴

3D collagen is a material that is often used with both HaCaTs and fibroblasts to recreate *in vivo* cellular environments. Additionally, the interactions that occur between collagen and cells play a key role in tissue remodeling and the wound-healing process. Since collagen is a natural molecule, it is biodegradable and biocompatible.⁶ The use of 3D collagen has led to a greater understanding of the growth, survival, and migration of cells.⁷ 3D collagen can be manipulated to imitate physiological conditions along with having properties that are controllable and adaptable.⁸ In the extracellular matrix, there is an abundance of collagen protein.⁹ Collagen can be used to form 3D hydrogels.⁶ 3D collagen is a versatile tool that can be used to study various types of cells. Specifically, collagen interacts with cells in ways that are crucial for wound healing processes and tissue remodeling.⁶

Ultraviolet (UV) rays are a well-known mutagen of human cells. Ultraviolet radiation can be divided into three categories: UV-A, UV-B, and UV-C. These categories of UV rays are divided based on wavelength. Ultraviolet B is defined as the ultraviolet rays from 320 to 286 nm. These are the rays that come from the sun that cause damage to the

skin and sunburns.¹⁰ Additionally, UV-B rays are carcinogenic. Severe sunburns from these types of ultraviolet radiation have caused an increase in melanoma, the most fatal form of skin cancer.¹¹

The mutagenic effects of ultraviolet radiation on human cells have been studied for years and are well known.¹¹ In an effort to reduce the likelihood of skin cancer, various active ingredients are added to topical sunscreens to absorb UV rays before they can penetrate into someone's skin. However, in some studies, active ingredients like octyl methoxycinnamate (also known commonly as octinoxate) have been linked to altered gene expression in fibroblast and breast cancer cell lines when UV rays break the active components down.¹² The exact degree to which this altered gene expression could cause mutagenesis or toxicity with alternative sunscreen active components is still unknown. The objective of this experiment was to determine the degree to which sunscreen can be toxic or carcinogenic. This was done by treating HaCat and NIH-3T3 cells in a collagen matrix with sunscreen and UV rays, and measuring their viability via a cell proliferation assay.

METHODS AND PROCEDURES

2.0 Acquiring and Passaging HaCaT and NIH-3T3 Fibroblast Cells

HaCaT cells from AddexBio (catalog number T0020001) were obtained and plated into a T-75 flask with Dulbecco's Modified Eagle Medium (DMEM) + 10% Fetal Bovine Serum (FBS). These were passaged as needed to keep cells at 95% confluency. NIH-3T3 fibroblast cells from ATCC (CRL-1658™) were obtained and plated into a T-75 flask with DMEM + 10% FBS. These were passaged as needed to keep cells at 95% confluency. All cell lines were placed in a 37-degree Celsius incubator at 5% carbon dioxide. Humidity was maintained in the incubator through a water tray at the bottom.

2.1. Determining Lethal Dosage of Sunscreen and UV Rays on HaCaT Cells (Phase I)

This phase aimed to test the lethality of both sunscreen and UV light on the cells. The tests were run on a 12-well plate with 1 mL of DMEM + 10% FBS medium and 200 µL of HaCaT cells in each well. In the first column, the wells were exposed to 20 seconds of UV light. In the second column, the wells were exposed to 10 seconds of UV light. The third column was not exposed to UV light, but each of the three wells had a different volume of sunscreen

(Neutrogena™ Beach Defense Water+Sun Protection Lotion SPF 30) in it, being 5, 15, and 25 μL of sunscreen respectively.

2.2 Creating the NIH-3T3 cells and collagen matrix with HaCaTs

The NIH-3T3 cells were washed, trypsinized, centrifuged, and then resuspended in 1 mL of complete medium. This mixture was added to collagen in a 1:11 ratio (total volume of 12 mL). Using a P-1000 micropipette, 500 μL of the collagen and cell mixture was pipetted into each well in two 12-well plates. The plates were incubated for an hour until the collagen was set. Once the matrix was set, 500 μL of HaCaT cells were added to half of the wells on each plate (6 wells out of 12 per plate). The two plates were then placed in the incubator to allow the HaCaT cells to settle and proliferate over a five-day period. At the end of this five-day period, 500 μL of fresh DMEM + 10% FBS medium was added to each well. They were then placed back in the incubator for 2 more days, at which point 500 μL of medium was added to each well again.

2.3 Determining the Lethal Dosage of Sunscreen and UV Rays on HaCaT Cells (Phase II)

Additional testing was performed to determine the proper UV exposure time and concentration of sunscreen. These tests were run on a 12-well plate with HaCaT cells seeded to 40% confluency in DMEM + 10% FBS medium. In the first column, the wells were exposed to 4 seconds of broad spectrum UV light at a wavelength of 254 nm (BioGlow® Dual Wavelength UV Lamp). The second column was exposed to 2 seconds of UV light. The third and fourth columns tested the amount of sunscreen in each, using volumes of 5 μL , 10 μL , 15 μL , 25 μL , 50 μL , and 100 μL of sunscreen. The sunscreen used was CareOne™ Sport Sunscreen Spray (SPF 30), which was sprayed into a sterile cylindrical tube for ease of pipetting. The active ingredients in this sunscreen are Avobenzone (3%), Homosalate (15%), Octisalate (5%), and Octocrylene (8%).

2.4 Treatment of NIH-3T3 and HaCaT Cell Collagen Matrix with Sunscreen and UV Rays

From the preliminary tests that were performed, it was determined that 3 seconds of UV rays at a wavelength of 254 nm and 1 μL of sunscreen would be used as treatments. 1 μL of sunscreen was pipetted into each designated area for sunscreen on both 12-well plates. Additionally, the plate being treated with UV rays was given 3 seconds of radiation after the sunscreen was added. The plate setup can be seen in Figure 1.

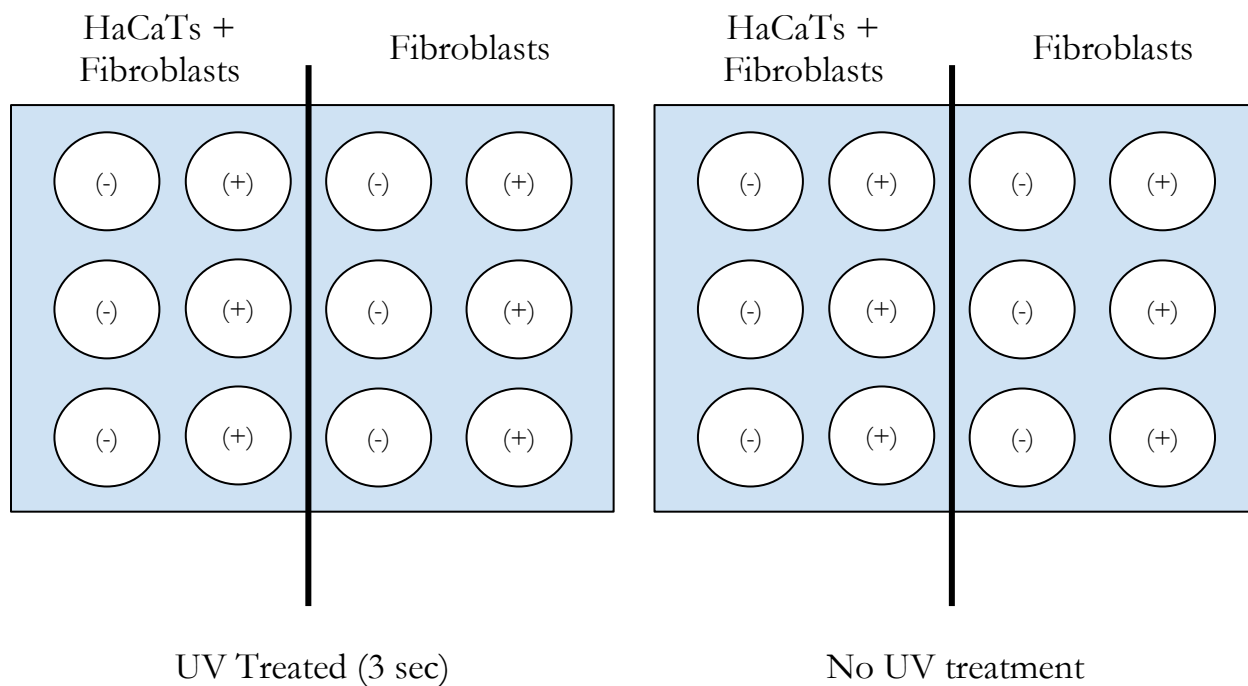


Figure 1. This diagram shows the plate maps for both the UV-treated and non-UV-treated plates, as described in section 2.4 of Methods and Procedures. The (-) symbol indicates no sunscreen was added to these wells. The (+) sign indicates that 1 μ L of sunscreen was added to these wells.

2.5 Cell Proliferation Assay

A cell proliferation assay was performed to determine how sunscreen and UV rays impacted cell growth and cytotoxicity. A cell count was performed in order to determine the density of cells for each variable that was tested. These cell counts were then used to determine how much cell suspension and medium to add to each well and how to perform the dilution for the assay. A 1X, 5X, and 25X dilution was pipetted into the wells of a 96-well plate for each variable being tested. The plate was then left in the incubator at 37 degrees Celsius for 48 hours. AlamarBlue dye (Invitrogen DAL1025) was added to each well to perform this assay. Each well received 15 μ L of alamarBlue dye. The 96-well plates were then returned to the incubator at 37 degrees Celsius for an hour. After an hour, the plate was taken out of the incubator to observe the color change in the wells. With no color change, it was placed back in the incubator for 24 hours. At that point, color changes were detected in the wells, and the plate was wrapped in aluminum foil and placed in the refrigerator.

2.6 Reading Cell Proliferation Assay and Imaging Wells

The 96-well plate was quantitatively analyzed using a fluorescence reading in the BioTek H1M2 plate reader. The excitation wavelength was set to 540 nm and the emission wavelength was set to 590 nm. The RFU values were not blank subtracted before graphing.

Each well that had been seeded was also imaged at a 10X brightfield in the Cytation 5 Imaging Reader by BioTek. Auto-focus and auto-exposure was used for all images.

RESULTS

Sunscreen and UV Ray Toxicity on HaCaT and NIH-3T3 Fibroblast Cells through a Cell Proliferation Assay

All treatment conditions followed an expected decrease in relative fluorescence units (RFUs) as one goes from a 1X dilution to a 25X dilution. The condition with the highest RFUs throughout all dilutions had no sunscreen and no UV treatment, and both HaCaT and NIH-3T3 fibroblast cells were present (Figure 2 and Figure 4G, 4H, 4I). The HaCat and NIH-3T3 cell condition that was (+) sunscreen (SS) and (-) UV treatment did not have cells present when counting in the hemocytometer and therefore was not seeded into a well.

In the HaCaT and NIH-3T3 fibroblast cell conditions, the cells that proliferated the least were in (+) UV and (-) SS (Figure 2 and Figure 4A, 4B, 4C). Comparatively, the cells in (+) UV and (+) SS (Figure 2 and Figure 4D, 4E, 4F) had slightly higher RFUs than those in (+) UV and (-) SS (Figure 2 and Figure 4A, 4B, 4C). The cells in (-) UV and (-) SS had the greatest number of RFUs of these three conditions (Figure 2 and Figure 4G, 4H, 4I).

HaCaT and Fibroblast Cells Viability (Treated with UV, sunscreen (SS), both, or none)

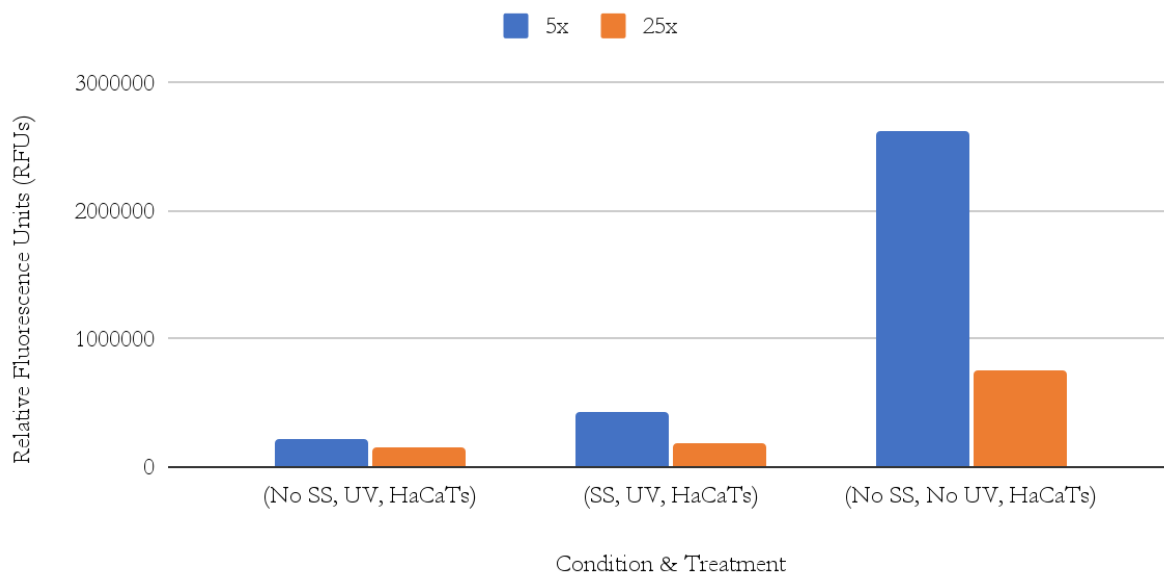


Figure 2. Graph of HaCaT and Fibroblast cells' viability after being treated with sunscreen, UV light, both, or neither via RFU values.

In the NIH-3T3 fibroblast cell wells, the cells that had the highest RFUs were in (-) UV and (-) SS (Figure 3 and Figure 5G, 5H, 5I). The cells in (+) UV and (-) SS had the next highest RFU values (Figure 3 and Figure 5A, 5B, 5C).

Comparatively, the cells in (+) UV and (+) SS had fewer RFUs than the two wells in (-) SS (Figure 3 and Figure 5D, 5E, 5F). Lastly, the cells in (-) UV and (+) SS had the smallest number of RFUs (Figure 3 and Figure 5J, 5K, 5L).

Fibroblast Cell Viability (Treated with UV, sunscreen (SS), none, or both)

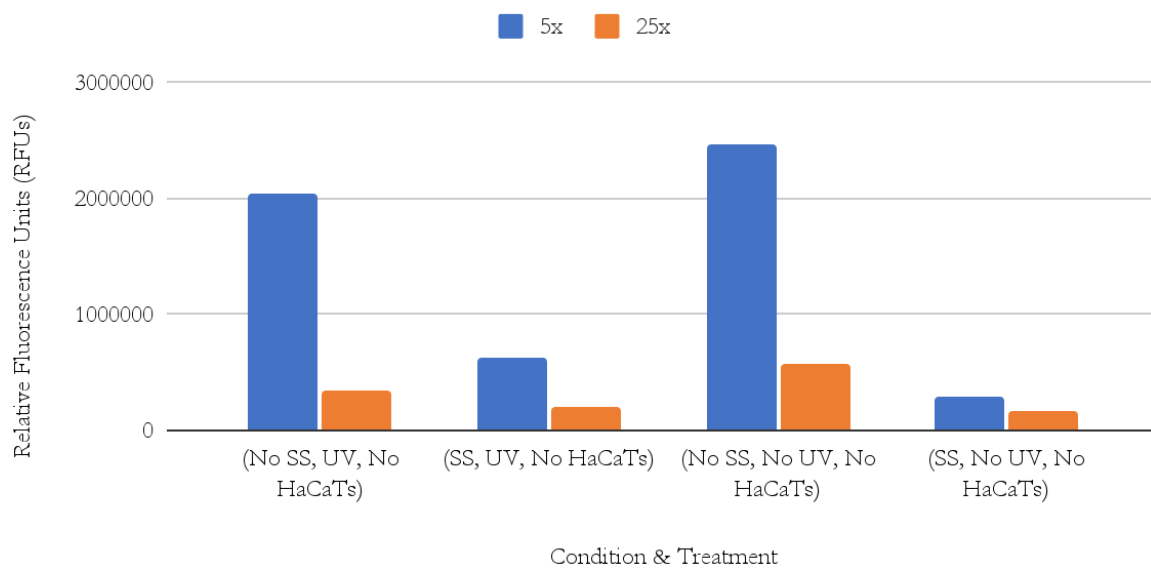


Figure 3. Graph of Fibroblast cells' viability via RFU values after being treated with sunscreen, UV light, both, or neither.

After imaging the different wells, all dilution series visibly followed the expected density decrease. Wells that were seeded with both HaCaTs and NIH-3T3 cells were confirmed visually to have both (see Figure 4), and wells seeded with only NIH-3T3 cells were confirmed visually to have only NIH-3T3 cells (see Figure 5).

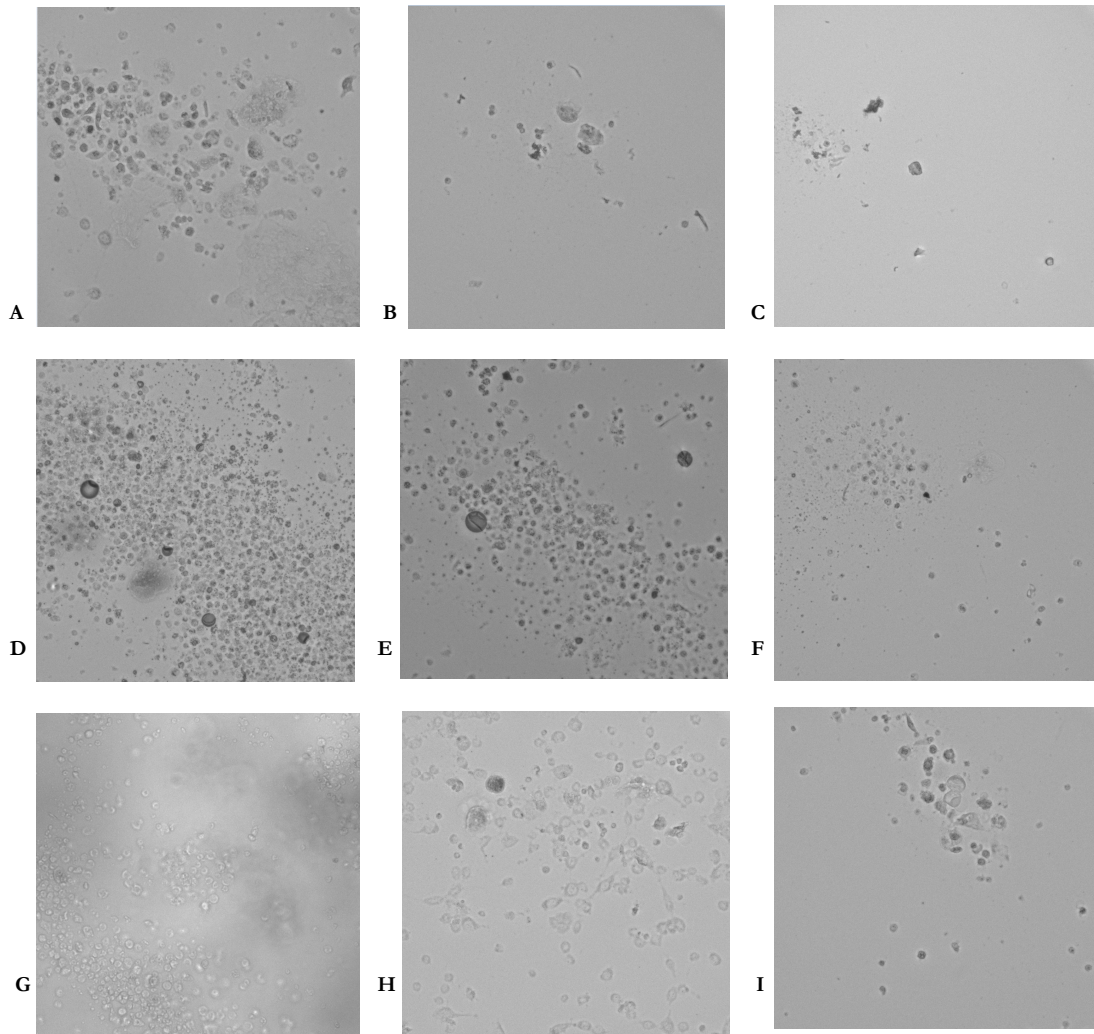


Figure 4. Plate imaging for wells with HaCaTs and NIH-3T3 cells. A (1X dilution), B (5X dilution), and C (25X dilution) are images from the wells that were (-) SS and (+) UV rays. D (1X dilution), E (5X dilution), and F (25X dilution) were images from the wells that are (+) SS and (+) UV rays. G (1X dilution), H (5X dilution), and I (25X dilution) are images from the wells that were (-) SS and (-) UV rays. These images show a successful dilution of each condition.

For wells with both HaCaTs and NIH-3T3 cells, the plate images for (-) SS and (+) UV rays showed the least amount of visible cells for all dilutions when compared to other treatment conditions (Figure 4A, 4B, 4C).

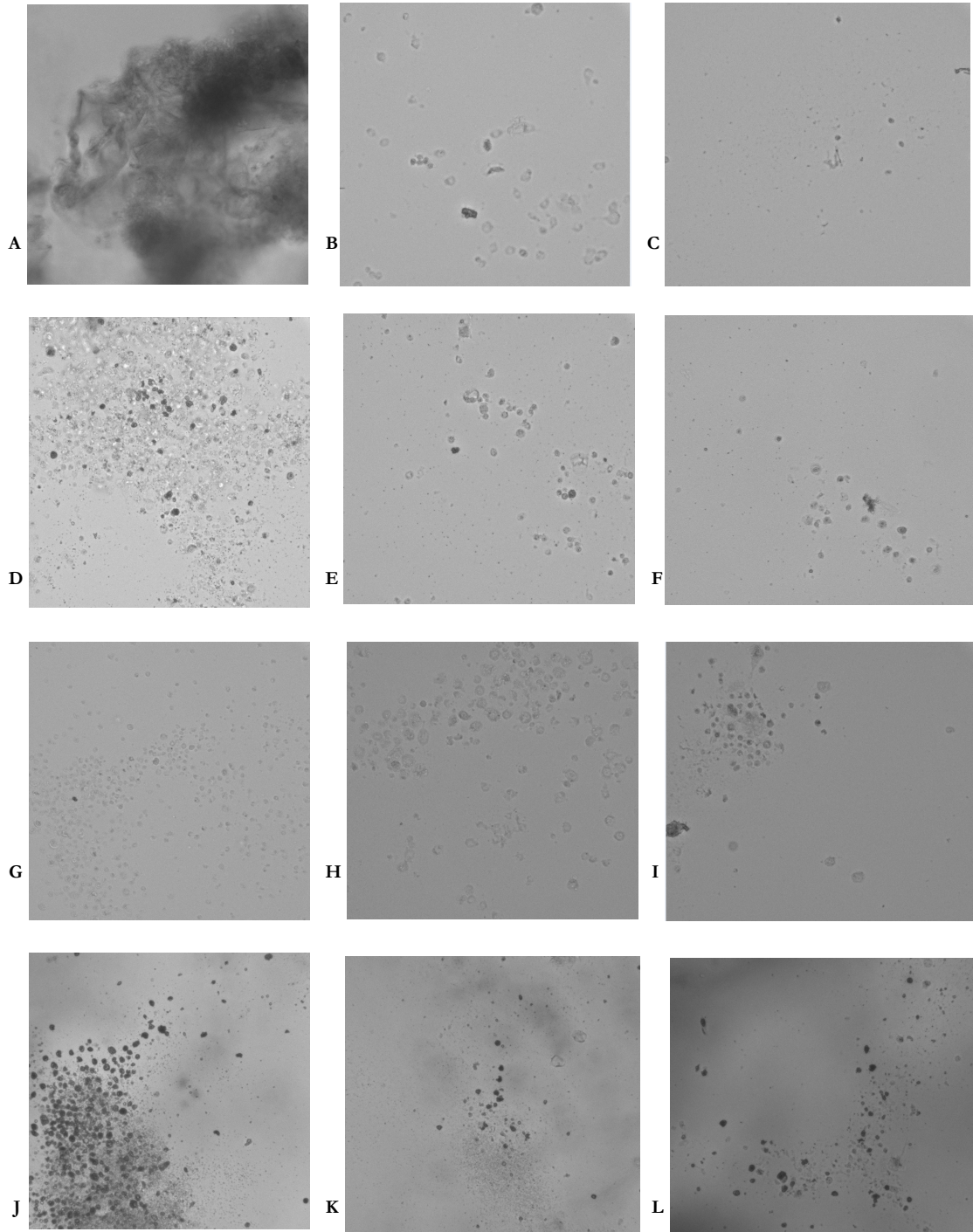


Figure 5. Plate imaging for wells with no HaCaT's, and only NIH-3T3 cells. A (1X dilution), B (5X dilution), and C (25X dilution) are images from the wells that were (-) SS and (+) UV rays. D (1X dilution), E (5X dilution), and F (25X dilution) are images from the wells that were (+) SS and (+) UV rays. G (1X dilution), H (5X dilution), and I (25X dilution) are images from the wells that were (-) SS and (-) UV rays. J (1X dilution), K (5X dilution), and L (25X dilution) are images from the wells that were (+) SS and (-) UV rays. These images show a successful dilution of each condition.

For wells that were seeded with only NIH-3T3 cells, the (-) ss and (+) UV rays visually appeared to have the least amount of cells from plate imaging (Figure 5A, 5B, 5C).

DISCUSSION

Through the creation of a three-dimensional cell culture model and performing a viability assay, the toxicity or potential carcinogenesis of sunscreen could be determined. As shown from comparing Figure 2 to Figure 3, UV and sunscreen treatment caused different effects in the wells with HaCaTs versus those without. In the wells with HaCaTs, the cells that were treated with sunscreen and UV rays had higher viability than treating the same cells with UV rays. Higher RFUs most likely means that there were more cells that survived and were proliferating. This suggests that the sunscreen had a protective element over the cells when they were exposed to UV rays. However, as seen in Figure 2, the addition of sunscreen to both cells reduced RFUs when compared to untreated HaCaT and NIH-3T3 cells. Due to experimental error, we cannot make any comparisons on the HaCaT and NIH-3T3 cells treated only with sunscreen, as there were no cells visible upon hemocytometer counting for that treatment group.

NIH-3T3 fibroblast cells grown alone have much lower RFUs when treated with sunscreen compared to cells treated with only UVs (see Figure 3). However, when cells are treated with both sunscreen and UV rays, they have higher RFUs than cells treated only with sunscreen. Along with the similar effect we saw with both HaCaT and 3T3 cells cultured together, this suggests that the UV rays themselves are making the sunscreen less toxic to the cells, possibly through degrading the chemicals.

Furthermore, in relation to our hypothesis that sunscreen may act as a carcinogenic or toxic compound to HaCaT and NIH-3T3 cells, it appears to negatively affect both cell types. When HaCaTs and NIH-3T3 cells are together, the addition of sunscreen to UV-treated cells reduces death. However, the sunscreen-treated cells still had much lower RFUs than the non-sunscreen-treated wells. When NIH-3T3 cells are cultured alone, the addition of sunscreen also reduces RFUs, but to a lesser degree of reduction than when the sunscreen is coupled with UV rays. Whether or not the sunscreen induced cancerous mutations in our cells is unknown, as the conditions with the highest RFUs were ones that had no sunscreen treatment (see Figures 2 and 3). In order to determine if something was cancerous, we made the

assumption that the wells treated with sunscreen would have much higher RFUs than the wells that were not treated with sunscreen.

Additionally, when we imaged all of our wells, the cells appeared to follow their dilution series as they should (see Figures 4 and 5). There were the most cells in the 1X dilutions, followed by the 5X, and much fewer cells were visible in the 25X dilutions. This confirms that our proliferation results were valid, and were not potentially affected by an error like simply seeding cells to the wrong density in one well.

CONCLUSIONS

Although we did not find that sunscreen induced carcinogenesis in HaCaT and NIH-3T3 cells, we did find that it can be toxic for both cell types. In the case of HaCaT cells grown with NIH-3T3 cells, sunscreen appears to kill some of the cells but still has a protective quality when coupled with UV ray treatment. In the case of NIH-3T3 cells grown alone, and both cell types coupled together, sunscreen becomes less toxic when it is coupled with UV ray treatment, than on its own. This implies that sunscreen is more toxic in the absence of UV rays. It would be worthwhile to repeat this experiment and screen cells with an assay that could detect biochemical molecules usually associated with cancer. It would also be interesting to determine the molecular mechanism for why sunscreen becomes less toxic to cells when those cells are also treated with UV rays.

ACKNOWLEDGEMENTS

We thank our Professor, Dr. Louis Roberts, and our Graduate Teaching Assistant, Yizhe Ma, for their endless guidance and assistance in developing our experiment. They both went above and beyond to help us and we are extremely grateful. We also thank the WPI Department of Biology and Biotechnology, the EmpOwER grant awarded by the Women's Impact Network for funding the research initiatives, and the Cell Engineering Research Equipment Suite (CERES) for the use of necessary plate reading and imaging instrumentation.

REFERENCES

1. Sorrell, J. M., & Caplan, A. I. (2009). Chapter 4 fibroblasts—A diverse population at the center of it all. *International Review of Cell and Molecular Biology*, 276, 161-214. [https://doi.org/10.1016/s1937-6448\(09\)76004-6](https://doi.org/10.1016/s1937-6448(09)76004-6)
2. Movat, H. Z., & Fernando, N. V. P. (1962). The fine structure of connective tissue: I. The fibroblast. *Experimental and Molecular Pathology*, 1(6), 509-534. [https://doi.org/10.1016/0014-4800\(62\)90040-0](https://doi.org/10.1016/0014-4800(62)90040-0)
3. Abercrombie, M. (1978). Fibroblasts. *J Clin Pathol Suppl (R Coll Pathol)*, 12, 1-6.
4. Colombo, I., Sangiovanni, E., Maggio, R., Mattozzi, C., Zava, S., Corbett, Y., Fumagalli, M., Carlino, C., Corsetto, P. A., Scaccabarozzi, D., Calvieri, S., Gismondi, A., Taramelli, D., & Dell'Agli, M. (2017, December 17). *HaCaT cells as a reliable in vitro differentiation model to dissect the inflammatory/repair response of human keratinocytes*. Mediators of Inflammation. Retrieved January 24, 2023, from <https://www.hindawi.com/journals/mi/2017/7435621/>
5. Seo, M.-D., Kang, T. J., Lee, C. H., Lee, A.-Y., & Noh, M. (2012, March). *HACAT keratinocytes and primary epidermal keratinocytes have different transcriptional profiles of cornified envelope-associated genes to T helper cell cytokines*. Biomolecules & therapeutics. Retrieved January 24, 2023, from <https://www.ncbi.nlm.nih.gov/pmc/articles/PMC3792214/#:~:text=HaCaT%20cells%20are%20the%20immortalized,can%20affect%20skin%20barrier%20homeostasis.>
6. Dinescu, S., Albu Kaya, M., Chitoiu, L., Ignat, S., Kaya, D. A., & Costache, M. (2019). Collagen-based Hydrogels and their applications for tissue engineering and regenerative medicine. *Polymers and Polymeric Composites: A Reference Series*, 1643-1664. https://doi.org/10.1007/978-3-319-77830-3_54
7. Artym, V. V., & Matsumoto, K. (2010). Imaging cells in three-dimensional collagen matrix. *Current Protocols in Cell Biology*, 48(1). <https://doi.org/10.1002/0471143030.cb1018s48>
8. Curtin, C., Nolan, J., Conlon, R., Deneweth, L., Gallagher, C., Tan, Y., Cavanagh, B., Asraf, A., Harvey, H., Miller-Delaney, S., Shohet, J., Bray, I., O'Brien, F., Stallings, R., & Piskareva, O. (2018). A physiologically relevant 3D collagen-based scaffold–neuroblastoma cell system exhibits chemosensitivity similar to orthotopic xenograft models. *Acta Biomaterialia*, 70, 84-97. <https://doi.org/10.1016/j.actbio.2018.02.004>
9. Yuan, Z., Memarzadeh, K., Stephen, A. S., Allaker, R. P., Brown, R. A., & Huang, J. (2018). Development of a 3D collagen model for the in vitro evaluation of magnetic-assisted osteogenesis. *Scientific Reports*, 8(1). <https://doi.org/10.1038/s41598-018-33455-2>

10. Giese, A. C. (2012). *Living with our sun's ultraviolet rays*. Springer. <https://doi.org/10.1007/978-1-4615-8744-6>
11. Narayanan, D. L., Saladi, R. N., & Fox, J. L. (2010). Review: Ultraviolet radiation and skin cancer. *International Journal of Dermatology*, 49(9), 978-986. <https://doi.org/10.1111/j.1365-4632.2010.04474.x>
12. Duale, N., Olsen, A., Christensen, T., Butt, S. T., & Brunborg, G. (2010). Octyl Methoxycinnamate Modulates Gene Expression and Prevents Cyclobutane Pyrimidine Dimer Formation but not Oxidative DNA Damage in UV-Exposed Human Cell Lines. *Toxicological Sciences*, 114(2), 272–284.
<https://doi.org/10.1093/toxsci/kfq005>